

ELUCIDATING THE ROLE OF THE ENERGY DEMANDS OF PHOTORESPIRATION IN
ACHIEVING ENERGY BALANCE

By

Kaila Ellis Smith

A DISSERTATION

Submitted to
Michigan State University
in partial fulfillment of the requirements
for the degree of

Plant Biology – Doctor of Philosophy
Molecular Plant Sciences – Dual Major

2024

ABSTRACT

The current annual food production cannot sustain population growth and is limited by rates of photosynthetic efficiency. Some strategies to improve photosynthetic efficiency include modification of the photorespiratory pathway which could substantially alter metabolic energy demands, specifically the ATP and reductant demands. Such altered energy demands might pose a problem in terms of photosynthetic efficiency because to operate efficiently and without photodamage the energy demand from metabolism must be matched with that supplied in a process referred to as energy balancing. There is a lot of focus on how processes which supply ATP and reductant mediate energy balancing, however, there is much less focus on how changes in metabolic demand drives these responses. In terms of metabolism, photorespiration consumes substantial amounts of energy making the pathway an important component in leaf energetics. The energetic costs of photorespiration are often discussed; however, less emphasis is placed on how the energy demands from photorespiration might be involved in achieving energy balance.

Overall, this dissertation explored the role of the energy demands of photorespiration in achieving energy balance. First, I contextualized the energy demands of photorespiration within the greater metabolic network by quantifying the contribution of individual pathways to energy demand. Next, I examined the impact of increased and decreased energy demands from photorespiration on the light reactions and found a novel role for the energy demands of photorespiration in energy balancing. More specifically, the ATP consumption from photorespiration assisted in maintaining photosynthetic efficiency. I leveraged the associated phenotype to create a screening platform which identified candidate genes involved in responding to dynamic shifts energy demand. I also examined whether the decreased photosynthetic efficiency associated with altered energetic demands might restore over time and

the regulation surrounding this. Finally, this dissertation concludes with future directions which would begin to address some of the outstanding questions raised throughout.

ACKNOWLEDGEMENTS

This dissertation would not be possible without the support of the amazing community surrounding me. I would foremost like to thank my advisor, Dr. Berkley Walker, for the opportunity to join his lab, the mentorship throughout my time as a graduate student, as well as the freedom to pursue scientific questions which genuinely interested me. Additionally, thank you to Drs. David Kramer, Thomas Sharkey, and Jianping Hu for serving on my committee, providing crucial feedback on my projects, and support. Additionally, to Drs. David Kramer and Thomas Sharkey for letting me extensively use your laboratory equipment. Thank you to my collaborators Drs. Polly Hsu and Larry Wu for offering their technical expertise on RNA-sequencing and being overall great collaborators.

I would also like to thank the entirety of the Walker lab for making the lab an enjoyable place to spend five years. I'd specifically like to thank Dr. Deserah Strand for not only the years of technical knowledge she advised me on but also for being an example of how to ask critical scientific questions. Thank you to Dr. Xinyu Fu who collaborated with me on numerous projects throughout my time and was always willing to go above and beyond. Dr. Mauricio Tejera was an excellent resource for coding knowledge and absolute joy to share a desk space including our spirited debates. Additionally, thank you to the other graduate students in the lab Luke Gregory, Anne Steensma, and Max Harman who were great friends to navigate through this process together oftentimes over ice cream. I would also like to thank the undergraduate research assistant, Sarah Davis, who was a tremendous help in a lot of this work.

Thank you to all of the students in both the PLB and MPS program for being overall great people. I'd like to specifically thank both Sara Kraeuter and Heather Sharick for being excellent resources and ensuring progress on my degree. Drs. Robert Last and Jyothi Kumar for

their leadership of the Plant Biotechnology for Health and Sustainability program. Additionally, thank you to both the staff at the MSU Technology Transfer office as well as Michael Best LLC for my internship opportunities and introducing me to the patent space.

Finally, I would like to thank my friends and family for their unconditional love and support during this program. My parents have always been my biggest supporters of my educational pursuits. Additionally, to all friends who never failed to listen or make me laugh during stressful situations. Lastly, thank you to both my fiancé, Matthew Hansen, and our dog, Potato, for being the absolute best.

TABLE OF CONTENTS

CHAPTER 1: Evaluating the contribution of plant metabolic pathways in the light to the ATP:NADPH demand using a meta-analysis of isotopically non-stationary metabolic flux analyses	1
Abstract	2
Introduction	3
Materials and methods	7
Results	9
Discussion	14
Figures and Tables	20
LITERATURE CITED	28
APPENDIX	32
 CHAPTER 2: The role of photorespiration in preventing feedback regulation via ATP synthase in <i>Nicotiana tabacum</i>	 34
Abstract	35
Introduction	35
Materials and methods	39
Results	42
Discussion	49
Figures and Tables	55
LITERATURE CITED	65
APPENDIX A: SUPPLEMENTAL FIGURES	72
APPENDIX B: THE PRODUCTION OF ATP AND NADPH THROUGH LINEAR ELECTRON FLOW	75
 CHAPTER 3: Identification of novel players involved in acclimating to dynamic shifts in energy demands in photosynthetic tissues using a novel chlorophyll fluorescence-based screen	 77
Abstract	78
Introduction	78
Materials and methods	82
Results	85
Discussion	93
Figures and Tables	98
LITERATURE CITED	108
 CHAPTER 4: The acclimatory response to periods with altered ATP:NADPH demand	 112
Abstract	113
Introduction	114
Materials and methods	117
Results	122
Discussion	126
Figures and Tables	130
LITERATURE CITED	138

CHAPTER 5: Conclusions and future directions	143
Summary	144
Future directions	148
LITERATURE CITED.....	152

CHAPTER 1:

Evaluating the contribution of plant metabolic pathways in the light to the ATP:NADPH demand using a meta-analysis of isotopically non-stationary metabolic flux analyses

Kaila Smith, Deserah D. Strand, and Berkley J. Walker

Submitted for publication in Photosynthesis Research

Abstract

Balancing the ATP:NADPH demand from plant metabolism with supply from photosynthesis is essential for preventing photodamage and operating efficiently, so understanding its drivers is important for integrating metabolism with the light reactions of photosynthesis and for bioengineering efforts that may radically change this demand. It is often assumed that the C3 cycle and photorespiration consume the largest amount of ATP and reductant in illuminated leaves and as a result mostly determine the ATP:NADPH demand. However, the quantitative extent to which other energy consuming metabolic processes contribute in large ways to overall ATP:NADPH demand remains unknown. Here, we used the metabolic flux networks of numerous recently published isotopically non-stationary metabolic flux analyses (INST-MFA) to evaluate flux through the C3 cycle, photorespiration, the oxidative pentose phosphate pathway, the tricarboxylic acid cycle, and starch/sucrose synthesis and characterize broad trends in the demand of energy across different pathways and compartments as well as in the overall ATP:NADPH demand. These data sets include a variety of species including *Arabidopsis thaliana*, *Nicotiana tabacum*, and *Camelina sativa* as well as varying environmental factors including high/low light, day length, and photorespiratory levels. Examining these datasets in aggregate reveals that ultimately the bulk of the energy flux occurred in the C3 cycle and photorespiration, however, the energy demand from these pathways did not determine the ATP:NADPH demand alone. Instead, a notable contribution was revealed from starch and sucrose synthesis which might counterbalance photorespiratory demand and result in fewer adjustments in mechanisms which balance the ATP deficit.

Introduction

Bioengineering in plants presents an attractive opportunity to exploit their ability to harness light and assimilate CO₂ through photosynthesis to produce unique specialized metabolites and other bioproducts. Because photosynthesis occurs in the chloroplast and chloroplast transformation results in reproducible expression, this makes chloroplasts a strong target for bioengineering strategies (Strand and Walker, 2023). However, to use photosynthetic machinery for bioengineering efforts the need for plants to balance energy harvested from the light reactions with that required by metabolism in order to operate efficiently and avoid damage must be considered (Kramer and Evans, 2011, Walker et al., 2020). Energy balancing mechanisms which supply additional ATP and transport reductant from the chloroplast exist to avoid these situations, but little is known regarding how much individual metabolic pathways contribute towards energy demand or the flexibility of such mechanisms in response to dynamic flux through metabolism. Through the perspective of energy balancing, this paper examines how different metabolic pathways contribute to the overall energy demand of the cell with considerations towards how these may impact bioengineering efforts in leaves.

The C₃ cycle and photorespiration are thought to require the largest amount of ATP and reductant in photosynthetic tissues (Noctor and Foyer, 1998, Walker et al., 2020, Walker et al., 2014). This claim stems in part from the fact that the *in vivo* activity of rubisco feeds carbon to all downstream metabolism and so is the dominate player in photosynthetic carbon metabolism. The C₃ cycle and photorespiration are fed carbon by rubisco following either the carboxylation or oxygenation, respectively, of ribulose 1,5-bisphosphate (RuBP). The C₃ cycle initiates when rubisco catalyzes the carboxylation of RuBP to form 2 molecules of 3-phosphoglycerate (3PGA). The 3PGA is converted to 1,3-bisphosphoglyceric acid and then to glyceraldehyde-3-phosphate

of which a portion is ultimately allocated towards starch and sucrose synthesis and the residual regenerates RuBP. Overall, the energetic demand for this process is assumed to be 3 ATP and 2 NADPH per CO₂ fixed by rubisco. Photorespiration begins with the oxygenation catalyzed by rubisco which produces one molecule of 3PGA and 2-phosphoglycolate (2PG) which through a series of a series of reactions is at least partially converted into 3PGA which enters the C₃ cycle. The process occurs across the chloroplast, peroxisome, and mitochondria and ultimately requires 3.5 ATP and 2 NADPH equivalents (Edwards and Walker, 1983). Given the flux of rubisco relative to other enzymes, cellular energetic demands are thought to mostly depend upon the distribution of flux through these pathways which varies based on environmental parameters.

Many key physiological approaches assume that the majority of ATP and NADPH equivalents are consumed by the C₃ cycle and photorespiration, with other energy-consuming processes either minor, or constant across measurement conditions. For example, measurements of mesophyll conductance to CO₂ using chlorophyll fluorescence assume the demand ratios above (Loreto et al., 1992, Gilbert et al., 2011, Warren, 2006). Investigations into the presence of the water-water cycle from rates of oxygen evolution and concurrent gas exchange rely on similar assumptions (Ruuska et al., 2000). These simplifying assumptions are also routinely made to estimate chloroplastic ATP:NADPH demand ratios as discussed further below (Walker et al., 2014). While these simplifications can be useful, they only reflect a portion of the total ATP and NADPH demand in the cell.

Although flux from the C₃ cycle and photorespiration dominate central metabolism, additional metabolic processes also alter the energetic landscape and include starch and sucrose synthesis, the tricarboxylic acid (TCA) cycle, the oxidative pentose phosphate pathway (OPPP), lipid biosynthesis, and nitrate fixation. During starch and sucrose synthesis, plants convert

carbon to sucrose for transport and starch for storage of carbohydrates. These processes require ATP and take place across the chloroplast and cytosol (McClain and Sharkey, 2019). The TCA cycle provides precursors for respiration, amino acid biosynthesis, and nitrogen metabolism and ultimately produces some ATP and NADPH in the mitochondria (Zhang and Fernie, 2018). The OPPP produces NADPH and pentose phosphates. There are two currently proposed OPPP pathways occurring in either the cytosol or the chloroplast, however, the exact location remains an area of active discussion (Xu et al., 2022, Xu et al., 2023, Wieloch et al., 2023). Lipid biosynthesis is an energetically expensive processes occurring in the chloroplast. Nitrate assimilation requires reducing equivalents and occurs in the cytosol in the chloroplast.

It can be useful to evaluate ATP and NADPH flux through individual pathways, however, the ratio of ATP:NADPH demand across many pathways collectively is often more informative from an energy balancing perspective. This is partly because the pool sizes of chloroplastic ATP and NADPH are relatively small compared to the high flux being produced from the light reactions and furthermore the light reactions produce ATP and NADPH in a constrained stoichiometry of ~ 1.3 through linear electron flow (LEF) (Hangarter and Good, 1982). The stoichiometry of ATP:NADPH production from the light reactions is constrained due to the coupling of proton and electron transfer. The ~ 1.3 ATP:NADPH production from LEF falls short of the ATP:NADPH demand from the largest ATP:NADPH consuming pathways, the C₃ cycle and photorespiration which demand 1.5 and 1.75, respectively (Noctor and Foyer, 1998). The discrepancy between supply and demand may lead to an ATP deficit (where ATP is insufficient relative to NADPH) if the chloroplast does not activate alternative ATP generating pathways in addition to LEF (Smith et al., 2023, Strand and Walker, 2023). An ATP deficit may lead to metabolic bottlenecks, lower assimilation, and ultimately yields. As outlined above, the

ATP:NADPH demand of the cell is often primarily determined by the proportion of flux through either the C3 cycle or photorespiration. However, the question arises as to how additional energy consuming metabolic pathways contribute to the ATP:NADPH demand and ultimately the ATP deficit.

Plants employ various energy balancing strategies to meet fluctuating cellular energetic demand. Within the chloroplast, alternative ATP generating processes are thought to play a large role in balancing an ATP deficit. These alternative pathways are cyclic electron flow (CEF), the malate valve, and the water-water cycle [reviewed in (Allen, 2003b, Scheibe, 2004, Asada, 1999, Kramer and Evans, 2011)]. Both CEF and the water-water cycle occur in the chloroplast whereas, the malate valve shuttles reductant between the chloroplast, peroxisome, and mitochondria. Given that metabolism and energy balancing occur across several organelles this then poses the question of how the distribution of ATP and NADPH from supplying processes is coordinated with consumption throughout the cell.

One approach for determining how each individual metabolic pathway contributes to the ATP:NADPH demand is to leverage metabolic flux networks. Isotopically non-stationary metabolic flux analysis (INST-MFA) is an increasingly used technique in plants for quantifying metabolic flux through central metabolism (Jazmin et al., 2014). Typically, the scope of these studies focuses on carbon flux, however, they can be used to resolve cellular energy flux by coupling each reaction to its associated ATP and NADPH demand. By evaluating the energy demand from different pathways, we can gain insight into how these pathways specifically contribute to ATP and NADPH demand. In this study, we used flux values from 8 different INST-MFA experiments which consist of a variety of species including *Arabidopsis thaliana*, *Nicotiana tabacum*, and *Camelina sativa* across environmental factors such as high/low light,

day length, and photorespiratory levels allowing us to characterize the flux of energy across different pathways and compartments (Ma et al., 2017, Fu et al., 2023, Xu et al., 2021, Xu et al., 2022, Xu et al., 2023). We found that while most of the energy demand did arise from the C3 cycle and photorespiration, the energy demand from these pathways did not account for total cellular demand with notable contributions from starch and sucrose synthesis. Ultimately, we suggest starch and sucrose synthesis may help counterbalance the energy demand from photorespiration to avoid the need for rapid adjustments in alternative ATP generating processes which may limit photosynthetic efficiency or cause photodamage.

Materials and methods

We compiled data from 8 different ^{13}C labeled INST-MFA data sets to use in our analysis. Within the INST-MFA data sets, individual reactions were grouped into their cellular compartment and respective pathways (Ma et al., 2017, Fu et al., 2023, Xu et al., 2021, Xu et al., 2022). The pathways we included in our analysis were the C3 cycle, photorespiration, starch and sucrose synthesis, the TCA cycle, and the OPPP as almost every data set had reported flux through these pathways with the exception of the OPPP being absent in *Arabidopsis thaliana* data sets (ATP and NADPH demands for each flux map available as supplementary material). Some other pathways which were excluded from our analysis include lipid biosynthesis and nitrate assimilation due to not having reported metabolite flux into those pathways. By categorizing the carbon flux from the individual reactions described below, we could calculate the energy demand for the various pathways and compartments. For the C3 cycle, we used the flux from 3PGA to triose phosphates (-1 ATP, -1 NADPH per turnover) and ribulose 5-phosphate (Ru5P) to RuBP (-1 ATP per turnover). For photorespiration, we used the carbon flux for glycine to serine (+1 NADH, -1 ATP, -2 Fd assuming the NH_4^+ recapture per turnover) and glycolate to

3PGA (-1 ATP per turnover). For the OPPP, we used carbon flux for glucose-6-phosphate to 6-phosphogluconolactone (6PG, +1 NADPH per turnover) and 6PG to Ru5P (+1 NADPH per turnover). For starch and sucrose synthesis, we only considered flux from fructose-6-phosphate to fructosyl (-1 ATP per turnover) and the glucosyl and fructosyl moieties of sucrose to sucrose-6-phosphate (-1 ATP per turnover). For the TCA cycle we used phosphoenolpyruvate to pyruvate (+1 ATP per turnover), isocitrate to alpha-ketoglutarate (AKG, +1 NADH per turnover), AKG to succinate (+1 NADH, +1 GTP per turnover), succinate to fumarate (+1 FADH₂ per turnover), malate to oxaloacetate (+1 NADH per turnover), AKG to glutamate (-1 NADH per turnover), and pyruvate to acetyl-CoA (+1 NADH per turnover). Despite the fact that these reactions use a variety of energy carriers as outlined above, for simplicity sake we will refer to reductant in terms of NADPH equivalents and nucleoside triphosphates in terms of ATP.

The percentage of ATP needed to be supplied by alternative ATP generating processes was calculated by subtracting the assumed 1.3 ATP:NADPH demand supplied by LEF from the ATP:NADPH demand from metabolism for each data set. This value was then divided again by the 1.3 value provided from the light reactions and multiplied by 100.

$$\text{Percentage of ATP needed from alternative electron processes} = \quad (1)$$

$$\left(\frac{\text{ATP:NADPH demand} - 1.3}{1.3} \right) * 100$$

Data handling, statistical analysis, and graphing were performed in R using dplyr and ggplot2 packages.

Results

Most leaf energy demand in the chloroplast comes from the C3 cycle and photorespiration

As described above, the largest energy-consuming pathways in photosynthetic tissues are thought to be the C3 cycle and photorespiration, however, the plant cell uses ATP and NADPH in a multitude of other pathways. To determine how much each pathway contributes to the total flux, we examined the flux from individual pathways by finding the absolute value of the energetic flux from each pathway and averaging this across all the flux data sets excluding those which manipulated levels of photorespiration using altered O₂ concentrations. ATP and NADPH energy use was the highest in the C3 cycle, with it requiring 4.2 mmol ATP g⁻¹ FW h⁻¹ and 2.7 mmol ATP g⁻¹ FW h⁻¹ which was ~90% of ATP and ~91% of NADPH total flux (Figure 1.1). Next largest was photorespiration with 0.34 mmol ATP g⁻¹ FW h⁻¹ and 0.17 mmol NADPH g⁻¹ FW h⁻¹ or about ~7% total of ATP and ~6% NADPH flux. Interestingly, the OPPP produced 59 μmol NADPH g⁻¹ FW h⁻¹ or 2% of total NADPH flux. Starch and sucrose synthesis required 99 μmol ATP g⁻¹ FW h⁻¹ or about 2% of total ATP flux. Finally, the TCA cycle produced 7 μmol ATP g⁻¹ FW h⁻¹ and 15 μmol NADPH g⁻¹ FW h⁻¹ which was less than 1% of total ATP and NADPH flux. These results highlight that, while C3 and photorespiration do dominate metabolism, small contributions from other pathways may have important roles in energy balancing. For example, if CEF must operate at 13% of LEF to supply the C3 cycle, then starch and sucrose synthesis consuming 2% of the total ATP demand may substantially impact the system (Strand et al., 2017).

Metabolism acts across all cellular compartments, requiring the plant to coordinate and transport ATP and NADPH. This need for this coordination invites the question of how the distribution of ATP and NADPH consumption is coordinated throughout the cell and how are

these demands met. To examine the energy flux in individual compartments, we took the absolute value of the energetic flux from each pathway and averaged this across all the flux data sets again excluding those which manipulated levels of photorespiration through altered oxygen concentrations. We found ATP and NADPH flux was highest in the chloroplast with it requiring 2.9 mmol ATP g⁻¹ FW h⁻¹ and 4.5 μmol NADPH g⁻¹ FW h⁻¹ which was 98% of total ATP flux and 88% of total NADPH flux (Figure 1.2). Within the peroxisome, 0.17 mmol NADPH g⁻¹ FW h⁻¹ was required which was 5% of NADPH flux. ATP and NADPH flux in the cytosol was 92 μmol ATP g⁻¹ FW h⁻¹ produced and 59 μmol NADPH g⁻¹ FW h⁻¹ produced which was 2% of both ATP and NADPH total flux. 0.16 mmol NADPH g⁻¹ FW h⁻¹ was produced in the mitochondria which was 5% of NADPH flux. This not only highlights the large amounts of ATP and NADPH required in the chloroplast, but also the amount of NADPH required in the peroxisome which is not typically thought of as an energetically important organelle.

Cellular ATP:NADPH demand and the percentage of ATP supplied by alternative ATP generating processes varied amongst species and conditions

The ATP deficit in the plant varies based on the proportion of flux through downstream metabolism which changes based on environmental conditions, however, the range of this variation is under-explored. We first examined the range of the ATP deficit by examining the ATP:NADPH demand in the chloroplast because it contains the majority of metabolic flux. ATP:NADPH demand was most similar between species and conditions in the chloroplast where demand ranged from 1.52-1.58 with the demand never rising above 1.6 (Figure 1.3A). Since the majority of chloroplastic flux is from the C3 cycle and photorespiration, the demand in the chloroplast should be almost identical to that from the C3 cycle and photorespiration. Indeed, these ratios were almost identical to the ATP:NADPH demand solely from photorespiration and

the C3 cycle, the exception being an increased ATP:NADPH demand in the 21% and 40% *Nicotiana tabacum* data sets likely from the inclusion of mitochondrial and peroxisomal reactions which introduced additional demand related to photorespiration (Figure 1.3B). This suggests that the ATP deficit experienced specifically within in the chloroplast is relatively similar between species and conditions such as gas concentrations, growth day length, and light intensities.

Given that the largest energy demand was found to be in the chloroplast with 98% of total ATP flux and 88% of total NADPH flux within the whole cell, it seemed likely that the cellular ATP:NADPH demand would also be relatively similar to the chloroplast between species and conditions (Figure 1.2). However, while the extent of ATP deficit varied little in the chloroplast, the total cellular ATP:NADPH demand was more variable and higher overall. More specifically, the demand among the different conditions ranged from 1.56 to 1.67 (Figure 1.3C). The larger variability among the environmental conditions in the species in the whole cell compared to the chloroplast alone suggests the potential for a larger role of other metabolism in determining the total ATP:NADPH demand rather than being solely determined by flux through the C3 cycle and photorespiration.

Ultimately, all the conditions above support the presence of an ATP deficit because they are all greater than the ~ 1.3 ATP:NADPH supplied by LEF. The discrepancy in ATP:NADPH between supply and demand must therefore be met by alternative ATP generating processes such as CEF, the malate valve, and the water-water cycle. We calculated the percentage of the ATP:NADPH which must be met by alternative ATP generating processes both in the whole cell as well as the chloroplast specifically for each data set. We found ATP demand which must be supplied by alternative ATP generating processes was between 20-29% in the whole cell from the

metabolism measured in the component MFA analyses. In the chloroplast specifically the ATP demand which must be supplied by alternative processes was reduced to 16-21% (Table 1). The discrepancy between the percentage of ATP demand which must be met by alternative processes in the whole cell and the chloroplast raises questions as to how the plant employs different energy balancing processes and their flexibility under dynamic conditions.

ATP and NADPH demand are reasonably estimated by rates of rubisco carboxylation and oxygenation

Due to difficulties associated with measuring ATP and NADPH demand related to their fast turnover times, one method of assessing the ATP and NADPH demand has been approximating the levels from the rate of rubisco carboxylation (v_c) and the rate of rubisco oxygenation (v_o) estimated from leaf gas exchange (Walker et al., 2020, Hangarter and Good, 1982, Sharkey, 1988). This demand is calculated by adding the products of v_c and v_o multiplied by the requirements for the C3 cycle (3 ATP and 2 NADPH) and photorespiration (3.5 ATP and 2 NADPH). Since energy demand estimates from v_c and v_o rely solely on the contributions from the C3 cycle and photorespiration, we compared demand estimated from v_c and v_o to not only flux data demand from the entire cell but as well to as solely from the C3 cycle and photorespiration. Overall, both total NADPH and ATP demand correlated strongly with demand calculated from v_c and v_o (Figure 1.4). Total ATP demand correlated the same in both in the entire cell and from the C3 cycle and photorespiration (Figure 1.4C-D). NADPH demand correlated slightly less in the entire cell when compared to from the C3 cycle and photorespiration (Figure 1.4A-B). Previously ATP:NADPH has been estimated from multiplying v_c and v_o by the respective demand outlined above for the C3 cycle and photorespiration (Walker et al., 2020). The data suggests the method reasonably estimates energetic demands calculated from flux networks. However, there

are slight imperfections as the relationships are not perfectly linear with the least linear being the cellular NADPH demand (Figure 1.4A).

In addition to the C3 cycle and photorespiration, starch and sucrose contribute notably to cellular ATP:NADPH demand

Since a majority of energetic demand comes from the C3 cycle and photorespiration, we hypothesized that most of the variability in the cellular ATP:NADPH demand between the individual data sets may be due to differences in the flux through these pathways. If this were the case, then the ATP:NADPH demand should be proportional to v_o/v_c . ATP:NADPH demand from just the C3 cycle and photorespiration correlated with rates of v_o/v_c more weakly than expected (but still significant) likely due to the slight imperfections in estimating ATP and NADPH demand described above (Figure 1.5A, $r^2 = 0.74$, $p < 0.05$, linear regression model). Interestingly, cellular ATP:NADPH for core metabolism and v_o/v_c were only weakly and insignificantly correlated (Figure 1.5B, $r^2 = 0.10$, $p > 0.05$). We then examined whether ATP:NADPH from the C3 cycle and photorespiration correlated with cellular demand and found an almost non-existent correlation (Figure 1.5C, $r^2 = 0.06$, $p > 0.05$, linear regression model). This suggests that while a majority of energy demand does come from the C3 cycle and photorespiration, differences in flux in these pathways do not entirely explain the increase or variation in ATP:NADPH demand.

Since the proportion of flux through the C3 cycle and photorespiration did not appear to determine cellular ATP:NADPH demand, we hypothesized a different metabolic pathway must also play a prominent role. Based on the ATP and NADPH flux values, it is likely that the increase in demand was arising from either the NADPH produced by the OPPP, or the ATP required from starch and sucrose synthesis (Figure 1.1). To test this, we alternatively subtracted energy consumption from either the combined starch and sucrose synthesis or the energy

produced from the OPPP to observe which would increase the correlation with cellular ATP:NADPH. When starch and sucrose biosynthesis was removed the relationship became mostly linear (Figure 1.6A, $r^2 = 0.95$, $p < 0.05$, linear regression model). However, when the OPPP was removed the relationship only slightly improved (Figure 1.6B, $r^2 = 0.25$, $p > 0.05$, linear regression model). This suggests that aside from the C3 cycle and photorespiration, starch and sucrose synthesis has the largest effect on cellular ATP:NADPH demand with a smaller role for the OPPP. To determine how the energy demand from starch synthesis scaled with net carbon assimilation, we investigated the relationship between the ATP required from starch and sucrose biosynthesis and v_c with the flux through the glycine decarboxylase complex subtracted to account for carbon loss from photorespiration. ATP consumption from starch and sucrose synthesis did scale relatively well with this net carbon assimilation displaying how ATP demand from starch and sucrose synthesis scales with net assimilation (Figure 1.7).

Discussion

Starch and sucrose synthesis may help counterbalance photorespiration to maintain cellular energy demand

These findings support the hypothesis that starch and sucrose synthesis counterbalance changes in cellular ATP:NADPH demand when accompanied by changes in net assimilation. Typically, cellular ATP:NADPH demand is thought to be determined mainly from the distribution of flux through photorespiration and the C3 cycle due to the large flux of these pathways (Figure 1.1) (Walker et al., 2020, Smith et al., 2023). If this were true, cellular ATP:NADPH demand would decrease or increase according to levels of photorespiration due to the extra ATP consumption from this pathway. However, in this study we show that the ATP:NADPH demand from the C3 cycle and photorespiration did not entirely explain cellular

demand (Figure 1.4). Instead, starch and sucrose synthesis also substantially contributed to cellular ATP:NADPH demand (Figure 1.5A). We propose this is because as photorespiration is reduced and net assimilation increases, there is more flux into carbon assimilation ultimately which also increases starch and sucrose synthesis (Figure 1.7) (Fu et al., 2023, Sharkey et al., 1985). Therefore, since starch and sucrose synthesis and photorespiration both increase the cellular ATP required as they inversely change perhaps this helps maintain a more similar ATP:NADPH demand.

Perhaps the inverse relationship between levels of photorespiration and starch and sucrose synthesis begins to explain why decreasing either result in a similar effect on the light reactions. Triose phosphate utilization (TPU), related to starch and sucrose synthesis, serves as a biochemical limitation of photosynthesis in C3 plants when plants are photosynthesizing rapidly and the turnover of triose phosphates into end products causes a decrease in available phosphate limiting the rate of photosynthesis via ATP synthase (McClain and Sharkey, 2023, Kiirats et al., 2009). Similarly, when photorespiration is decreased it also results in a decrease in ATP synthase conductivity likely due to a decrease in ATP consumption (Smith et al., 2023). Additionally, when either of these metabolic pathways are disrupted, mechanisms that supply additional ATP, such as CEF, appear to increasingly compensate. For example, CEF increases when the flow of triose phosphates into sucrose is altered via a mutation in the C3 cycle enzyme fructose 1,6-bisphosphate (Livingston et al., 2010a). Likewise, there is an increase in CEF when the flow of the photorespiratory pathway is interrupted via a peroxisomal hydroxypyruvate reductase (*hpr1*) knockout (Li et al., 2019). Both of these instances occur due to an increase in peroxide as potentially a signal that metabolism has been disrupted. Overall, the similar impacts on both the light reactions and CEF when either starch and sucrose synthesis or photorespiration are

impaired further highlight the potential role of starch and sucrose synthesis aiding in counterbalancing photorespiration to maintain similar cellular ATP:NADPH demand.

Contributions from starch and sucrose synthesis to ATP:NADPH demand could decrease the need for rapid adjustments from alternative ATP generating processes in dynamic environments

The extent of the variation of ATP:NADPH demand under different conditions and species has not been explored, however, here we show that the chloroplast ATP:NADPH demand varied less than cellular ATP:NADPH demand between various species and conditions. The chloroplast ATP:NADPH demand was almost identical to the ATP:NADPH demand solely the C3 cycle and photorespiration with the exception of in the 21% and 40% *Nicotiana tabacum* data sets likely from the inclusion of mitochondria and peroxisome introducing additional photorespiratory demand outside of the chloroplast (Figure 1.3). This suggests that the ATP deficit specifically within in the chloroplast is relatively similar between species and conditions such as day length and light intensities. However, we found while the extent of ATP deficit varied little in the chloroplast, the total cellular ATP:NADPH demand was more variable with higher overall demand (Figure 1.3C). The variability appears to be due to differences in the flux in starch and sucrose biosynthesis between the species and conditions.

The counterbalance between photorespiration and starch and sucrose synthesis would be beneficial because it would decrease the need to dynamically adjust alternative ATP generating processes as cellular ATP:NADPH demand varies. As shown here, the percentage of alternative processes needed to supply ATP can be quite substantial and ranged between 20-29% in the whole cell (Table 1). The increased variability in the whole cell ATP:NADPH demand observed under different environmental conditions and species suggests cellular demand is likely rapidly

changing according to the environment (Figure 1.3C). The proposed counterbalance between starch and sucrose synthesis and photorespiration could be beneficial to avoid potentially rather large adjustments in alternative processes which could be experienced under dynamic environments. For example, if the plant were to experience an increase in ATP:NADPH demand and then accordingly increase CEF this would result in an increase in proton motive force and ultimately the downregulation of the light reactions and photosynthesis (Livingston et al., 2010b, Alric and Johnson, 2017, Allen, 2003a). This perhaps begins to resolve why altering flux through the C3 cycle or photorespiration does not always appear to activate CEF as expected from changes in energetic demands or under sub-saturating light intensities (Smith et al., 2023, Walker et al., 2014).

C3 cycle and photorespiration within the chloroplast represented the majority of energy demand

Ultimately, the flux from starch and sucrose synthesis is still small proportionally to the large flux from the C3 cycle and photorespiration. The C3 cycle represented most of the flux with ~90% of ATP and ~91% of reductant and photorespiration accounted for only ~7% of ATP and ~6% of reductant. This proportional energy demand for photorespiration is much lower than previous estimates, however, this is because other calculations partition the energy required to regenerate the 3PGA recycled from photorespiration back into Ribulose-5-phosphate, whereas ours account for this energy as part of the C3 cycle (Walker et al., 2016, Edwards and Walker, 1983). In contrast, starch and sucrose synthesis only accounted for about 2% of ATP consumption (Figure 1.1). These calculations highlight that while other metabolic pathways may have more energetic significance than expected, the C3 cycle and photorespiration still dominate in terms of absolute flux.

Given the large amounts of ATP and NADPH required by the C3 cycle and photorespiration as calculated here, bioengineering efforts focused on decreasing the rate of photorespiration may need to consider maintaining native energy demands to not perturb the energetic balance between supply and demand. Recently, bioengineering efforts have focused on decreasing the CO₂ and NH₄⁺ released from photorespiration to improve photosynthetic efficiency (South et al., 2019, Kebeish et al., 2007, Basler et al., 2016, Peterhansel et al., 2013b). However, strategies for reengineering photorespiration, commonly referred to as photorespiratory bypasses, also impose novel energetic requirements which may not be met by intrinsic cellular energetic flexibility. These bypasses alter the total ATP and NADPH required by photorespiration and as a result the ATP:NADPH ratio increases or decreases depending on the engineered pathway (Peterhansel et al., 2013a). An increase or decrease in the ATP:NADPH ratio may negatively impact the light reactions or the regulation of alternative processes, highlighting the need to resolve the fundamental bioenergetics linked to photorespiration. More specifically, when the ATP:NADPH demand decreases due to reduced photorespiration this causes a decrease in electron transfer and may eventually limit crop yields (Smith et al., 2023).

The complex energetic interplay between the peroxisome and the mitochondria

In this analysis we explored how metabolism acts across several organelles as well as in the exterior cytosol. While the chloroplast required the most ATP and NADPH, there was a larger contribution from the peroxisome than we anticipated. More specifically, the chloroplast required approximately ~98% of the ATP and ~88% of the NADPH compared to the other cellular compartments (Figure 1.2). However, the peroxisome, not typically thought of as an energetically important organelle, required approximately ~5% of the reducing power.

It is often assumed that the conversion of glycine to serine during photorespiration in the mitochondria produces reductant which offsets the demand in the peroxisome for glycerate synthesis (Raghavendra et al., 1998). These processes are then accordingly linked in corresponding metabolic flux models and then resulted here in the 5% of the reductant produced in the mitochondria matching the 5% reductant required in the peroxisome. However, there is evidence glycine can be exported from photorespiration, which would reduce the reductant ultimately available to the peroxisome by decreasing the stoichiometry of glycine decarboxylation (Fu et al., 2023, Harley and Sharkey, 1991b, Busch et al., 2018). Albeit this glycine export likely occurs at low rates and would therefore not largely reduce the reductant available. Additionally, the reductant produced in the conversion of glycine to serine could be used in the mitochondrial electron transport chain, which would lead to a decrease in reductant supply to the peroxisome (Shameer et al., 2019). If this were true, it is possible some of the reductant not provided from the mitochondria could be provided to the peroxisome from the 2% of NADPH produced by the OPPP as observed here.

Conclusions

Overall, this work highlights how the energetic landscape is diverse and complicated. While the C3 cycle and photorespiration represented most of the energetic flux, additional metabolic pathways, most notably starch and sucrose synthesis, drove variation in energy demands between species and environmental conditions. Additionally, the contribution of starch and sucrose synthesis in ATP:NADPH demand proposed an important mechanism for homeostasis in the complicated energetic landscape. Ultimately, by deepening our understanding of the interactions within the energetic landscape we can more accurately inform and address challenges in metabolic engineering to increase both crop yields and desired products.

Figures and Tables

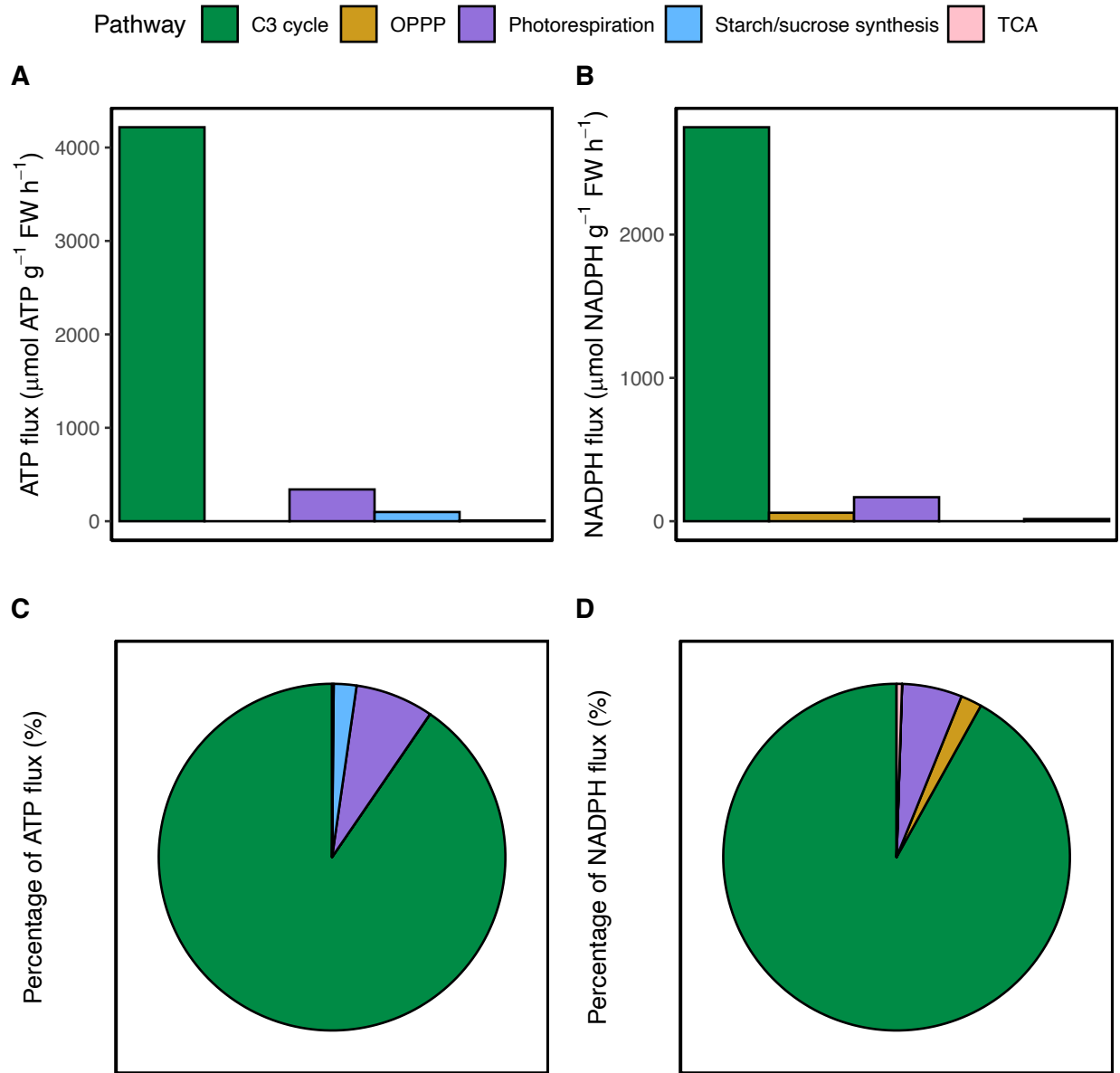


Figure 1.1. The relative flux of ATP and NADPH through individual metabolic pathways. Relative flux of A) ATP and B) NADPH through individual pathways were determined by finding the absolute value of the total energetic flux from each pathway then averaging across all data sets. Data sets which manipulated levels of photorespiration using altered O_2 concentrations were not included. The fluxes were then expressed in the percentage of the total C) ATP and D) NADPH flux.

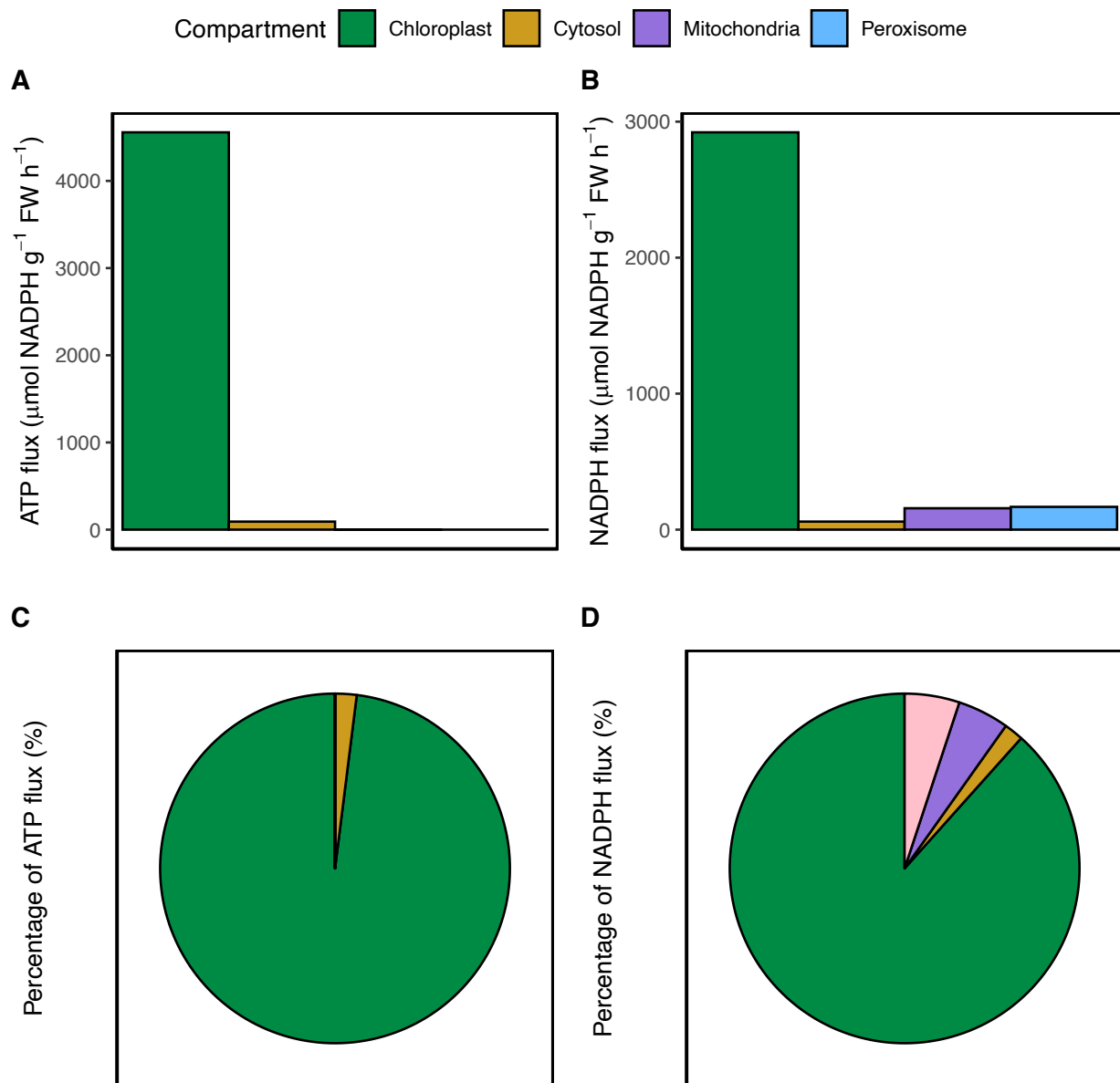


Figure 1.2. The relative flux of ATP and NADPH through individual compartments.

Relative flux of A) ATP and B) NADPH through individual compartments were determined by finding the absolute value of the total energetic flux from each compartment then averaging across all data sets. Data sets which manipulated levels of photorespiration using altered O₂ concentrations were not included. The fluxes were then expressed in the percentage of the total C) ATP and D) NADPH flux.

Species ● Arabidopsis HL ● Camelina 2021 ● Camelina LD ● Nicotiana 2% O2 ● Nicotiana 40% O2
 ● Arabidopsis LL ● Camelina 2022 ● Camelina SD ● Nicotiana 21% O2

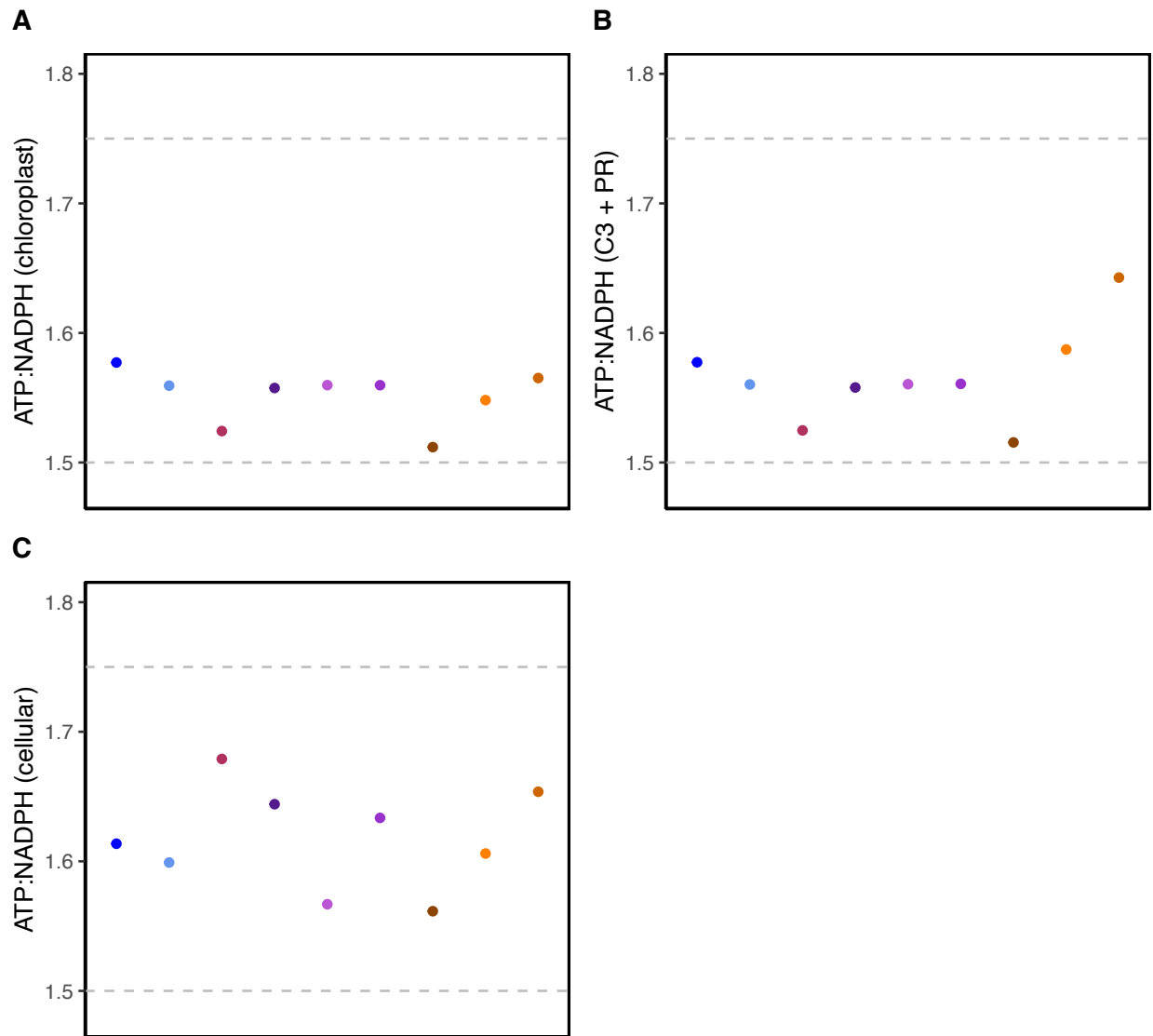


Figure 1.3. The dynamicity of the ATP:NADPH demand across different conditions and species. Shown are the ATP:NADPH demand for the different data sets at the scale of A) the chloroplast, B) from solely the C3 cycle and photorespiration (PR), and C) cellular.

ATP:NADPH demand were calculated by totaling the ATP and NADPH demand separately from the carbon flux then taking the ratio of ATP:NADPH. The dashed gray lines constrain the graphs and represent the energy demand for the C3 cycle (lower) and photorespiration (upper).

Table 1.1. ATP needed to be supplied by alternative ATP generating processes. Shown is the percentage ATP needed to be supplied by alternative electron processes in both the whole cell and the chloroplast for each data set. Details of these calculations are found in the text.

Dataset	ATP needed to be supplied by alternative electron processes in the whole cell (%)	ATP needed to be supplied by alternative electron processes in the chloroplast (%)
Arabidopsis HL	24	21
Arabidopsis LL	23	19
Camelina LD	20	20
Camelina SD	25	20
Camelina 2021	29	17
Camelina 2022	26	19
Nicotiana 21% O ₂	23	19
Nicotiana 2% O ₂	20	16
Nicotiana 40% O ₂	27	20

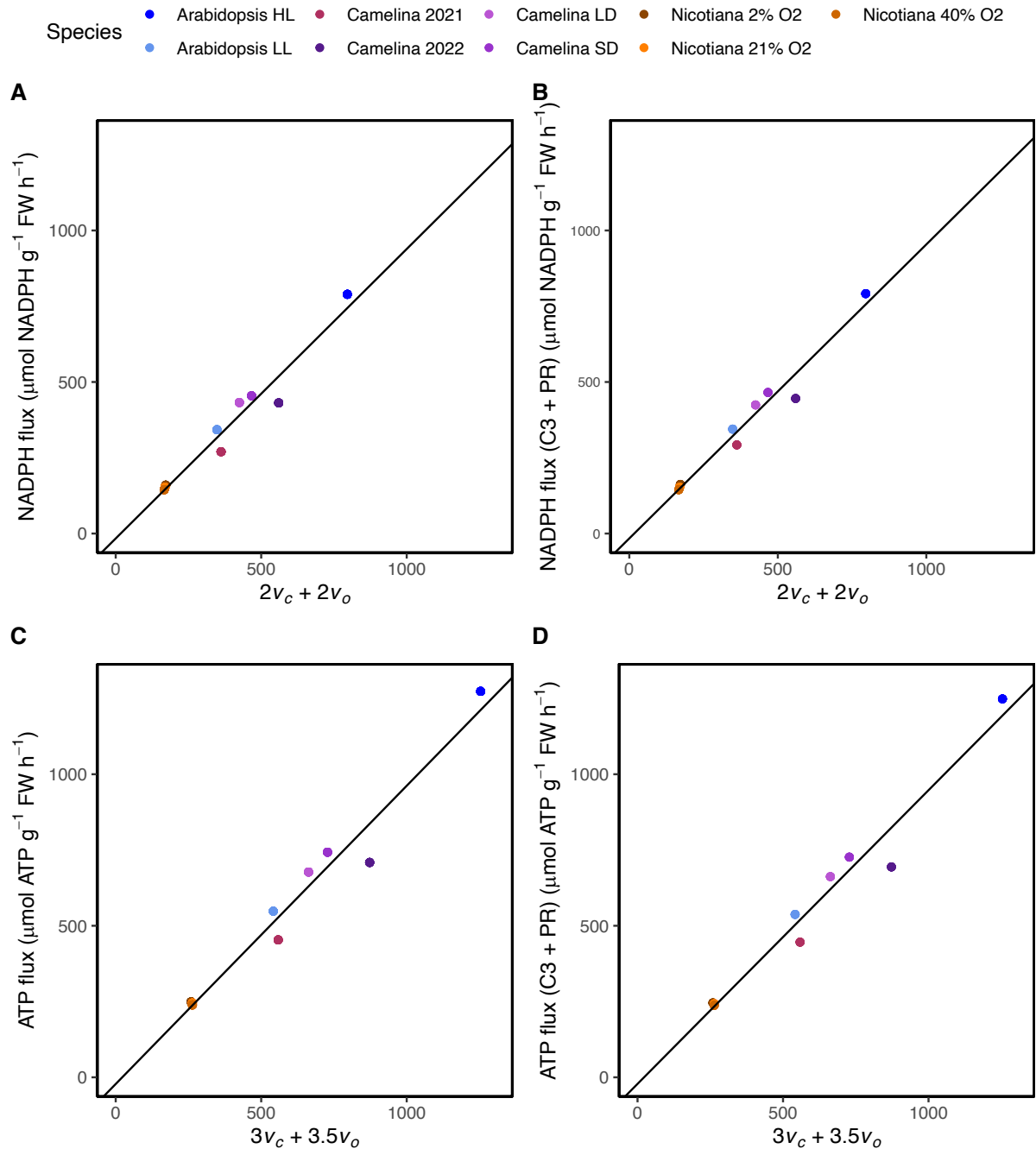


Figure 1.4. Comparison between the values calculated for ATP and NADPH fluxes. First, shown are the comparisons between the estimated NADPH flux as calculated by adding the products of v_c and v_o multiplied by the NADPH demand from the C3 cycle and PR, respectively, with the NADPH flux through A) the cell ($r^2 = 0.94$, $p < 0.05$, linear regression model) B) through solely the C3 cycle and photorespiration (PR) ($r^2 = 0.96$, $p < 0.05$, linear regression model). Then, then same comparisons are made for ATP flux through C) the cell ($r^2 = 0.96$, $p < 0.05$, linear regression model) and D) and solely the C3 cycle and PR ($r^2 = 0.96$, $p < 0.05$, linear regression model). The solid black lines represent the results of the results of the linear regression models.

Species

- Arabidopsis HL
- Camelina 2021
- Camelina LD
- Nicotiana 2% O₂
- Nicotiana 40% O₂
- Arabidopsis LL
- Camelina 2022
- Camelina SD
- Nicotiana 21% O₂

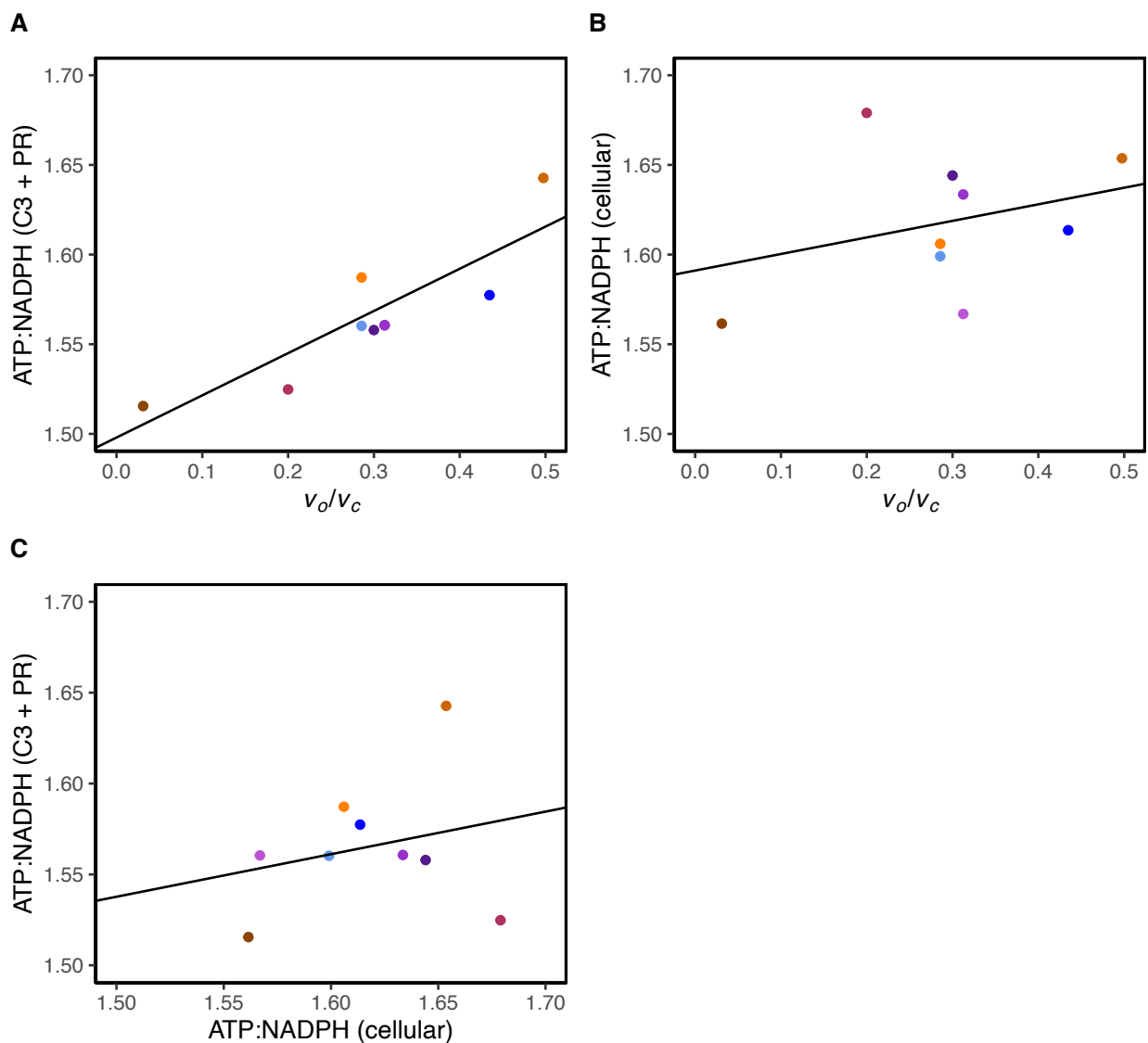


Figure 1.5. The contribution of the C3 cycle and photorespiration in determining cellular ATP:NADPH demand. First, A) the relationship between the ATP:NADPH demand from the C3 cycle and photorespiration and v_o/v_c ($r^2 = 0.74$, $p < 0.05$, linear regression model). Then, B) the relationship between cellular ATP:NADPH and v_o/v_c ($r^2 = 0.10$, $p > 0.05$, linear regression model) and finally between C) the ATP:NADPH demand from the C3 cycle and photorespiration and cellular ATP:NADPH demand ($r^2 = 0.06$, $p > 0.05$, linear regression model). The solid black lines represent the results of the results of the linear regression models.

Species

- Arabidopsis HL
- Camelina 2021
- Camelina LD
- Nicotiana 2% O₂
- Nicotiana 40% O₂
- Arabidopsis LL
- Camelina 2022
- Camelina SD
- Nicotiana 21% O₂

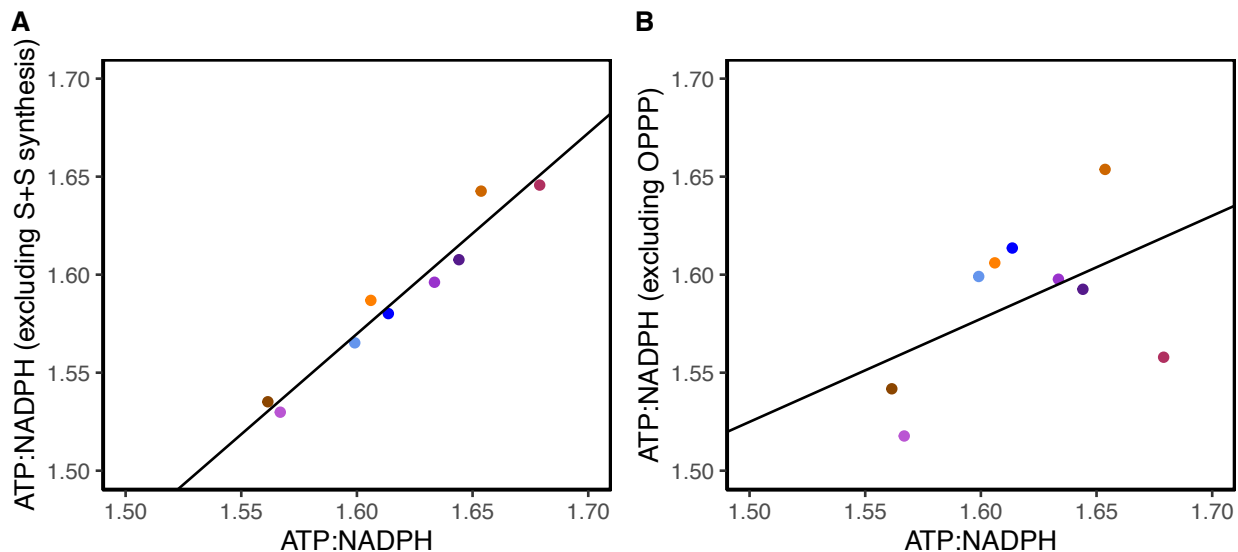


Figure 1.6. The removal of metabolic pathways to evaluate their contribution towards the cellular ATP:NADPH. First, removal of A) starch and sucrose (S+S) synthesis ($r^2 = 0.95$, $p < 0.05$, linear regression model) and B) the OPPP ($r^2 = 0.25$, $p > 0.05$, linear regression model) to evaluate their contribution in determining cellular ATP:NADPH demand. The solid black lines represent the results of the results of the linear regression models.

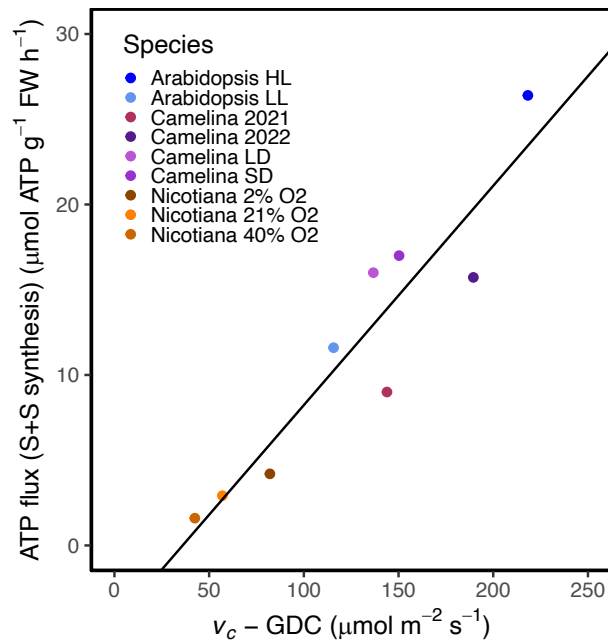


Figure 1.7. The relationship between ATP flux through starch and sucrose synthesis and the net carbon fixed. Shown is the relationship between the ATP flux through starch and sucrose synthesis (S+S) and the net carbon fixed as calculated by the rate of rubisco carboxylation (v_c) minus the flux through the glycine decarboxylase complex (GDC). ATP flux through starch and sucrose synthesis was found by taking the absolute value of the sum of the ATP flux through each ATP consuming reaction in starch and sucrose synthesis for every data set. The solid black line displays the results of the linear regression model ($r^2 = 0.25$, $p > 0.05$).

LITERATURE CITED

- ALLEN, J. F. 2003. Cyclic, pseudocyclic and noncyclic photophosphorylation: new links in the chain. *Trends in Plant Science*, 8, 15-19.
- ASADA, K. 1999. The water-water cycle in chloroplasts: scavenging of active oxygens and dissipation of excess photons. *Annual review of plant biology*, 50, 601-639.
- BASLER, G., KÜKEN, A., FERNIE, A. R. & NIKOLOSKI, Z. 2016. Photorespiratory bypasses lead to increased growth in *Arabidopsis thaliana*: are predictions consistent with experimental evidence? *Frontiers in bioengineering and biotechnology*, 4, 31.
- BOCKWOLDT, M., HEILAND, I. & FISCHER, K. 2019. The evolution of the plastid phosphate translocator family. *Planta*, 250, 245-261.
- BUSCH, F. A., SAGE, R. F. & FARQUHAR, G. D. 2018. Plants increase CO₂ uptake by assimilating nitrogen via the photorespiratory pathway. *Nature plants*, 4, 46-54.
- EDWARDS, G. & WALKER, D. 1983. *C Three C Four: Mechanisms, Cellular and Environmental Regulation of Photosynthesis*, Univ of California Press.
- FU, X., GREGORY, L. M., WEISE, S. E. & WALKER, B. J. 2023. Integrated flux and pool size analysis in plant central metabolism reveals unique roles of glycine and serine during photorespiration. *Nature Plants*, 9, 169-178.
- HANGARTER, R. P. & GOOD, N. E. 1982. Energy thresholds for ATP synthesis in chloroplasts. *Biochimica et Biophysica Acta (BBA)-Bioenergetics*, 681, 397-404.
- HARLEY, P. C. & SHARKEY, T. D. 1991. An improved model of C₃ photosynthesis at high CO₂: reversed O₂ sensitivity explained by lack of glycerate reentry into the chloroplast. *Photosynthesis Research*, 27, 169-178.
- JAZMIN, L. J., O'GRADY, J. P., MA, F., ALLEN, D. K., MORGAN, J. A. & YOUNG, J. D. 2014. Isotopically nonstationary MFA (INST-MFA) of autotrophic metabolism. *Methods Mol Biol*, 1090, 181-210.
- KEBEISH, R., NIESSEN, M., THIRUVEEDHI, K., BARI, R., HIRSCH, H.-J., ROSENKRANZ, R., STÄBLER, N., SCHÖNFELD, B., KREUZALER, F. & PETERHÄNSEL, C. 2007. Chloroplastic photorespiratory bypass increases photosynthesis and biomass production in *Arabidopsis thaliana*. *Nature biotechnology*, 25, 593-599.
- KIIRATS, O., CRUZ, J. A., EDWARDS, G. E. & KRAMER, D. M. 2009. Feedback limitation of photosynthesis at high CO₂ acts by modulating the activity of the chloroplast ATP synthase. *Functional Plant Biology*, 36, 893-901.
- KRAMER, D. M. & EVANS, J. R. 2011. The importance of energy balance in improving photosynthetic productivity. *Plant Physiol*, 155, 70-8.

- LI, J., TIETZ, S., CRUZ, J. A., STRAND, D. D., XU, Y., CHEN, J., KRAMER, D. M. & HU, J. 2019. Photometric screens identified Arabidopsis peroxisome proteins that impact photosynthesis under dynamic light conditions. *The Plant Journal*, 97, 460-474.
- LIVINGSTON, A. K., CRUZ, J. A., KOHZUMA, K., DHINGRA, A. & KRAMER, D. M. 2010. An Arabidopsis mutant with high cyclic electron flow around photosystem I (hcef) involving the NADPH dehydrogenase complex. *Plant Cell*, 22, 221-33.
- MA, F., JAZMIN, L. J., YOUNG, J. D. & ALLEN, D. K. 2017. Isotopically Nonstationary Metabolic Flux Analysis (INST-MFA) of Photosynthesis and Photorespiration in Plants. *Methods Mol Biol*, 1653, 167-194.
- MCCLAIN, A. M. & SHARKEY, T. D. 2019. Triose phosphate utilization and beyond: from photosynthesis to end product synthesis. *Journal of Experimental Botany*, 70, 1755-1766.
- MCCLAIN, A. M. & SHARKEY, T. D. 2023. Rapid CO₂ changes cause oscillations in photosynthesis that implicate PSI acceptor-side limitations. *Journal of Experimental Botany*, 74, 3163-3173.
- NOCTOR, G. & FOYER, C. H. 1998. A re-evaluation of the ATP :NADPH budget during C₃ photosynthesis: a contribution from nitrate assimilation and its associated respiratory activity? *Journal of Experimental Botany*, 49, 1895-1908.
- NGUYEN-QUOC, B. & FOYER, C. H. 2001. A role for 'futile cycles' involving invertase and sucrose synthase in sucrose metabolism of tomato fruit. *Journal of Experimental Botany*, 52, 881-889.
- PETERHANSEL, C., BLUME, C. & OFFERMANN, S. 2013a. Photorespiratory bypasses: how can they work? *J Exp Bot*, 64, 709-15.
- PETERHANSEL, C., KRAUSE, K., BRAUN, H. P., ESPIE, G. S., FERNIE, A. R., HANSON, D. T., KEECH, O., MAURINO, V. G., MIELEWCZIK, M. & SAGE, R. F. 2013b. Engineering photorespiration: current state and future possibilities. *Plant Biol (Stuttg)*, 15, 754-8.
- RAGHAVENDRA, A. S., REUMANN, S. & HELDT, H. W. 1998. Participation of mitochondrial metabolism in photorespiration. Reconstituted system of peroxisomes and mitochondria from spinach leaves. *Plant Physiol*, 116, 1333-7.
- SALERNO, G. L. & CURATTI, L. 2003. Origin of sucrose metabolism in higher plants: when, how and why? *Trends in plant science*, 8, 63-69.
- SCHEIBE, R. 2004. Malate valves to balance cellular energy supply. *Physiologia plantarum*, 120, 21-26.
- SHARKEY, T. D. 1988. Estimating the rate of photorespiration in leaves. *Physiologia Plantarum*, 73, 147-152.

- SHARKEY, T. D., BERRY, J. A. & RASCHKE, K. 1985. Starch and Sucrose Synthesis in *Phaseolus vulgaris* as Affected by Light, CO₂, and Abscisic Acid. *Plant Physiol*, 77, 617-20.
- SHARKEY, T. D. 2024. The end game(s) of photosynthetic carbon metabolism. *Plant Physiology*.
- SMITH, K., STRAND, D. D., KRAMER, D. M. & WALKER, B. J. 2023. The role of photorespiration in preventing feedback regulation via ATP synthase in *Nicotiana tabacum*. *Plant, Cell & Environment*.
- SOUTH, P. F., CAVANAGH, A. P., LIU, H. W. & ORT, D. R. 2019. Synthetic glycolate metabolism pathways stimulate crop growth and productivity in the field. *Science*, 363, eaat9077.
- STRAND, D. D., FISHER, N. & KRAMER, D. M. 2017. The higher plant plastid NAD(P)H dehydrogenase-like complex (NDH) is a high efficiency proton pump that increases ATP production by cyclic electron flow. *J Biol Chem*, 292, 11850-11860.
- STRAND, D. D. & WALKER, B. J. 2023. Energetic considerations for engineering novel biochemistries in photosynthetic organisms. *Front Plant Sci*, 14, 1116812.
- STREB, S. & ZEEMAN, S. C. 2012. Starch metabolism in *Arabidopsis*. *Arabidopsis Book*, 10, e0160.
- WALKER, B. J., KRAMER, D. M., FISHER, N. & FU, X. 2020. Flexibility in the energy balancing network of photosynthesis enables safe operation under changing environmental conditions. *Plants*, 9, 301.
- WALKER, B. J., STRAND, D. D., KRAMER, D. M. & COUSINS, A. B. 2014. The Response of Cyclic Electron Flow around Photosystem I to Changes in Photorespiration and Nitrate Assimilation. *Plant Physiology*, 165, 453-462.
- WALKER, B. J., VANLOOKE, A., BERNACCHI, C. J. & ORT, D. R. 2016. The Costs of Photorespiration to Food Production Now and in the Future. *Annu Rev Plant Biol*, 67, 107-29.
- WIELOCH, T., AUGUSTI, A. & SCHLEUCHER, J. 2023. A model of photosynthetic CO₂ assimilation in C₃ leaves accounting for respiration and energy recycling by the plastidial oxidative pentose phosphate pathway. *New Phytologist*, 239, 518-532.
- XU, Y., FU, X., SHARKEY, T. D., SHACHAR-HILL, Y., WALKER & J, B. 2021. The metabolic origins of non-photorespiratory CO₂ release during photosynthesis: a metabolic flux analysis. *Plant Physiology*, 186, 297-314.
- XU, Y., KOROMA, A. A., WEISE, S. E., FU, X., SHARKEY, T. D. & SHACHAR-HILL, Y. 2023. Daylength variation affects growth, photosynthesis, leaf metabolism, partitioning, and metabolic fluxes. *Plant Physiology*, 194, 475-490.

XU, Y., WIELOCH, T., KASTE, J. A. M., SHACHAR-HILL, Y. & SHARKEY, T. D. 2022. Reimport of carbon from cytosolic and vacuolar sugar pools into the Calvin–Benson cycle explains photosynthesis labeling anomalies. *Proceedings of the National Academy of Sciences*, 119, e2121531119.

ZHANG, Y. & FERNIE, A. R. 2018. On the role of the tricarboxylic acid cycle in plant productivity. *Journal of Integrative Plant Biology*, 60, 1199-1216.

APPENDIX

Carbon assimilated photosynthetically through the C₃ cycle is either used in the formation of starch in the chloroplast or is exported to the cytosol for synthesis of sucrose (Sharkey, 2024). More specifically, the triose phosphates exported from the C₃ cycle may be used for either the synthesis of ADP-glucose in the chloroplast for starch synthesis or translocated to the cytosol for sucrose synthesis. Both processes consume ATP making them energetically important pathways and the specifics of the ATP consumption of both pathways will be described below.

Starch is a complex polysaccharide consisting of two glucose polymers and represents the most significant carbon reserve in plants (Streb and Zeeman, 2012). The first committed step of starch biosynthesis is the formation of ADP-glucose from triose phosphates exported from the C₃ cycle and occurs in the chloroplast. The triose phosphates exported from the C₃ cycle are converted to glucose-1-phosphate where the enzyme ADP-glucose pyrophosphorylase can then catalyze the formation of ADP-glucose from ATP and glucose-1-phosphate. The ADP-glucose is then used for starch elongation. Overall, starch biosynthesis in plants is a complex process which requires one ATP molecule for each hexose added.

Sucrose is a disaccharide consisting of a fructosyl and glucosyl moiety which plays several central roles (Salerno and Curatti, 2003). Triose phosphates from the C₃ cycle are transported from the cytosol via the triose phosphate translocator for sucrose biosynthesis (Bockwoldt et al., 2019). These triose phosphates are then converted to fructose-1,6-bisphosphate by the action of adolase and then to fructose-6-phosphate by fructose diphosphatase. The fructose-6-phosphate is then converted to glucose-6-phosphate and subsequently glucose-1-phosphate by hexose phosphate isomerase and phosphoglucomutase,

respectively. Glucose-1-phosphate is then converted to UDP-glucose by UDP-glucose pyrophosphorylase and requires one molecule of UTP which is energetically equivalent to one molecule of ATP. UDP-glucose is then converted to sucrose. Ultimately, sucrose biosynthesis requires one ATP molecule for each sucrose produced.

The ATP demand associated with starch synthesis can increase from the continuous synthesis and degradation of sucrose in a process referred to as sucrose cycling (Nguyen-Quoc and Foyer, 2001). Sucrose cycling involves the breakdown of sucrose into fructose and glucose and subsequent synthesis back into sucrose. First, sucrose can be hydrolyzed by invertase to form fructose and glucose. The fructose can then be converted back to fructose-6-phosphate by fructokinase which requires one molecule of ATP. The sucrose molecule can be converted to glucose and then to glucose-6-phosphate by hexokinase also requiring one molecule of ATP. The fructose-6-phosphate and glucose-6-phosphate formed can then ultimately be converted back to sucrose requiring two ATP. Therefore, one cycle through sucrose cycling would require four total ATP which would substantially increase the ATP demand associated with sucrose biosynthesis.

CHAPTER 2:

The role of photorespiration in preventing feedback regulation via ATP synthase in

Nicotiana tabacum

Kaila Smith, Deserah D. Strand, David M. Kramer and Berkley J. Walker

Modified from Smith K, Strand DD, Kramer DM, Walker BJ (2024). The role of photorespiration in preventing feedback regulation via ATP synthase in *Nicotiana tabacum*. *Plant Cell Environ.* 47(2):416-428. DOI: 10.1111/pce.14759.

Abstract

Photorespiration consumes substantial amounts of energy in the forms of ATP and reductant making the pathway an important component in leaf energetics. Because of this high reductant demand, photorespiration is proposed to act as a photoprotective electron sink. However, photorespiration consumes more ATP relative to reductant than the C3 cycle meaning increased flux disproportionately increases ATP demand relative to reductant. Here we explore how energetic consumption from photorespiration impacts the flexibility of the light reactions in *Nicotiana tabacum*. Specifically, we demonstrate that decreased photosynthetic efficiency (ϕ_{II}) at low photorespiratory flux was related to feedback regulation at the chloroplast ATP synthase. Additionally, decreased ϕ_{II} at high photorespiratory flux resulted in the accumulation of photoinhibition at PSII centers. These results are contrary to the proposed role of photorespiration as a photoprotective electron sink. Instead, our results suggest a novel role of ATP consumption from photorespiration in maintaining ATP synthase activity, with implications for maintaining energy balance and preventing photodamage that will be critical for plant engineering strategies.

Introduction

Photorespiration is a metabolic pathway in plants which consumes ATP and reductant (NADPH, NADH, and ferredoxin) and releases previously fixed carbon as CO₂. Photorespiration occurs as a result of the oxygenation of ribulose-1,5-bisphosphate at rubisco producing 2-phosphoglycolate which through the photorespiration pathway is partially recycled back into the C3 cycle. These energetic costs and CO₂ release make photorespiration an attractive target for improving crop productivity by reducing carbon loss and redirecting energy flux into yield-limiting metabolism. Several strategies to re-engineer the photorespiratory pathway have already

been implemented in plants, each which are expected to alter plant energetics (Kebeish et al., 2007, Maier et al., 2012, South et al., 2019). Given the large energy flux consumed by photorespiration (30-40% in an illuminated leaf), it is important to understand how it interacts with leaf bioenergetics to optimize efforts to reengineer carbon fixation and to understand how any engineering strategy requiring energy from the chloroplast might impact photosynthesis. One proposed function of photorespiration regarding leaf energetics is to dissipate “excess” photochemical energy produced in excess of that which can be consumed by CO₂ assimilation, thus acting a photoprotective mechanism (Walker et al., 2016, Sharkey, 1988, Osei-Bonsu et al., 2021, Guan and Gu, 2009). However, substantial rates of photorespiration are not necessary for plant growth given the recovery of photorespiratory mutants at high CO₂ as well as the existence of C4 plants which maintain minimal photorespiration due to biochemical carbon concentrating mechanisms indicating that any protective effort would be most significant when CO₂ is limiting (Timm et al., 2012, Somerville and Ogren, 1980, Kennedy, 1976). If this is the case, would re-engineered photorespiratory pathways that abolish or reduce this energy sink be detrimental to the photosynthetic electron transport machinery? This is a core question we examine in this work through the lens of energy balancing.

To avoid damage to the photosynthetic apparatus, plants must balance the energy from harvested light with the energy demand of central metabolism (Walker et al., 2020, Kramer and Evans, 2011). Harvested light energy is converted to chemical energy in the form of ATP and NADPH using the thylakoid electron transport chain. Linear electron flow (LEF) through the thylakoid electron transport chain is coupled to proton translocation into the lumen by water splitting, plastoquinone reduction and protonation at photosystem II (PSII), and plastoquinol oxidation and deprotonation at the cytochrome *bf* (*bf*) complex [reviewed in (Eberhard et al.,

2008)]. The accumulation of protons in the lumen, coupled with electron flux generates a protonmotive force (*pmf*), which provides the energy to drive ATP synthesis at chloroplast F₀F₁ ATP synthase. After plastoquinol oxidation, electrons are passed from the *bf* complex to plastocyanin, photosystem I (PSI), ferredoxin (Fd) and finally to NADPH (Kramer et al., 2004a). This ATP and NADPH then primarily powers the C3 cycle or photorespiration where the relative stoichiometry of demand must match that of the light reactions to prevent metabolic congestion through substrate limitations, which in turn can lead to downregulation of electron transfer or photodamage (Avenson et al., 2005a, Cruz et al., 2005). For example, depletion of substrates for ATP synthase can limit efflux of protons from the lumen, resulting in increased *pmf* that, in turn, controls electron transfer by slowing oxidation of plastoquinol at the *bf* complex and activating the pH dependent *q_E* (energy dependent quenching) form of nonphotochemical quenching (NPQ). Activation of *q_E* can then prevent the accumulation of reactive electron transfer intermediates which can lead to photodamage of PSII and PSI and can limit efficiency (Muller et al., 2001, Takizawa et al., 2007, Takizawa et al., 2008).

LEF alone is constrained to produce a stoichiometry of ATP:NADPH of ~1.33 whereas the C3 cycle demands 1.5 ATP:NADPH, ultimately introducing an ATP deficit between these two processes (Kramer and Evans, 2011). Further, the value of 1.5 increases as flux increases through the photorespiratory pathway. For example, the pathway of photorespiration has an energy demand of 1.75 ATP:NADPH on a marginal basis (Fu and Walker, 2022, Noctor and Foyer, 1998). However, this actual demand stoichiometry would change when rates of CO₂ loss from photorespiration outpace rates of gross carbon uptake and require anaplerotic uptake of carbon would need to compensate. Thus the practical limit of the ATP:NADPH demand ratio determined without having to account for the anaplerotic source of additional carbon would be determined at

the CO₂ compensation point where ratio of rubisco carboxylation (v_c) and oxygenation rate (v_o) would be close to 0.5 which results in an ATP:NADPH ratio of ~1.67. Therefore, in the photosynthetic cells of C3 leaves, when net CO₂ uptake is occurring but photorespiration is also active, the ATP:NADPH ratio required by carbon assimilation is likely to be somewhere between 1.5 and 1.67, with the exact value depending on the carboxylation to oxygenation ratio in response to environmental conditions. Several alternative pathways have been proposed to supplement an ATP deficit in the chloroplast (*e.g.* cyclic electron flow, the “malate valve”, and the Mehler-Asada reaction, also known as the water-water cycle) [reviewed in (Scheibe, 2004, Miyake, 2010, Kramer and Evans, 2011)]. However, an ATP deficit may not always be the case since environment, development, or synthetic pathways may actually lead to an ATP surplus in the chloroplast (Strand and Walker, 2023). Despite many proposed mechanisms for balancing the chloroplast energy supply and demand, it is still somewhat unclear how dynamic these responses are *in vivo*.

Here, we examine the *in vivo* flexibility of the light reactions to downstream metabolic changes in ATP:NADPH demand by manipulating flux through photorespiration by altering oxygen availability. In this work, low photorespiratory flux decreased photosynthetic efficiency (ϕ_{II}) which we attributed to increased feedback regulation at ATP synthase. We propose this to be from insufficient ATP consumption generating a substrate limitation under a period of ATP surplus (*i.e.*, a deficit of NADPH relative to ATP). Additionally, ϕ_{II} decreased under high photorespiratory flux, possibly from the accumulation of photoinhibition, contrary to the proposed role of photorespiration as a photoprotective electron sink.

Materials and methods

Plant material and growth

Nicotiana tabacum (c.v. petit Havana) was grown in soil in a growth chamber with a photoperiod of 18 hours ($\sim 100 \mu\text{mol photons m}^{-2} \text{ s}^{-1}$) and 6 hours of darkness. *Nicotiana tabacum* (c.v. SNN) and ATPC1 antisense lines were grown in soil in a growth chamber with a photoperiod of 16 hours ($\sim 100 \mu\text{mol photons m}^{-2} \text{ s}^{-1}$) and 8 hours of darkness. Plants were fertilized weekly with a quarter strength Hoagland solution until measurements. All experiments were performed on intact, fully expanded leaves between 17-19 cm long.

Gas exchange measurements

Both steady-state and net assimilation (A) in response to intercellular CO_2 ($A\text{-}C_i$) were measured using gas exchange on the youngest, fully expanded leaves using a LI-6800 with a 3 x 3 cm measuring head (LI-COR Biosciences, Lincoln, Nebraska, USA) at $1000 \mu\text{mol photons m}^{-2} \text{ s}^{-1}$. Altered O_2 concentrations (2%, 21%, or 40%) were provided using a mass flow controller which entered the auxiliary air inlet of the LI-6800 with appropriate band-broadening corrections for the infra-red gas analyzers to account for the altered O_2 background. During all gas exchange measurements, leaf temperature was maintained at 25°C and vapor pressure deficit was controlled at $1.2 \text{ kPa H}_2\text{O}$. Steady-state assimilation was measured once the leaf reached a stable level of A and stomatal conductance under each O_2 concentration after 30 min. To estimate biochemical limitations to A from an $A\text{-}C_i$ curves under limited photorespiration, assimilation was measured as a function of intercellular CO_2 (C_i) under 2% O_2 . The curve was fit to calculate the rubisco, RuBP-regeneration, and triose-phosphate utilization (TPU) limitations using the msuRACiFit package in RStudio (Gregory et al., 2021). The fit used the values of $2.001 \mu\text{mol m}^{-2} \text{ s}^{-1} \text{ Pa}^{-1}$, $0.653 \mu\text{mol m}^{-2} \text{ s}^{-1}$, and 4.044 Pa , for mesophyll conductance (g_m) respiration in the

light (R_l), and CO_2 compensation point in the absence of R_l (Γ^*) which were determined previously for *Nicotiana tabacum* grown under the identical conditions and the same growth chamber (Fu et al., 2023).

Calculating ATP:NADPH demand

ATP:NADPH demand was estimated based on A values measured under the steady state for each O_2 concentration and the intercellular CO_2 concentration (C_i) using the following equations (Walker et al., 2020, Farquhar et al., 1980).

$$A = v_c - 0.5v_o - R_l \quad (1)$$

$$v_c = \frac{A + R_l}{1 - \frac{\Gamma^*}{C_c}} \quad (2)$$

$$v_o = \frac{v_c - A - R_l}{0.5} \quad (3)$$

$$C_c = C_i - \frac{A}{g_m} \quad (4)$$

To estimate the rubisco carboxylation (v_c) and oxygenation rate (v_o), from A , Equation (1) can be expressed in terms of v_c (2) to then solve for v_o (3). For these calculations, Equation (4) converts the concentration of CO_2 in the intercellular airspace (C_i) to the partial pressure of CO_2 at the site of rubisco (C_c). Finally, both the NADPH and ATP demand were calculated by multiplying the energy requirements for the C3 cycle and photorespiration (PR below) by the respective carboxylation or oxygenation rates and combining these values (Sharkey, 1988).

$$\text{ATP demand from the C3 cycle and PR} = 3v_c + 3.5v_o \quad (5)$$

$$\text{NADPH demand from the C3 cycle and PR} = 2v_c + 2v_o \quad (6)$$

In Vivo spectroscopic assays

All spectroscopic measurements were made using intact fully expanded leaves as outlined above. O₂ concentrations (2%, 21%, or 40%) were obtained using a mass flow controller system feeding into a LI-6400 XT (LI-COR Biosciences, Lincoln, Nebraska, USA) which mixed in 400 ppm CO₂. The resulting gas mixture was then fed into the leaf cuvette of an in-house constructed integrated diode emitter array spectrophotometer (Hall et al., 2013, Kanazawa et al., 2017) to measure steady-state chlorophyll *a* fluorescence and electrochromic shift (ECS) parameters. Plants were dark adapted for 30 min prior to experiments. Actinic light intensities ranged between 100 - 850 μmol photons m⁻² s⁻¹ and the plants were illuminated for 12 min at each individual intensity to reach a steady state, and then dark adapted for 12 min to allow for the relaxation of *q_E*. Saturation pulse parameters were calculated from a multiphase flash, and used to calculate φ_{II}, LEF, NPQ, *q_E*, and *q_I* as previously described (Baker, 2008, Loriaux et al., 2013). LEF was calculated as

$$\text{LEF} = \phi_{II} * i * 0.43 \quad (7)$$

where *i* is the actinic light intensity.

To examine the impact of changing photorespiratory flux on the proton circuit, we took advantage of the ECS of membrane-embedded pigments. The peak of this shift occurs around 520 nm in higher plants (Witt, 1974, Witt, 1979). The relative extent of the *pmf* is measured from the total amplitude of this absorbance shift (ECS_{*t*}) during a 300 ms dark interval after steady state illumination (Sacksteder and Kramer, 2000). The initial slope of the ECS decay during a dark interval is relative to the rate of transthylakoid proton flux (ν_{H⁺}). The first order rate constant of the ECS decay reflects the rate constant of transthylakoid efflux, or proton conductivity of the thylakoid membrane (g_{H⁺}) and was determined by fitting the ECS decay to a

first order exponential. The contribution of LEF to pmf (pmf_{LEF}) was calculated as described previously (Avenson et al., 2005b).

Statistical analysis

Curve fitting, statistical analysis, and graphing were performed in R (dplyr and ggplot2 packages) and python (SciPy package). All p values less than 0.05 were considered significant and denoted in the figure legends.

Results

High photorespiratory flux increased the ATP:NADPH demand from the C3 cycle and photorespiration

Assimilation (A) was measured under saturating light conditions ($1000 \mu\text{mol photons m}^{-2} \text{s}^{-1}$) under 2% O_2 (low photorespiratory flux), 21% O_2 (normal photorespiratory flux), and 40% O_2 (high photorespiratory flux). v_o increased with O_2 concentrations while v_c did not significantly change (Figure 2.1A and B). As expected, A decreased as O_2 increased (Figure 2.1C). Decreased v_c and A in with increased v_o demonstrates the redistribution of flux through photorespiration as O_2 increases.

Theoretically, ATP:NADPH demand should increase as the relative rates of photorespiration increase given its differential energy demands. Because rubisco carboxylation and oxygenation constrain ATP and NADPH through central metabolism, v_o and v_c can be used to estimate total ATP and NADPH demand from the C3 cycle and photorespiration specifically (Huma et al., 2018, Walker et al., 2020). The estimated ratios of ATP:NADPH demands from the C3 cycle and photorespiration increased significantly as v_o increased relative to v_c , consistent with a higher relative ATP demand for photorespiration (Figure 2.1D, $p < 0.05$, one-way ANOVA, Tukey's post-hoc test). Since the C3 cycle and photorespiration comprise the bulk of energy

demand, these relative overall trends will persist, although the absolute values will depend on other energy-consuming processes that occur at lower rates the metabolic as discussed further below.

High CO₂ is often considered to have similar effects as decreasing O₂ on suppressing photorespiration. However, v_o was ~5 fold smaller when photorespiration was suppressed by 2% O₂ compared to increasing CO₂ to 1000 Pa (Figure 2.2A, $p < 0.05$, one-way ANOVA, Tukey's post-hoc test). Consequently, the ATP:NADPH demand from the C3 cycle and photorespiration also decreased under 2% O₂ compared to 1000 Pa CO₂ indicating CO₂ and O₂ changes are not equivalent for suppressing photorespiration and ATP:NADPH demand (Figure 2.2B, $p < 0.05$, one-way ANOVA, Tukey's post-hoc test). This difference can be explained at least partially by the differences in the O₂:CO₂ ratios of these treatments. Another confounding variable when considering using high CO₂ for suppressing photorespiration is that high CO₂ can also impose triose-phosphate utilization (TPU) limitations, which occur when free P_i is limiting due to restricted cycling of phosphorylated intermediates of carbon fixation and would possibly confound the perceived response of the light reactions of photosynthesis to changes in photorespiratory ATP:NADPH demand measured below (Kiirats et al., 2009). To determine if 2% O₂ was TPU limiting under near ambient CO₂ concentrations, we measured assimilation as a function of intercellular CO₂ (A/C_i) to estimate the biochemical limitations to carbon assimilation at our highest experimental light intensity. These results show that at 40 Pa CO₂ (approximately 34.8 C_c Pa) the leaf was not TPU limited under 2% O₂ (Figure 2.3). This was only measured at 2% O₂ to confirm that TPU was not limiting under the conditions which also appeared to have differential ATP synthase activity (discussed below).

Altering flux through photorespiration decreased photosynthetic efficiency driven by different forms of NPQ

We next sought to understand the impact of altered photorespiratory flux has on light-driven proton and electron transport in the thylakoid. Changes in metabolism can lead to altered photosynthetic efficiency (ϕ_{II}) due to changes in the feedback regulation of light harvesting or PSII acceptor side limitations and may impact electron transfer rates (Kanazawa and Kramer, 2002, Walker et al., 2014). Under 2% and 40% O₂, ϕ_{II} decreased relative to ambient (21%) which resulted into a decreased rate of LEF (Figure 2.4A and B). The effects of O₂ were dependent on PAR, with decreased LEF apparent as low as $\sim 200 \mu\text{mol of photons m}^{-2} \text{ s}^{-1}$ under 40% O₂ and $\sim 400 \mu\text{mol of photons m}^{-2} \text{ s}^{-1}$ under 2% O₂.

The decreased ϕ_{II} observed under both high and low O₂ were surprising from an energy-balancing perspective given that they displayed opposite changes in ATP:NADPH demand. We thus looked to identify the underlying causes of the altered ϕ_{II} . First, we tested if ϕ_{II} was modulated through either a change in the redox state of the acceptor side of PSII (i.e., Q_A-redox state) and/or in increased dissipation of absorbed light energy through NPQ (Kanazawa and Kramer, 2002). Under both high and low O₂, the redox state of the plastoquinone pool (estimated by the 1-qL parameter) was more reduced compared to ambient (Figure 2.4C) (Kramer et al., 2004b). Changing O₂ from ambient also resulted in increased NPQ with the highest amount of total NPQ, with the largest increase at 2% O₂ (Figure 2.4D). However, when NPQ was partitioned into its components under 2% O₂, the increased NPQ compared to ambient O₂ was comprised mainly of q_E , with a minimal contribution from the photoinhibition-related q_I form (Muller et al., 2001) (Figure 2.5). By contrast, under 40% O₂, the situation was reversed, with q_I comprising a larger fraction relative to q_E . The difference in NPQ partitioning indicates responses

by the electron transport chain to O₂ content leading to decreased ϕ_{II} were strongly dependent on gas composition.

We also see that O₂ content changes the accumulation of NPQ components independent from electron flux (Figure A2.1A and B). Under both 2% and 40 % O₂ q_E increased as a function of LEF, with 2% O₂ having the largest impact (Figure A2.1A). Under 40% O₂, q_I increased whereas q_L decreased under 2% O₂ indicating accumulation of the quenchers independent of total electron flux (Figure A2.1B). While both 2% and 40% O₂ have slightly more reduced plastiquinone pools than 21%, this reductions in 2% O₂ seems to be stronger at higher light excitation pressure and LEF (A2.1C). In Figure A2.1D, we see that under 2% O₂, despite lower rates of LEF, we have increased total pmf (as measured by ECS_{*t*}), while the 40% O₂ treatment does not deviate from the ambient O₂ relationship.

Low photorespiratory flux introduced feedback regulation via ATP synthase

In the absence of any other changes in the system, increased pmf should have resulted in increased lumen acidification and stronger activation of q_E . We therefore hypothesized that the increased q_E at 2% O₂ was due to increased lumen acidification associated with an increase in thylakoid pmf . Consistent with this model, the ECS_{*t*} signal, a measure of the light-induced thylakoid pmf (see Methods), was higher under 2% O₂ beginning at 200 $\mu\text{mol photon m}^{-2} \text{s}^{-1}$ and is most obvious at 400 $\mu\text{mol photons m}^{-2} \text{s}^{-1}$ (Figure 2.6A). In contrast, ECS_{*t*} decreased under 40% O₂ starting at 400 $\mu\text{mol photons m}^{-2} \text{s}^{-1}$ and became more prominently lower at 1000 $\mu\text{mol photons m}^{-2} \text{s}^{-1}$. Total pmf can increase either from an increase in transthylakoid proton flux (v_{H^+}) or from a decrease in transthylakoid proton conductivity (g_{H^+}), which is mostly attributable to ATP synthase activity. Figure 2.6B shows that the O₂-dependence of the g_{H^+} parameter.

Specifically, we found a decrease g_{H^+} under 2% O₂ which suggests that the corresponding observed increase in *pmf* can indeed be explained by decreased g_{H^+} .

Because ATP synthase is sensitive to downstream metabolic demand, we hypothesized that under 2% O₂, there was a metabolic factor leading to downregulation of the complex. This effect could arise from the lowering of the ATP:NADPH demand from metabolism and subsequent substrate limitation of ADP or Pi. To test this possibility, we examined the O₂-dependence of the g_{H^+} parameter in an ATPC1 antisense line (ATPC1) (Rott et al., 2011). These tobacco plants accumulate ~12% of wild type ATP synthase complexes, leading to low assimilation rates and decreased growth. These plants are severely limited in their capacity for electron transport to supply assimilation and photorespiration, therefore, should not become limited by their capacity to consume ATP or NADPH. Figure 2.7 shows the response of ATPC1 and its wild type tobacco background (SNN) to 21% and 2% O₂. In SNN, 2% O₂ leads to a decrease in g_{H^+} , similar to the petit Havana ecotype shown above. In ATPC1, there is no change in g_{H^+} , suggesting that when the ability to supply ATP is limited, the regulatory signal for ATP synthase downregulation is also missing.

The impact of this missing signal is also seen when comparing the changes of the photosynthetic circuit as a function of LEF in the ATPC1 plants. In the SNN (wild type) plants, we see changes in the NPQ components q_E and q_I in response to low O₂ similar to how the Petit Havana plants respond (Figure A2.1-2). Much like the Petit Havana plants, the q_E component of NPQ is more sensitive to LEF at 2% O₂ and q_I accumulates to lower levels for a given rate of LEF at 2% (Figure A2.2A-B). Interestingly, the decreased LEF/1- q_L relationship at higher excitation pressure seen under 2% O₂ is more pronounced in the SNN ecotype than Petit Havana (Figure A2.2C). Total *pmf* (as measured by ECS_i) is also increased relative to LEF under 2% O₂

(Figure A2.2D). When we perform the same experiments in the ATPC1 plants, we see little to no differences between the 2% and 21% O₂ conditions, except for the q_I /LEF relationship, further supporting the interpretation of a downstream metabolic signal impacting ATP synthase activity (Figure A2.3).

These results support that 2% O₂ increased q_E due to an increase in total pmf , however, there are other factors that may influence q_E independently, some of which involve the membrane-embedded proteins PsBS and violaxanthin de-epoxidase (VDE). These proteins respond to the ΔpH component of pmf and additionally VDE is proposed to be redox regulated, therefore, changes in q_E can also arise from changes in the relative contribution of ΔpH to total pmf and/or changes in the redox state of the stroma (Baier and Dietz, 2005, Hall et al., 2008). Increasing or decreasing O₂ concentration from ambient increased the sensitivity of q_E to total ECS_{*t*} (seen by the increase in slope in Figure 2.8), suggesting that there may be other changes in addition to g_{H^+} that contribute to the q_E .

Photoinhibition increased under high photorespiratory flux

As described above, under elevated (40%) O₂ q_I comprised a larger fraction of NPQ relative to q_E (Figure 2.5B). The regulatory q_E component of NPQ acts as a photoprotective process by limiting the amount of excitation energy received by the light harvesting complexes of PSII to prevent photodamage. The q_I component of NPQ is the slowly reversible quenching that leads to long term downregulation of photosynthesis and is most often associated with photodamage of PSII reaction centers (Krause, 1988, Demmig-Adams and Adams III, 2006). At 2% O₂, there is less q_I than what is present at ambient O₂. However, a larger fraction of q_I accumulated at 40% O₂, despite similar levels of q_E as ambient O₂ (Figure 2.5A-B). The increase

of q_I with photorespiratory flux and decreased q_E at 2% does not support the proposed role of photorespiration as a photoprotective electron sink.

In ATPC1 q_E remained constant in response to 2% O₂, further supporting the hypothesis that the changes in q_E are predominantly from changes in g_H^+ (Figure 2.9A). The absence of decreased g_H^+ under 2% O₂ allows us the opportunity to test the direct role of O₂ on q_I on q_E . Most oftentimes q_E regulates light harvesting to prevent photoinhibition during excess light (Li et al., 2002). Surprisingly, q_I still decreased at 2% O₂ compared to 21% O₂ despite no changes in q_E (Figure 2.9A-B). While, ATPC1 has higher q_I and higher q_E in general compared to the wild type this is consistent with what has been observed with ATP synthase mutants (Davis et al., 2016). Despite no changes in q_E 2% O₂ changes q_I still increased supporting that in the case of changing O₂ changes in q_I are independent of q_E and likely independent of photorespiratory flux as previously suggested (Heber et al., 1996).

CEF is not activated under altered photorespiratory flux

Due to the increased ATP:NADPH demand from increased flux through photorespiration, we hypothesized that exposure to 40% O₂ would activate cyclic electron flow (CEF), a route of alternative electron transfer that provides extra ATP without producing NADPH (Bendall and Manasse, 1995, Strand et al., 2016b). To test our hypothesis, we utilized two estimates of the relative contributions of CEF including plots of v_H^+ against LEF and the extents of pmf estimated by ECS_{*t*} that calculated for contribution LEF alone (pmf_{LEF}) (Avenson et al., 2005a). Surprisingly, both showed no clear differences under the different O₂ levels, suggesting that activation of CEF played a minimal roles in compensating for altered ATP:NADPH demand (Figure 2.10A-B).

Discussion

This work reveals the response of the light reactions that supply ATP and NADPH to changes in demand from the C3 cycle and photorespiration. Overall, with decreased photorespiration there was short term inflexibility in the light reactions as indicated by the feedback regulation via ATP synthase. The feedback regulation via ATP synthase likely occurred as a result of the non-relaxation of alternative routes of electron transfer. This non (or slow)-relaxation may create a temporary ATP surplus when the additional ATP consumption from photorespiration is removed.

Alternative electron transport other than CEF may be meeting the short-term energetic demands for photorespiration

Due to the increased ATP:NADPH demand of photorespiration over that of the C3 cycle, we hypothesized that we would see dynamic flexibility in meeting these demands in the chloroplast. The chloroplast has many possible routes of alternative electron transfer to augment an ATP deficit. We hypothesized that out of these many routes, CEF would respond to photorespiratory flux (Strand et al., 2016a). We expected an increase in CEF under 40% O₂ to meet the higher ATP:NADPH demand and a decrease in CEF under 2% to meet the lower demand. Instead, the *in vivo* assays for CEF indicated no substantial changes in the relative rates of electron transfer from CEF (Figure 2.10A-B). While there may be small changes in CEF outside the measurable range of the instrumentation, we suggest instead that alternative processes are modulated to balance the chloroplast supply with demand on the short term. This lack of activation of CEF in response to altered ATP demands was surprising given its strong association with balancing the energy budget of the chloroplast and the finding that it changes as

expected from an energy balancing perspective during changes in CO₂ concentrations (Walker et al., 2014). However, the regulation of CEF is complex.

One route of CEF, the photosynthetic complex I has multiple levels of regulation, part of which involves synthesis of chloroplast and nuclear encoded genes which may lead to slower activation of CEF (Strand et al., 2015, Lascano et al., 2003a, Lascano et al., 2003b). Since CEF through the photosynthetic complex I is the route of CEF most often associated with a stress response *in vivo*, the activation of CEF through this pathway may be an acclimatory response if the plants were subjected to sustained periods of altered photorespiratory flux (Strand et al., 2015). The lack of CEF activation instead argues that other alternative electron transport pathways, such as the malate valve, may be more involved in supplying a dynamic ATP deficit.

It is possible the effect of altered O₂ may influence alternative electron transport pathways such as the Mehler-Asada reaction. The activity of the Mehler-Asada reaction in angiosperms is currently debated with values for C3 plants varying between less than 1% to 10% of total linear electron flux. As the Mehler-Asada reaction reduces O₂ to produce H₂O₂, it is reasonable to expect that reducing or increasing O₂ concentration from 21% might scale the Mehler-Asada reaction accordingly. Such an increased into flux in the Mehler-Asada reaction would increase production of reactive oxygen species within the chloroplast and might explain the higher proportion of q_l observed (Figure 2.5B). However, there is evidence the Mehler-Asada reaction along with stromal redox regulation does not scale significantly with O₂ concentration (Ruuska et al., 2000, Nakamoto and Edwards, 1983).

ATP consumption from photorespiration prevents feedback regulation from ATP synthase

Perhaps the most interesting result from this work is the downregulation of ATP synthase in response to decreased (2%) O₂. Changes in g_{H^+} have been shown to arise from redox regulation and metabolic limitations and additionally proposed to be in response to phosphorylation on certain ATP synthase subunits (Hisabori et al., 2002, Kohzuma et al., 2013, Wu et al., 2007). Decreased g_{H^+} had previously been reported in starchless mutants at 2% O₂ and proposed to be related to substrate limitation caused by inability to produce free P_i in the stroma during TPU limitation resulting from reduced triose-phosphate utilization or export (Kierats et al., 2009, McClain et al., 2023). This “classic” TPU limitation results in decreased *A*. Under 2% O₂ *A* increases, however, photosynthetic efficiency decreases, suggesting that there may be unrealized potential due to limitations on the electron transport chain. After demonstrating the low g_{H^+} under 2% O₂ is linked to a metabolic change and this metabolic change is not classic TPU limitation, the question arises as to what metabolic change leads to the downregulation of ATP synthase (Figure 2.3, 2.6B).

We propose after relaxing an ATP deficit (in this case a shift from 21% to 2% O₂) the plant doesn't relax an alternative ATP generating pathway(s) and is unable to turnover this excess ATP which leads to substrate limitation of ATP synthase. This substrate limitation leads to feedback regulation of light harvesting and electron transfer from the buildup of protons in the lumen. Ultimately, it might be that photorespiration acts as an ATP consuming pathway to maintain a pool of substrate for ATP synthase.

The feedback regulation via ATP synthase under the ATP:NADPH demand at 2% is evidence that the chloroplast is not always experiencing an ATP deficit and in some cases an ATP surplus (Kramer and Evans, 2011). Evolutionary pressure for energy balancing may have been

primarily for ATP deficit conditions, creating more pathways to address a deficit rather than a surplus. An ATP surplus could be addressed through identified ATP/ADP+P_i transporters, but their contribution to chloroplast energetics isn't clear (Voon et al., 2018, Heldt, 1969).

Additionally, it is unknown if the plant is able to eventually acclimate to lower ATP:NADPH demand by activating ATP export or deactivating alternative pathways of ATP generation.

While this interpretation relies on estimates of ATP:NADPH demand solely from the C₃ cycle and photorespiration, they still illustrate the relative overall trend that occurs when photorespiration is increased. More specifically, ATP:NADPH demand values might be impacted by other metabolic processes which both consume energy and are linked to photorespiration such as nitrate assimilation and starch and sucrose biosynthesis. Nitrate assimilation, which consumes reductant, has been proposed to increase with photorespiration, however, this likely occurs on a longer scale than utilized in this study (Rachmilevitch et al., 2004). The measurements in this study occurred in a time scale shorter than two hours, after two hours of exposure to low CO₂ nitrate reductase activity does not change likely due to the ability to export nitrate out of the vacuole for at least two hours after nitrate deprivation (Kaiser et al., 2000). Additionally, changes in nitrate assimilation and therefore the accompanying energy demands are relatively small compared to LEF. For example, measured rates demonstrate that nitrate assimilation is 5-10% that of CO₂ assimilation, and work illustrating a decrease in nitrate assimilation following multiple hours under 2% O₂ relative to 21% shows only a 0-50%, meaning the effects on total LEF demand will still be small (Bloom et al., 2010). Other ATP consuming processes such as starch and sucrose biosynthesis decrease as photorespiration increases, however, their flux changes are still an order of magnitude less than the changes in photorespiratory fluxes (Fu et al., 2023). Therefore, while ATP consumption from starch and sucrose biosynthesis may increase the

ATP demand in both the 2% and 21% O₂ conditions, this increase is not expected to be substantial enough to change our interpretations.

While our data strongly supports photorespiration acting as an ATP consuming pathway to maintain a pool of substrate for ATP synthase, measurements of chloroplastic ATP:ADP pools would provide critical validation of our hypothesis. The genetically encoded FRET would be one *in vivo* approach but are complicated by the need to measure mature leaves under both actinic light and different O₂ concentrations (Lim et al., 2020). Other measurements using *in vitro* methods are technically challenging due to fast turnover times, the use of ATP throughout the entire cell, and difficulty in isolating intact, but metabolically inactive chloroplasts from whole leaf tissues (Arrivault et al., 2009).

Photoinhibition increased under high photorespiratory flux contrary to the proposed role as a photoprotective electron sink

The downregulation of ATP synthase at 2% O₂ strongly supports the idea of photorespiration as an ATP consuming pathway in addition to an electron sink, allowing the chloroplast to avoid substrate limitations on ATP synthase. This idea contradicts the function of photorespiration as photoprotective, usually inferred by increases in total NPQ (Guan and Gu, 2009, Hendrickson et al., 2003). When we separate NPQ into the components kinetically (q_I and q_E), we show higher photorespiratory flux led to an increased accumulation of the slow relaxing component, q_I , and low photorespiratory flux led to an increase in faster relaxing component, q_E , which would not be expected if photorespiration provided the often cited critical photoprotective electron sink (Figure 2.5A-B). Increased q_E at 2% O₂ could be interpreted as protective against accumulation of q_I , however, at 21% and 40% O₂ q_E levels are indistinguishable at the highest light intensity and the 40% O₂ treatment leads to increased q_I . Additionally, q_E is insensitive to O₂

in ATPC1, but q_l was not (Figure 2.9A-B). These data suggest sensitivity of q_l directly to O_2 concentration, and not metabolism, as previously proposed in (Heber et al., 1996). While in this study our data are not conclusive on the general photoprotective capacity of photorespiration, our results do not support the pathway as a photoprotective electron sink.

Considerations for metabolic engineering

The function of photorespiration in preventing feedback regulation via ATP synthase presents an important consideration for plant engineering strategies specifically targeted towards improving the efficiency of photorespiration. This work demonstrates that attempts to re-engineer photorespiration might result in inflexibility in the light reactions which are not sufficient to maintain optimum electron transport rates. Additionally, because ATP synthase is a central regulator of the photosynthetic electron transport chain, maintaining appropriate feedback regulation of this complex is important to optimally balance photosynthetic efficiency with photoprotection. This is especially important under dynamic conditions such as those encountered under field conditions where energy demand changes rapidly (Slattery et al., 2018, Suorsa et al., 2012). If an engineering strategy for photorespiration introduces an increased electron sink relative to ATP demand, native ATP-consuming processes may not be sufficient and result in down-regulation of photosynthetic efficiency (Strand and Walker, 2023). However, there may be yet unknown longer term acclimatory responses the plant could use to meet new synthetic energy demands.

Figures and Tables

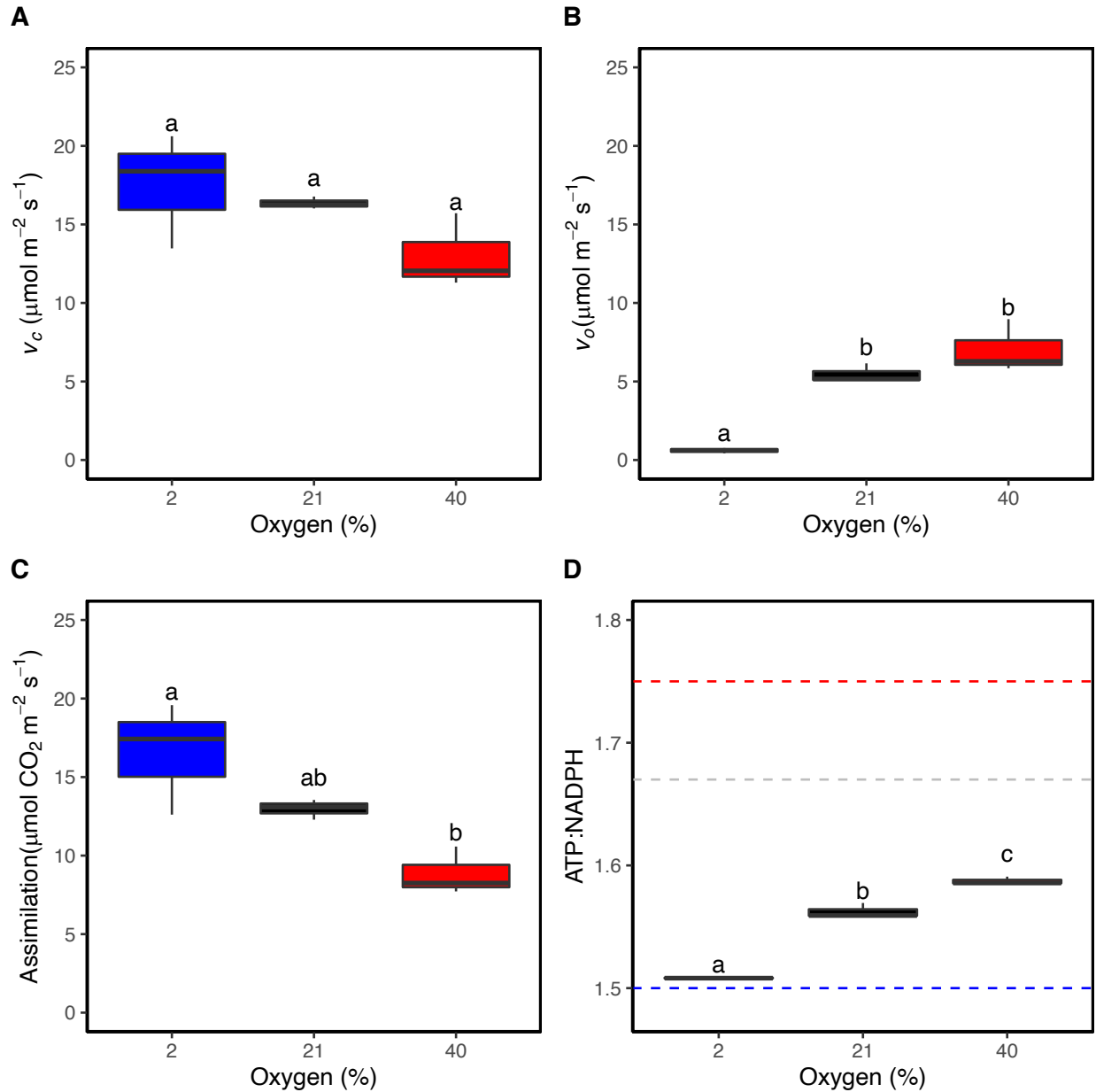


Figure 2.1. Response of net photosynthesis to altered oxygen concentration. Represented by A) rubisco carboxylation (v_c) B) rubisco oxygenation (v_o) C) net assimilation and D) estimated ATP:NADPH demands from the C3 cycle and photorespiration (PR above). The red and blue dashed line represents the energy demand of the photorespiratory and C3 cycle pathways, respectively. The gray dashed line represents the likely ATP:NADPH ratio at the photorespiratory CO_2 compensation point. Plants were measured at $1000 \mu\text{mol photons m}^{-2} \text{ s}^{-1}$ at 2%, 21%, and 40% O_2 with 400 ppm CO_2 . ATP:NADPH demand were calculated using v_c and v_o and the energy requirements for photorespiration. Shown are the means \pm SD ($n = 3$). Different letters denote statistically significant differences among O_2 concentrations ($p < 0.05$, one-way ANOVA, Tukey's post-hoc test).

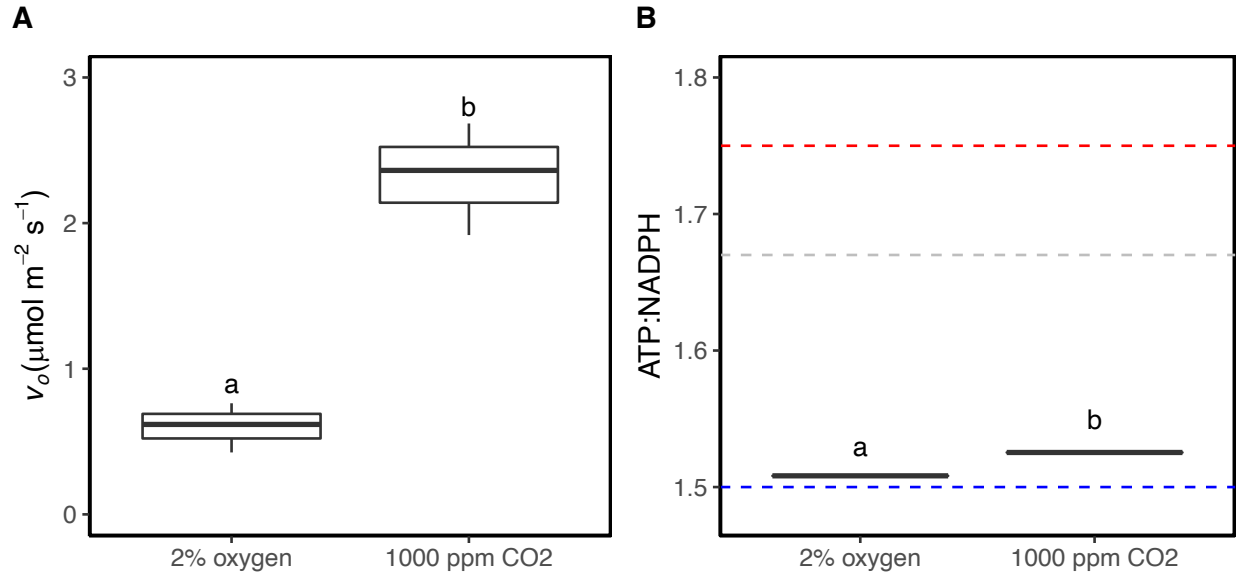


Figure 2.2. Comparison between different photorespiratory treatments. Displayed is the comparison of the amount of suppression of A) rubisco oxygenation (v_o) and B) estimated ATP:NADPH demands from the C₃ cycle and photorespiration (PR above). The red and blue dashed line represents the energy demand of the photorespiratory and C₃ cycle pathways, respectively. The gray dashed line represents the likely ATP:NADPH ratio at the photorespiratory CO₂ compensation point. Plants were measured at 1000 $\mu\text{mol photons m}^{-2} \text{s}^{-1}$ either at 2% O₂ and 400 ppm CO₂ or 21% O₂ and 1000 ppm CO₂. ATP:NADPH demand were calculated using v_c and v_o and the energy requirements for photorespiration. Shown are the means \pm SD ($n = 3$). Different letters denote statistically significant differences among O₂ concentrations ($p < 0.05$, one-way ANOVA, Tukey's post-hoc test).

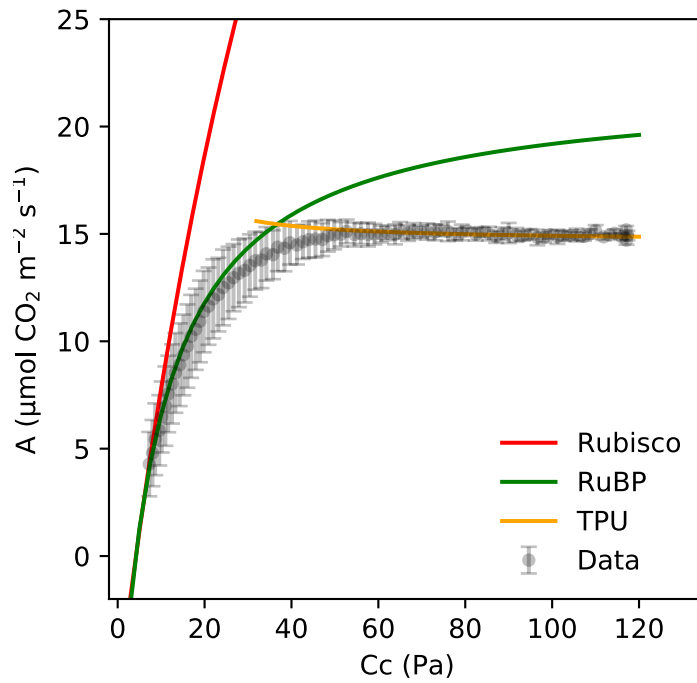


Figure 2.3. Assimilation as a function of C_c (Pa) for calculation of biochemical limitations. Plants were measured at 2% O_2 . Biochemical limitations were fitted for rubisco (red), RuBP-regeneration (blue), and TPU (yellow). Shown are the means \pm SD ($n = 3$).

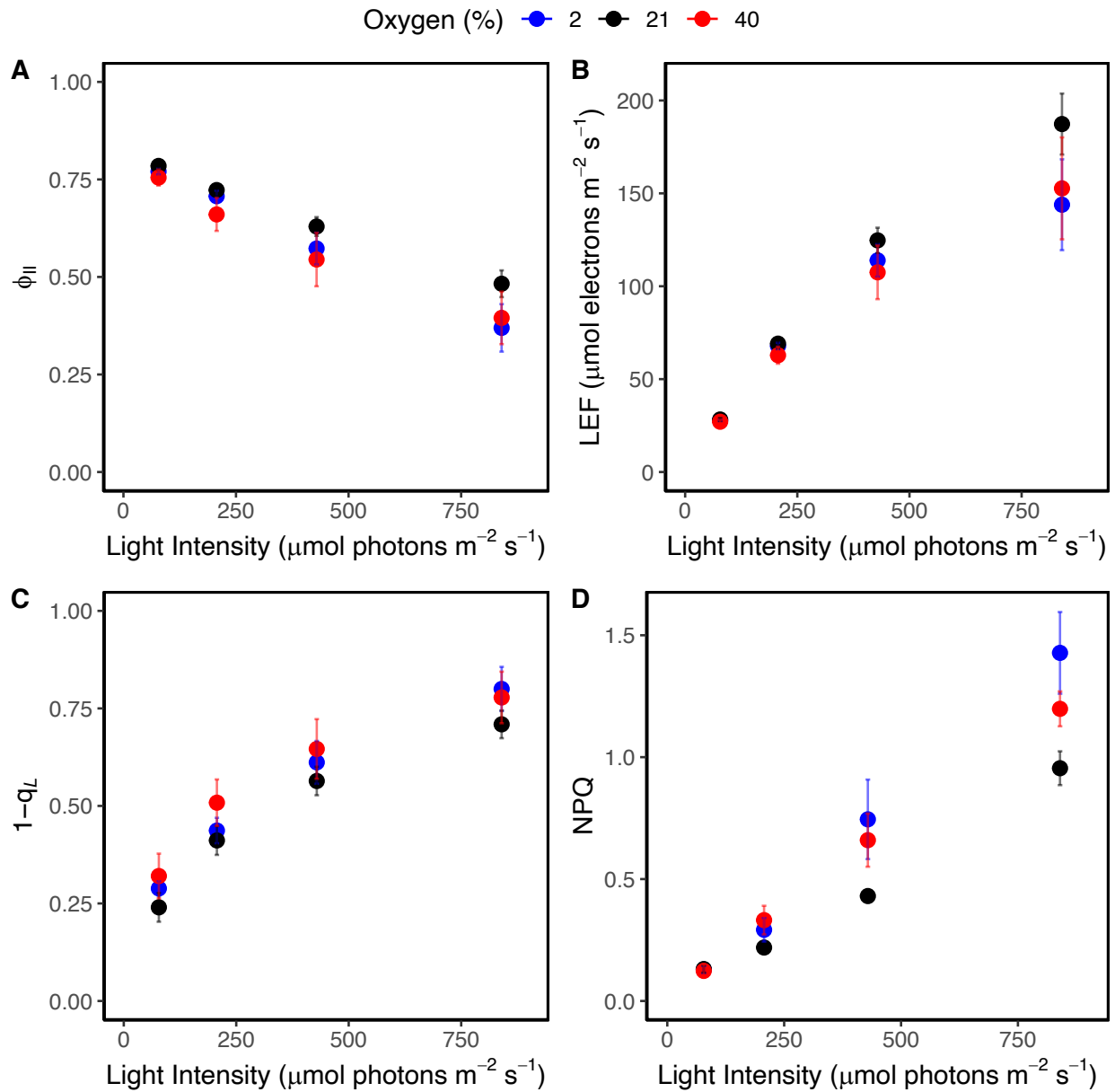


Figure 2.4. The response of the light reactions to altered photorespiratory flux. A) Changes in photosynthetic efficiency (ϕ_{II}) B) linear electron transport (LEF) C) the plastoquinone redox state ($1-q_L$) and D) nonphotochemical quenching (NPQ). Plants were measured at 2%, 21%, and 40% O_2 with 400 ppm CO_2 as a steady state function of light intensity. Shown are the means \pm SD ($n = 4$).

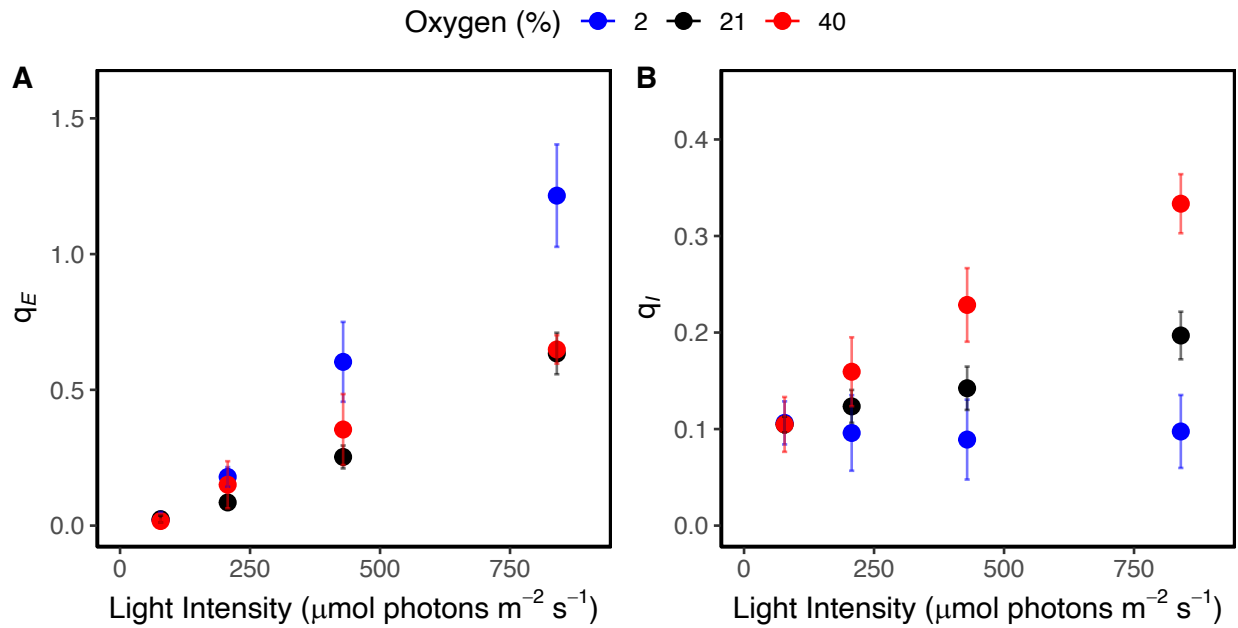


Figure 2.5. Changes in NPQ components in response to altered photorespiratory poise. A) The extent of the rapidly reversible pH dependent component of NPQ (q_E) and B) the long-lived component of NPQ (q_I). Plants were measured at 2%, 21%, and 40% O_2 with 400 ppm CO_2 as a steady state function of light intensity. Shown are the means \pm SD ($n = 4$).

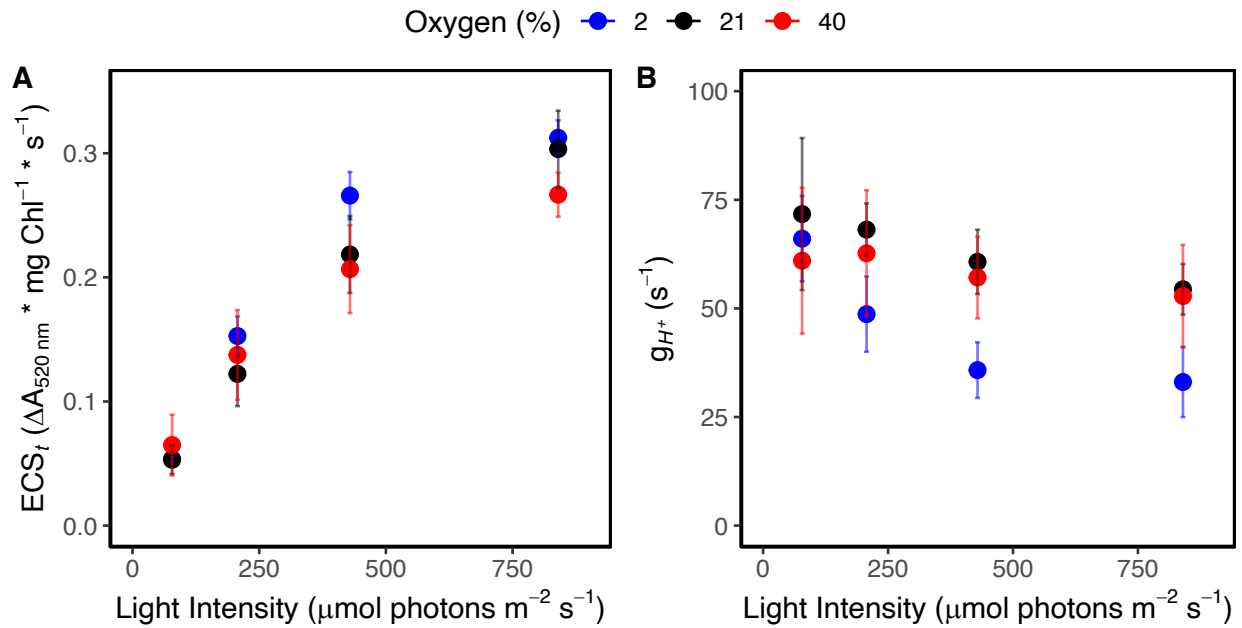


Figure 2.6. The response of the proton circuit to altered photorespiratory flux. A) The total extent of *pmf* (as measured by ECS_t) and B) the response of ATP synthase kinetics as measured by the rate constant of transthylakoid proton efflux (g_{H^+}). Plants were measured at 2%, 21%, and 40% O_2 with 400 ppm CO_2 as a steady state function of light intensity. Shown are the means \pm SD ($n = 4$).

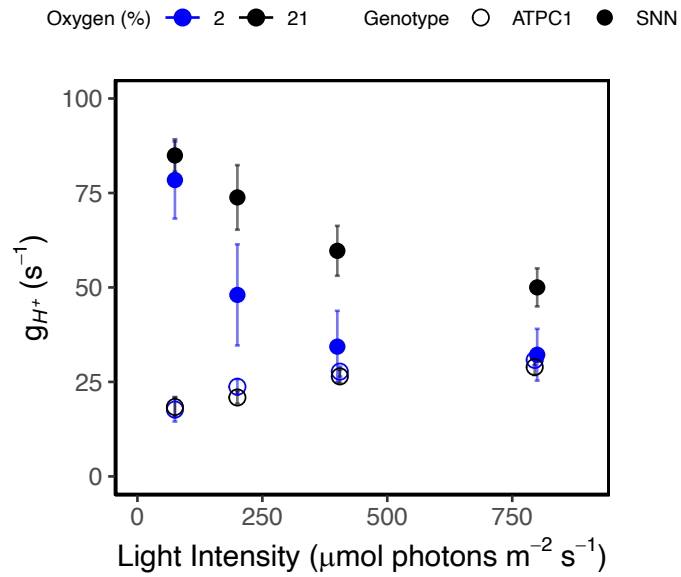


Figure 2.7. Comparison of ATP synthase conductivity (g_{H^+}) in response to decreased O_2 in ATPC1 antisense lines. ATPC1 antisense lines were compared to their background (c.v. SNN). Plants were measured at 2% and 21% with 400 ppm CO_2 as a steady state function of light intensity. Shown are the means \pm SD (n = 4).

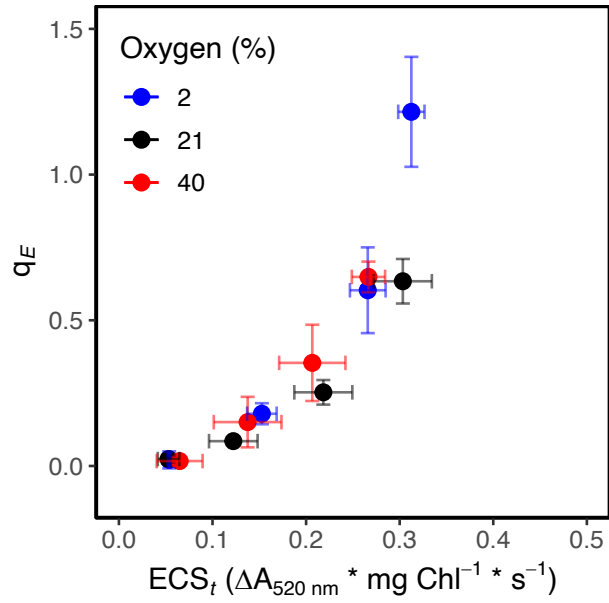


Figure 2.8. Sensitivity of q_E to total ECS_t . Plants were measured at 2%, 21%, and 40% O_2 with 400 ppm CO_2 . Shown are the means \pm SD (n = 4).

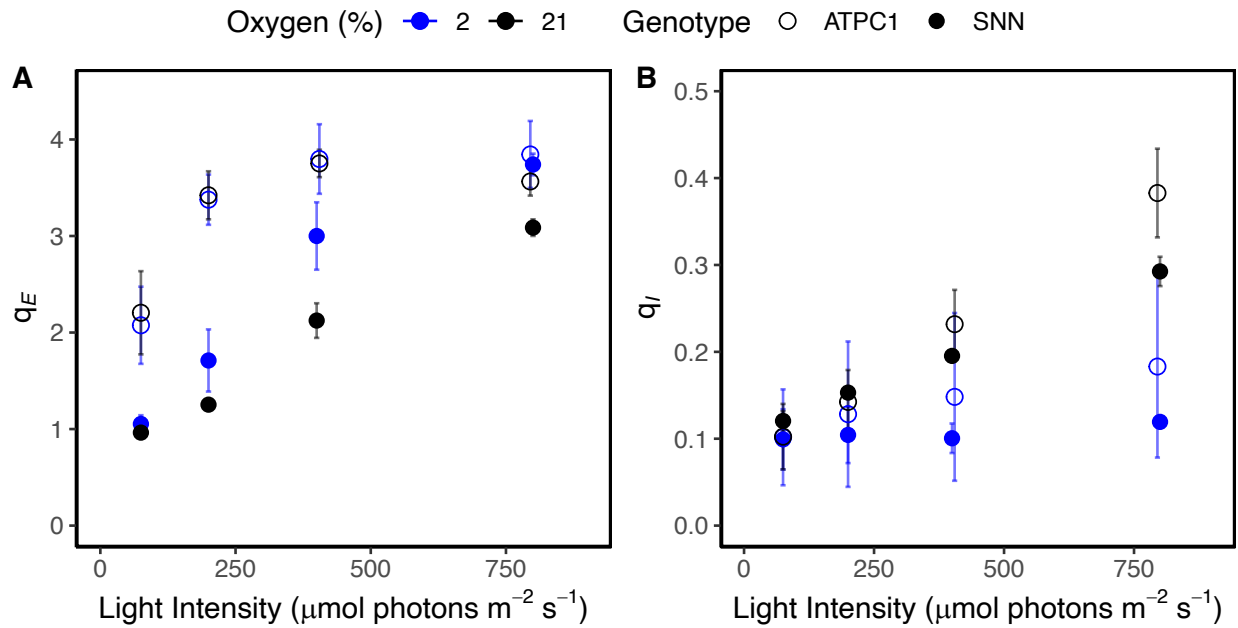


Figure 2.9. Changes in NPQ components in response to altered photorespiratory poise in ATPC1 antisense lines. A) The extent of the rapidly reversible pH dependent component of NPQ (q_E) and B) the long-lived component of NPQ (q_I). ATPC1 antisense lines were compared to their background (c.v. SNN). Plants were measured at 2% and 21% with 400 ppm CO_2 as a steady state function of light intensity. Shown are the means \pm SD ($n = 4$).

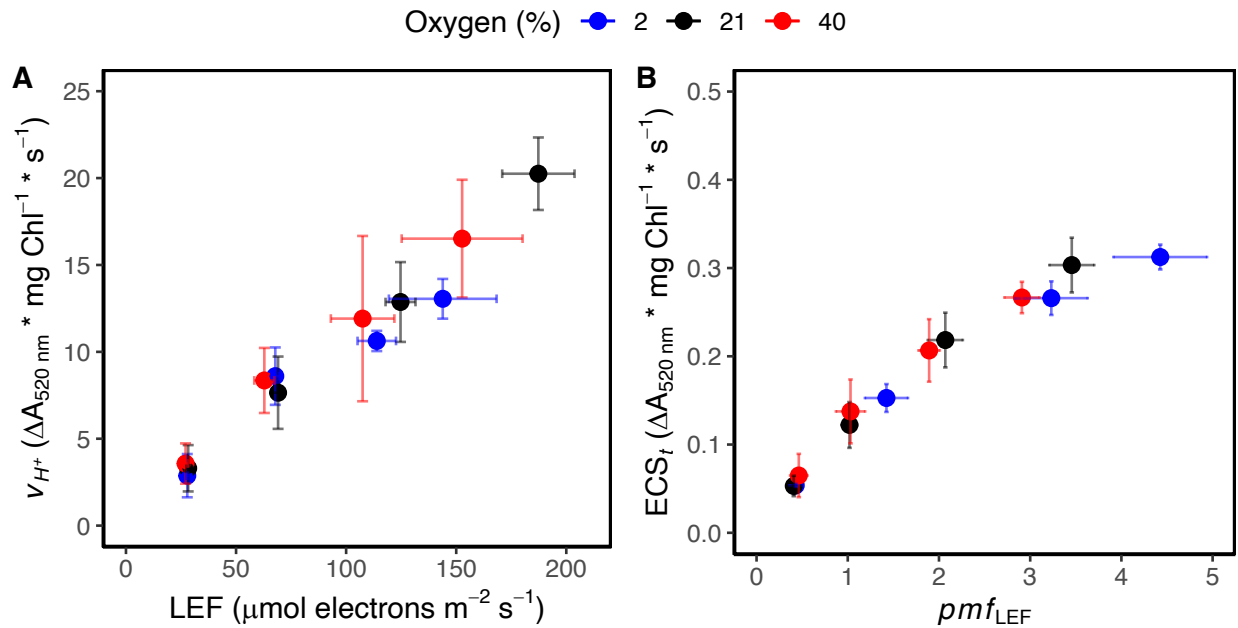


Figure 2.10. Plasticity of cyclic electron flow in response to changes in photorespiratory poise. A) Steady state transthylakoid proton flux (v_{H^+}) as a function of linear electron flow (LEF). B) Total extent of pmf (as measured by ECS_t) as a function of pmf generated from LEF alone (pmf_{LEF}) in the steady state. Plants were measured at 2%, 21%, and 40% O_2 with 400 ppm CO_2 . Shown are the means \pm SD ($n = 4$).

LITERATURE CITED

- ARRIVAUULT, S., GUENTHER, M., IVAKOV, A., FEIL, R., VOSLOH, D., VAN DONGEN, J. T., SULPICE, R. & STITT, M. 2009. Use of reverse-phase liquid chromatography, linked to tandem mass spectrometry, to profile the Calvin cycle and other metabolic intermediates in *Arabidopsis* rosettes at different carbon dioxide concentrations. *The Plant Journal*, 59, 826-839.
- AVENSON, T. J., CRUZ, J. A., KANAZAWA, A. & KRAMER, D. M. 2005a. Regulating the proton budget of higher plant photosynthesis. *Proc Natl Acad Sci U S A*, 102, 9709-13.
- AVENSON, T. J., KANAZAWA, A., CRUZ, J. A., TAKIZAWA, K., ETTINGER, W. E. & KRAMER, D. M. 2005b. Integrating the proton circuit into photosynthesis: progress and challenges. *Plant, Cell & Environment*, 28, 97-109.
- BAIER, M. & DIETZ, K.-J. 2005. Chloroplasts as source and target of cellular redox regulation: a discussion on chloroplast redox signals in the context of plant physiology. *Journal of experimental botany*, 56, 1449-1462.
- BAKER, N. R. 2008. Chlorophyll fluorescence: a probe of photosynthesis in vivo. *Annu. Rev. Plant Biol.*, 59, 89-113.
- BENDALL, D. S. & MANASSE, R. S. 1995. Cyclic photophosphorylation and electron transport. *Biochimica et Biophysica Acta (BBA)-Bioenergetics*, 1229, 23-38.
- BLOOM, A. J., BURGER, M., ASENSIO, J. S. R. & COUSINS, A. B. 2010. Carbon dioxide enrichment inhibits nitrate assimilation in wheat and *Arabidopsis*. *Science*, 328, 899-903.
- CRUZ, J. A., AVENSON, T. J., KANAZAWA, A., TAKIZAWA, K., EDWARDS, G. E. & KRAMER, D. M. 2005. Plasticity in light reactions of photosynthesis for energy production and photoprotection. *Journal of experimental botany*, 56, 395-406.
- DAVIS, G. A., KANAZAWA, A., SCHÖTTLER, M. A., KOHZUMA, K., FROEHLICH, J. E., RUTHERFORD, A. W., SATOH-CRUZ, M., MINHAS, D., TIETZ, S., DHINGRA, A. & KRAMER, D. M. 2016. Limitations to photosynthesis by proton motive force-induced photosystem II photodamage. *eLife*, 5, e16921.
- DEMMIG-ADAMS, B. & ADAMS III, W. W. 2006. Photoprotection in an ecological context: the remarkable complexity of thermal energy dissipation. *New phytologist*, 172, 11-21.
- EBERHARD, S., FINAZZI, G. & WOLLMAN, F. A. 2008. The dynamics of photosynthesis. *Annu Rev Genet*, 42, 463-515.
- FARQUHAR, G. D., VON CAEMMERER, S. & BERRY, J. A. 1980. A biochemical model of photosynthetic CO₂ assimilation in leaves of C₃ species. *Planta*, 149, 78-90.

- FU, X., GREGORY, L. M., WEISE, S. E. & WALKER, B. J. 2023. Integrated flux and pool size analysis in plant central metabolism reveals unique roles of glycine and serine during photorespiration. *Nature Plants*, 9, 169-178.
- FU, X. & WALKER, B. J. 2022. Dynamic Response of Photorespiration in Fluctuating Light Environments. *Journal of Experimental Botany*.
- GREGORY, L. M., MCCLAIN, A. M., KRAMER, D. M., PARDO, J. D., SMITH, K. E., TESSMER, O. L., WALKER, B. J., ZICCARDI, L. G. & SHARKEY, T. D. 2021. The triose phosphate utilization limitation of photosynthetic rate: Out of global models but important for leaf models. *Plant, Cell & Environment*, 44, 3223-3226.
- GUAN, X. & GU, S. 2009. Photorespiration and photoprotection of grapevine (*Vitis vinifera* L. cv. Cabernet Sauvignon) under water stress. *Photosynthetica*, 47, 437-444.
- HALL, C. C., CRUZ, J., WOOD, M., ZEGARAC, R., DEMARS, D., CARPENTER, J., KANAZAWA, A. & KRAMER, D. 2013. Photosynthetic measurements with the idea spec: an integrated diode emitter array spectrophotometer/fluorometer. *Photosynthesis Research for Food, Fuel and the Future*. Springer.
- HALL, M., SCHRÖDER, W. P. & KIESELBACH, T. 2008. Thioredoxin interactions of the chloroplast lumen of *Arabidopsis thaliana* indicate a redox regulation of the Xanthophyll cycle. *Photosynthesis. Energy from the Sun*. Springer.
- HEBER, U., BLIGNY, R., STREB, P. & DOUCE, R. 1996. Photorespiration is essential for the protection of the photosynthetic apparatus of C3 plants against photoinactivation under sunlight. *Botanica Acta*, 109, 307-315.
- HELDT, H. W. 1969. Adenine nucleotide translocation in spinach chloroplasts. *FEBS Lett*, 5, 11-14.
- HENDRICKSON, L., BALL, M. C., OSMOND, C. B., FURBANK, R. T. & CHOW, W. S. 2003. Assessment of photoprotection mechanisms of grapevines at low temperature. *Functional Plant Biology*, 30, 631-642.
- HISABORI, T., KONNO, H., ICHIMURA, H., STROTMANN, H. & BALD, D. 2002. Molecular devices of chloroplast F1-ATP synthase for the regulation. *Biochimica et Biophysica Acta (BBA) - Bioenergetics*, 1555, 140-146.
- HUMA, B., KUNDU, S., POOLMAN, M. G., KRUGER, N. J. & FELL, D. A. 2018. Stoichiometric analysis of the energetics and metabolic impact of photorespiration in C3 plants. *The Plant Journal*, 96, 1228-1241.
- KAISER, W. M., KANDLBINDER, A., STOIMENOVA, M. & GLAAB, J. 2000. Discrepancy between nitrate reduction rates in intact leaves and nitrate reductase activity in leaf extracts: what limits nitrate reduction in situ? *Planta*, 210, 801-807.

- KANAZAWA, A. & KRAMER, D. M. 2002. In vivo modulation of nonphotochemical exciton quenching (NPQ) by regulation of the chloroplast ATP synthase. *Proceedings of the National Academy of Sciences*, 99, 12789-12794.
- KANAZAWA, A., OSTENDORF, E., KOHZUMA, K., HOH, D., STRAND, D. D., SATO-CRUZ, M., SAVAGE, L., CRUZ, J. A., FISHER, N. & FROEHLICH, J. E. 2017. Chloroplast ATP synthase modulation of the thylakoid proton motive force: implications for photosystem I and photosystem II photoprotection. *Frontiers in Plant Science*, 719.
- KEBEISH, R., NIESSEN, M., THIRUVEEDHI, K., BARI, R., HIRSCH, H.-J., ROSENKRANZ, R., STÄBLER, N., SCHÖNFELD, B., KREUZALER, F. & PETERHÄNSEL, C. 2007. Chloroplastic photorespiratory bypass increases photosynthesis and biomass production in *Arabidopsis thaliana*. *Nature biotechnology*, 25, 593-599.
- KENNEDY, R. A. 1976. Photorespiration in C₃ and C₄ plant tissue cultures: significance of Kranz anatomy to low photorespiration in C₄ plants. *Plant physiology*, 58, 573-575.
- KIIRATS, O., CRUZ, J. A., EDWARDS, G. E. & KRAMER, D. M. 2009. Feedback limitation of photosynthesis at high CO₂ acts by modulating the activity of the chloroplast ATP synthase. *Functional Plant Biology*, 36, 893-901.
- KOHZUMA, K., DAL BOSCO, C., MEURER, J. & KRAMER, D. M. 2013. Light- and metabolism-related regulation of the chloroplast ATP synthase has distinct mechanisms and functions. *J Biol Chem*, 288, 13156-63.
- KRAMER, D. M., AVENSON, T. J. & EDWARDS, G. E. 2004a. Dynamic flexibility in the light reactions of photosynthesis governed by both electron and proton transfer reactions. *Trends Plant Sci*, 9, 349-57.
- KRAMER, D. M. & EVANS, J. R. 2011. The importance of energy balance in improving photosynthetic productivity. *Plant Physiol*, 155, 70-8.
- KRAMER, D. M., JOHNSON, G., KIIRATS, O. & EDWARDS, G. E. 2004b. New Fluorescence Parameters for the Determination of QA Redox State and Excitation Energy Fluxes. *Photosynth Res*, 79, 209.
- KRAUSE, G. H. 1988. Photoinhibition of photosynthesis. An evaluation of damaging and protective mechanisms. *Physiologia plantarum*, 74, 566-574.
- LASCANO, H. R., CASANO, L. M., MARTIN, M. & SABATER, B. 2003a. The activity of the chloroplastic Ndh complex is regulated by phosphorylation of the NDH-F subunit. *Plant Physiology*, 132, 256-262.
- LASCANO, H. R., CASANO, L. M., MARTÍN, M. & SABATER, B. 2003b. The Activity of the Chloroplastic Ndh Complex Is Regulated by Phosphorylation of the NDH-F Subunit. *Plant Physiology*, 132, 256-262.

- LI, X.-P., MÜLLER-MOULÉ, P., GILMORE, A. M. & NIYOGI, K. K. 2002. PsbS-dependent enhancement of feedback de-excitation protects photosystem II from photoinhibition. *Proceedings of the National Academy of Sciences*, 99, 15222-15227.
- LIM, S.-L., VOON, C. P., GUAN, X., YANG, Y., GARDESTRÖM, P. & LIM, B. L. 2020. In planta study of photosynthesis and photorespiration using NADPH and NADH/NAD⁺ fluorescent protein sensors. *Nature Communications*, 11, 3238.
- LORIAUX, S., AVENSON, T., WELLES, J., MCDERMITT, D., ECKLES, R., RIENSCHÉ, B. & GENTY, B. 2013. Closing in on maximum yield of chlorophyll fluorescence using a single multiphase flash of sub-saturating intensity. *Plant, cell & environment*, 36, 1755-1770.
- MAIER, A., FAHNENSTICH, H., VON CAEMMERER, S., ENGQVIST, M., WEBER, A., FLUGGE, U. & MAURINO, V. 2012. Glycolate oxidation in *A. thaliana* chloroplasts improves biomass production. *Frontiers in Plant Science*, 3, 38.
- MCCLAIN, A. M., CRUZ, J. A., KRAMER, D. M. & SHARKEY, T. D. 2023. The time course of acclimation to the stress of triose phosphate use limitation. *Plant, Cell & Environment*, 46, 64-75.
- MIYAKE, C. 2010. Alternative electron flows (water–water cycle and cyclic electron flow around PSI) in photosynthesis: molecular mechanisms and physiological functions. *Plant and Cell Physiology*, 51, 1951-1963.
- MITCHELL, P. 1976. Possible molecular mechanisms of the protonmotive function of cytochrome systems. *Journal of theoretical biology*, 62, 327-367.
- MULLER, P., LI, X. P. & NIYOGI, K. K. 2001. Non-photochemical quenching. A response to excess light energy. *Plant Physiol*, 125, 1558-66.
- NAKAMOTO, H. & EDWARDS, G. E. 1983. Influence of Oxygen and Temperature on the Dark Inactivation of Pyruvate, Orthophosphate Dikinase and NADP-Malate Dehydrogenase in Maize. *Plant Physiol*, 71, 568-73.
- NOCTOR, G. & FOYER, C. H. 1998. A re-evaluation of the ATP: NADPH budget during C₃ photosynthesis: a contribution from nitrate assimilation and its associated respiratory activity? *Journal of Experimental Botany*, 49, 1895-1908.
- ORT, D. R. & YOCUM, C. F. 1996. *Oxygenic photosynthesis: the light reactions*, Springer Science & Business Media.
- OSEI-BONSU, I., MCCLAIN, A. M., WALKER, B. J., SHARKEY, T. D. & KRAMER, D. M. 2021. The roles of photorespiration and alternative electron acceptors in the responses of photosynthesis to elevated temperatures in cowpea. *Plant Cell Environ*, 44, 2290-2307.

- RACHMILEVITCH, S., COUSINS, A. B. & BLOOM, A. J. 2004. Nitrate assimilation in plant shoots depends on photorespiration. *Proceedings of the National Academy of Sciences*, 101, 11506-11510.
- ROTT, M., MARTINS, N. F., THIELE, W., LEIN, W., BOCK, R., KRAMER, D. M. & SCHÖTTLER, M. A. 2011. ATP synthase repression in tobacco restricts photosynthetic electron transport, CO₂ assimilation, and plant growth by overacidification of the thylakoid lumen. *Plant Cell*, 23, 304-21.
- RUUSKA, S. A., BADGER, M. R., ANDREWS, T. J. & VON CAEMMERER, S. 2000. Photosynthetic electron sinks in transgenic tobacco with reduced amounts of Rubisco: little evidence for significant Mehler reaction. *Journal of Experimental Botany*, 51, 357-368.
- SACKSTEDER, C. A. & KRAMER, D. M. 2000. Dark-interval relaxation kinetics (DIRK) of absorbance changes as a quantitative probe of steady-state electron transfer. *Photosynthesis research*, 66, 145-158.
- SACKSTEDER, C. A., KANAZAWA, A., JACOBY, M. E. & KRAMER, D. M. 2000. The proton to electron stoichiometry of steady-state photosynthesis in living plants: a proton-pumping Q cycle is continuously engaged. *Proceedings of the National Academy of Sciences*, 97, 14283-14288.
- SCHEIBE, R. 2004. Malate valves to balance cellular energy supply. *Physiologia plantarum*, 120, 21-26.
- SEELERT, H., POETSCH, A., DENCHER, N. A., ENGEL, A., STAHLBERG, H. & MÜLLER, D. J. 2000. Proton-powered turbine of a plant motor. *Nature*, 405, 418-419.
- SHARKEY, T. D. 1988. Estimating the rate of photorespiration in leaves. *Physiologia Plantarum*, 73, 147-152.
- SLATTERY, R. A., WALKER, B. J., WEBER, A. P. & ORT, D. R. 2018. The impacts of fluctuating light on crop performance. *Plant physiology*, 176, 990-1003.
- SOMERVILLE, C. & OGREN, W. 1980. Photorespiration mutants of *Arabidopsis thaliana* deficient in serine-glyoxylate aminotransferase activity. *Proceedings of the National Academy of Sciences*, 77, 2684-2687.
- SOUTH, P. F., CAVANAGH, A. P., LIU, H. W. & ORT, D. R. 2019. Synthetic glycolate metabolism pathways stimulate crop growth and productivity in the field. *Science*, 363, eaat9077.
- STRAND, D. D., FISHER, N., DAVIS, G. A. & KRAMER, D. M. 2016a. Redox regulation of the antimycin A sensitive pathway of cyclic electron flow around photosystem I in higher plant thylakoids. *Biochimica et Biophysica Acta (BBA) - Bioenergetics*, 1857, 1-6.

- STRAND, D. D., FISHER, N. & KRAMER, D. M. 2016b. Distinct energetics and regulatory functions of the two major cyclic electron flow pathways in chloroplasts. *Chloroplasts: Current research and future trends*. Caister Academic Press Poole, UK.
- STRAND, D. D., LIVINGSTON, A. K., SATOH-CRUZ, M., FROEHLICH, J. E., MAURINO, V. G. & KRAMER, D. M. 2015. Activation of cyclic electron flow by hydrogen peroxide in vivo. *Proceedings of the National Academy of Sciences*, 112, 5539-5544.
- STRAND, D. D. & WALKER, B. J. 2023. Energetic considerations for engineering novel biochemistries in photosynthetic organisms. *Front Plant Sci*, 14, 1116812.
- SUORSA, M., JÄRVI, S., GRIECO, M., NURMI, M., PIETRZYKOWSKA, M., RANTALA, M., KANGASJÄRVI, S., PAAKKARINEN, V., TIKKANEN, M. & JANSSON, S. 2012. PROTON GRADIENT REGULATION5 is essential for proper acclimation of Arabidopsis photosystem I to naturally and artificially fluctuating light conditions. *The Plant Cell*, 24, 2934-2948.
- TAKIZAWA, K., KANAZAWA, A., CRUZ, J. & KRAMER, D. 2007. In vivo thylakoid proton motive force. Quantitative non-invasive probes show the relative lumen pH-induced regulatory responses of antenna and electron transfer. *Biochim. Biophys. Acta*, 1767, 1233-1244.
- TAKIZAWA, K., KANAZAWA, A. & KRAMER, D. M. 2008. Depletion of stromal P(i) induces high 'energy-dependent' antenna exciton quenching (q(E)) by decreasing proton conductivity at CF(O)-CF(1) ATP synthase. *Plant Cell Environ*, 31, 235-43.
- TIMM, S., MIELEWCZIK, M., FLORIAN, A., FRANKENBACH, S., DREISSEN, A., HOCKEN, N., FERNIE, A. R., WALTER, A. & BAUWE, H. 2012. High-to-low CO₂ acclimation reveals plasticity of the photorespiratory pathway and indicates regulatory links to cellular metabolism of Arabidopsis.
- VOLLMAR, M., SCHLIEPER, D., WINN, M., BÜCHNER, C. & GROTH, G. 2009. Structure of the c14 rotor ring of the proton translocating chloroplast ATP synthase. *Journal of Biological Chemistry*, 284, 18228-18235.
- VOON, C. P., GUAN, X., SUN, Y., SAHU, A., CHAN, M. N., GARDESTRÖM, P., WAGNER, S., FUCHS, P., NIETZEL, T., VERSAW, W. K., SCHWARZLÄNDER, M. & LIM, B. L. 2018. ATP compartmentation in plastids and cytosol of *Arabidopsis thaliana* revealed by fluorescent protein sensing. *Proceedings of the National Academy of Sciences*, 115, E10778-E10787.
- WALKER, B. J., KRAMER, D. M., FISHER, N. & FU, X. 2020. Flexibility in the energy balancing network of photosynthesis enables safe operation under changing environmental conditions. *Plants*, 9, 301.
- WALKER, B. J., STRAND, D. D., KRAMER, D. M. & COUSINS, A. B. 2014. The Response of Cyclic Electron Flow around Photosystem I to Changes in Photorespiration and Nitrate Assimilation *Plant Physiology*, 165, 453-462.

- WALKER, B. J., VANLOOCKE, A., BERNACCHI, C. J. & ORT, D. R. 2016. The Costs of Photorespiration to Food Production Now and in the Future. *Annu Rev Plant Biol*, 67, 107-29.
- WITT, H. T. 1974. PRIMARY ACTS OF ENERGY CONSERVATION IN THE FUNCTIONAL MEMBRANE OF PHOTOSYNTHESIS. *Annals of the New York Academy of Sciences*, 227.
- WITT, H. T. 1979. Energy conversion in the functional membrane of photosynthesis. Analysis by light pulse and electric pulse methods. The central role of the electric field. *Biochim Biophys Acta*, 505, 355-427.
- WU, G., ORTIZ-FLORES, G., ORTIZ-LOPEZ, A. & ORT, D. R. 2007. A point mutation in atpC1 raises the redox potential of the Arabidopsis chloroplast ATP synthase gamma-subunit regulatory disulfide above the range of thioredoxin modulation. *J Biol Chem*, 282, 36782-9.

APPENDIX A: SUPPLEMENTAL FIGURES

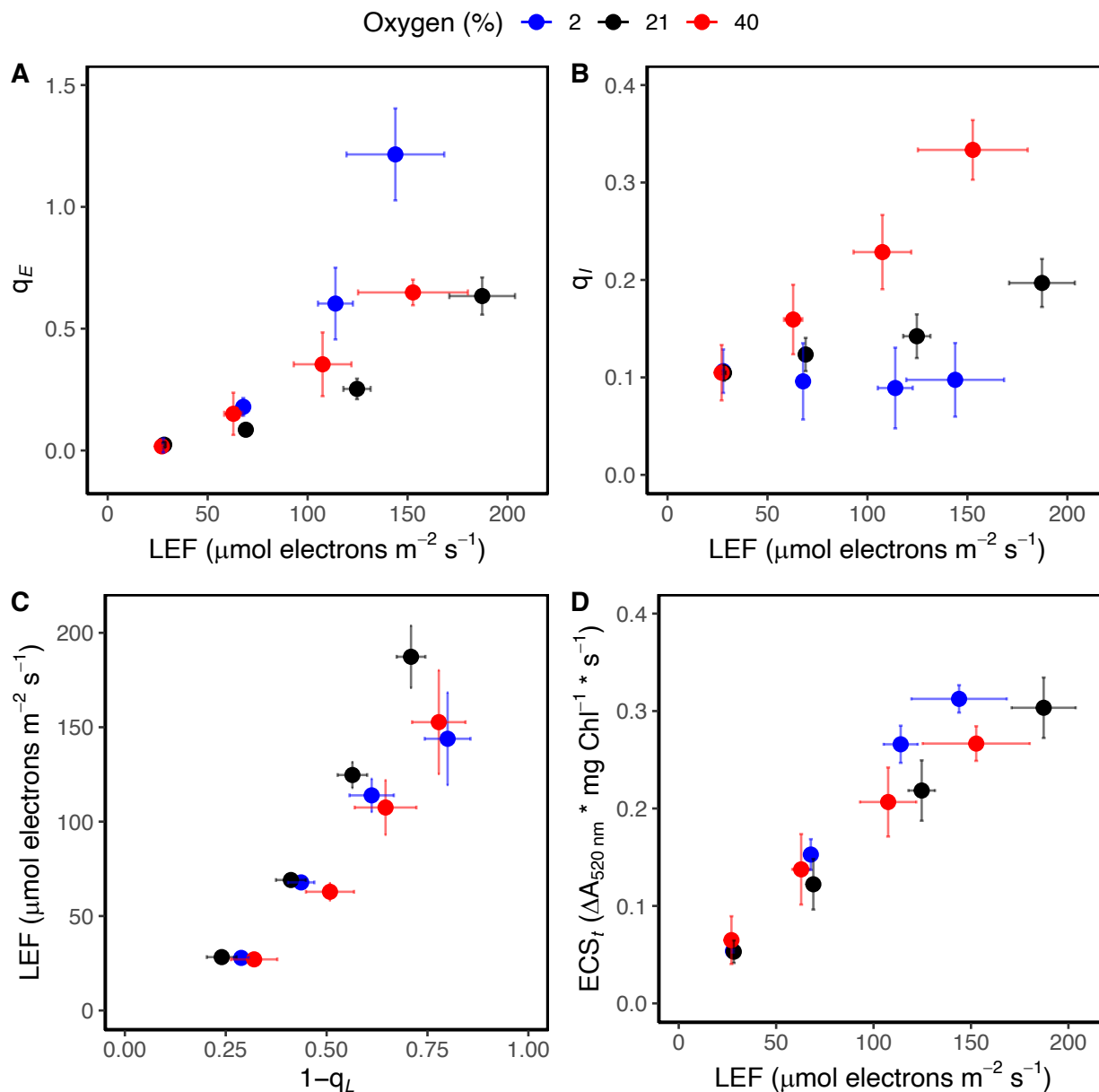


Figure A2.1. The relationship between different light reaction parameters and linear electron flow (LEF) in response to altered photorespiratory flux. The extent of the rapidly reversible pH dependent component of NPQ (q_E) and B) the long-lived component of NPQ (q_I) as a function of LEF. C) LEF as function of the plastoquinone redox state ($1-q_L$). D) The total extent of *pmf* (as measured by ECS_t). Plants were measured at 2%, 21%, and 40% O₂ with 400 ppm CO₂ as a steady state function of light intensity. Shown are the means \pm SD (n = 4).

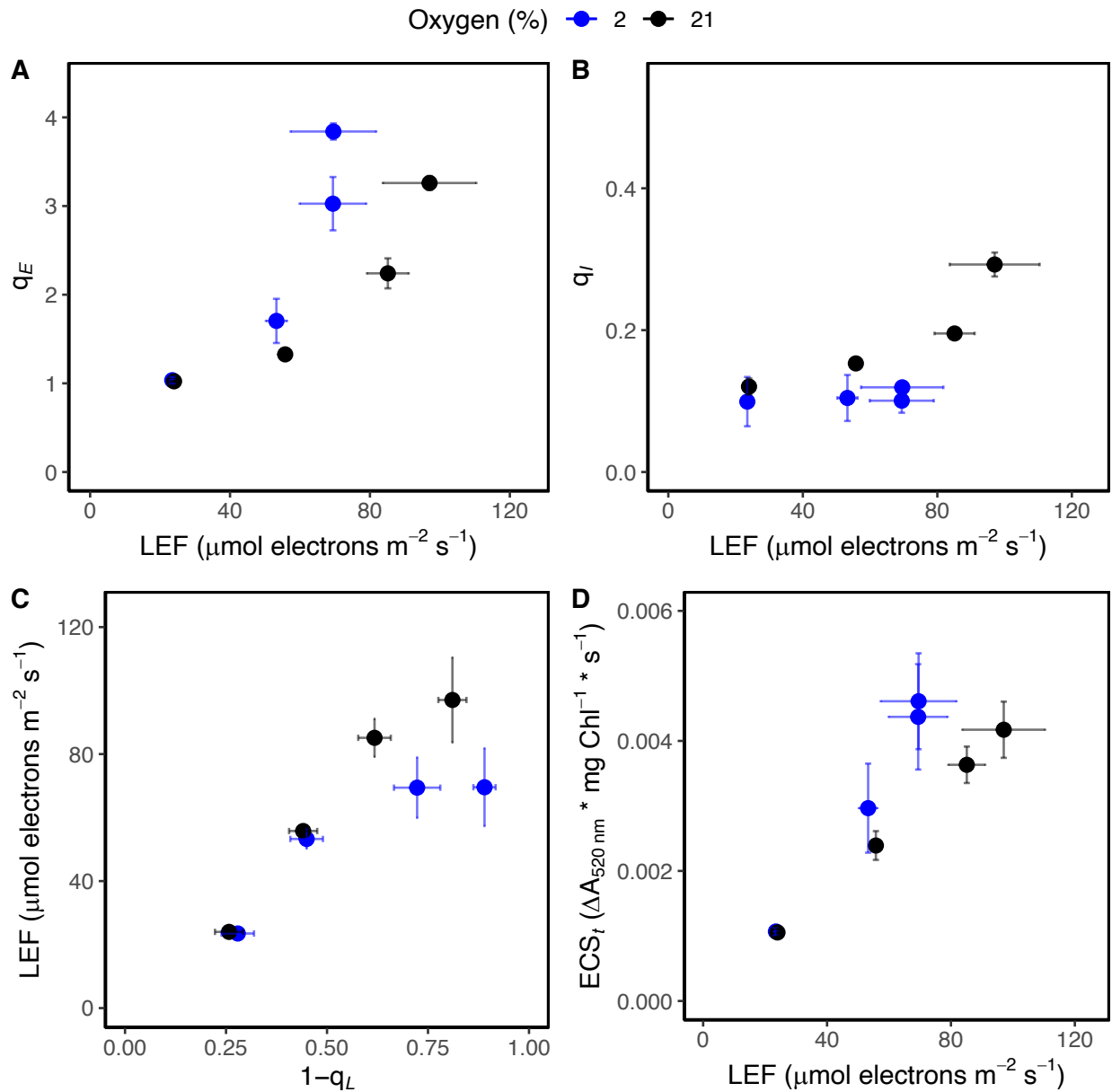


Figure A2.2. The relationship between different light reactions parameters and linear electron flow (LEF) in response to altered photorespiratory flux in *N. tabacum* SNN plants. The extent of the rapidly reversible pH dependent component of NPQ (q_E) and B) the long-lived component of NPQ (q_I) as a function of LEF. C) LEF as function of the plastoquinone redox state ($1-q_L$). D) The total extent of *pmf* (as measured by ECS_t). Plants were measured at 2% and 21% O_2 with 400 ppm CO_2 as a steady state function of light intensity. Shown are the means \pm SD ($n = 4$).

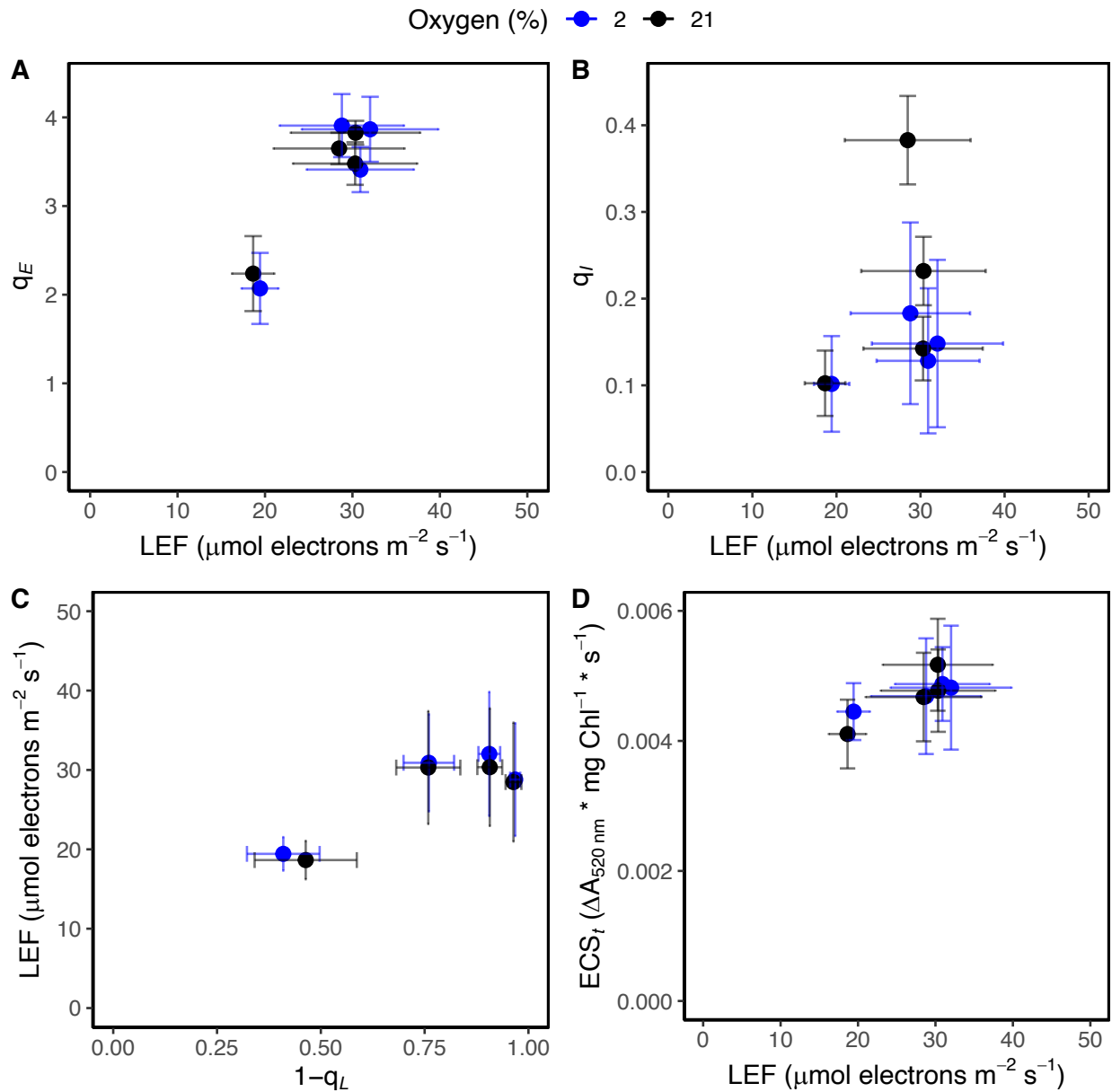


Figure A2.3. The relationship between different light reactions parameters and linear electron flow (LEF) in response to altered photorespiratory flux in ATPC1 antisense lines. The extent of the rapidly reversible pH dependent component of NPQ (q_E) and B) the long-lived component of NPQ (q_I) as a function of LEF. C) LEF as function of the plastoquinone redox state ($1-q_L$). D) The total extent of *pmf* (as measured by ECS_t). Plants were measured at 2% and 21% O_2 with 400 ppm CO_2 as a steady state function of light intensity. Shown are the means \pm SD ($n = 4$).

APPENDIX B: THE PRODUCTION OF ATP AND NADPH THROUGH LINEAR ELECTRON FLOW

Harvested light energy is converted to chemical energy in the form of ATP and NADPH using the thylakoid electron transport chain. Linear electron flow (LEF) through the thylakoid electron transport chain begins with the photoexcitation of photosystem II (PSII) which results in the extraction of electrons from water via water splitting and the reduction of plastoquinone to plastoquinol. Meanwhile, photoexcitation of photosystem I (PSI) oxidizes plastocyanin which reduces ferredoxin and then NADP^+ to NADPH via ferredoxin: NADP^+ oxidoreductase (Ort and Yocum, 1996). PSII and PSI are linked in series by the cytochrome *bf* complex which transfers electrons from plastoquinol to plastocyanin through the action of the Q cycle (Sacksteder et al., 2000). LEF is coupled to proton translocation into the lumen by water splitting, plastoquinone reduction and protonation at PSII, and plastoquinol oxidation and deprotonation at the cytochrome *bf* complex. The accumulation of protons in the lumen, coupled with electron flux generates a protonmotive force, which provides the energy to drive ATP synthesis at ATP synthase (Mitchell, 1976). The production of ATP and NADPH is tightly coupled in LEF resulting in a fixed ATP:NADPH output which will be described in detail below.

LEF produces ATP and NADPH in a fixed stoichiometry of approximately 1.28 ATP:NADPH. The absorption of four photons by PSII and four photons by PSI results in the extraction of four electrons from two molecules of water releasing four protons into the lumen. The four electrons can then reduce two molecules of NADP^+ through LEF. During LEF, transport of these four electrons results in the translocation of eight protons into the lumen through the action of the Q cycle. Together these 12 protons assist in generating proton motive force which fuels ATP synthesis at ATP synthase. As a result of ATP synthase having 14 c-subunits, ATP

synthase requires 14 protons to synthesize three ATP (Seelert et al., 2000, Vollmar et al., 2009).

Thus, the eight photons absorbed for linear electron flux can generate two molecules of NADPH and 2.57 ATP (12 protons x 3 ATP/14 protons) resulting in a ratio of 1.28 ATP:NADPH.

CHAPTER 3:

Identification of novel players involved in acclimating to dynamic shifts in energy demands in photosynthetic tissues using a novel chlorophyll fluorescence-based screen

Kaila Smith, Deserah D. Strand, Sarah Davis, David M. Kramer and Berkley J. Walker

Abstract

Plants must balance the energy supplied from the light reactions of photosynthesis with the demand from metabolism to avoid photodamage and operate efficiently. The processes involved in creating this balance ultimately generate an energetic network throughout the cell which is responsible for responding to dynamic shifts in the ATP:NADPH demand caused by the environment. However, many questions remain as to how flexible this network is and how these processes are coordinated during such large shifts in demand. To address this, we developed a novel chlorophyll fluorescence-based screen targeted towards identifying specific players involved in acclimating to dynamic shifts in ATP:NADPH demand. More specifically, the screen leveraged a recently discovered energy and photorespiratory-related phenotype in which the pH-dependent form of nonphotochemical quenching increases only under low photorespiratory conditions. By combining this phenotype with an O₂ transient which forced photorespiratory flux and subsequent ATP:NADPH demand to transition from low to high, we were able to identify novel energetic phenotypes. We identified both knockout and ethyl methanesulfonate-mutagenized plants which displayed a deviated response to the O₂ transient from the wild type suggesting these genes are involved in responding to shifts in the ATP:NADPH demand.

Introduction

To perform efficiently without photodamage, photosynthetic organisms must match the energy supplied from the light reactions with what is demanded from metabolism (Kramer and Evans, 2011, Walker et al., 2020). However, this can be challenging as linear electron flow through the light reactions produce a fixed stoichiometry of ~1.33 ATP:NADPH whereas metabolism consumes a greater ratio (Hangarter and Good, 1982, Kramer and Evans, 2011). More specifically, the ATP:NADPH demand from metabolism is mostly determined by flux

through the C3 cycle and photorespiration which consume 1.5 and 1.75 ATP:NADPH, respectively (Noctor and Foyer, 1998). The exact ATP:NADPH demand then falls somewhere between those values depending on the carboxylation (the driver for the C3 cycle) to oxygenation (the driver for photorespiration) ratio in response to environmental conditions. Ultimately, the discrepancy between the ATP:NADPH provided from the light reactions with that demanded from metabolism generates an ATP deficit (Smith et al., 2023, Strand and Walker, 2023). However, there are alternative processes which aid in overcoming this ATP deficit including cyclic electron flow (CEF), the malate valve, and the water-water cycle [reviewed in (Scheibe, 2004, Miyake, 2010, Kramer and Evans, 2011)]. Together these supply and demand processes create an energetic network which acts across the entire cell and rapidly changes in response to dynamic environments raising the question as to how each individual component responds and how these responses are coordinated. Resolving these mechanisms can not only answer fundamental questions in cellular bioenergetics, but also inform bioengineering efforts which may substantially alter energetics.

As described above, the ATP:NADPH demand of metabolism changes depending upon the ratio of carboxylation to oxygenation at rubisco. The carboxylation reaction of ribulose-1,5-bisphosphate (RuBP) catalyzed by rubisco results in the formation of two molecules of 3-phosphoglycerate (3PGA) which are metabolized by the C3 cycle to either regenerate RuBP or be exported as triose phosphates. Whereas the oxygenation reaction of RuBP catalyzed by rubisco results in the formation of one 3PGA molecule and one 2-phosphoglycolate (2PG) molecule. The 2PG is then recycled to 3PGA through a series of metabolic reactions known as photorespiration which in the process consumes both ATP and reductant. The consumption of ATP and reductant intimately links photorespiration to the plant's energetic landscape. In fact,

photorespiration is estimated to consume approximately 30-40% of energy flux in an illuminated leaf (Walker et al., 2016).

One proposed role of relatively large reductant consumption from photorespiration is to provide photoprotection to avoid photosystem damage (Osei-Bonsu et al., 2021, Guan and Gu, 2009, Kozaki and Takeba, 1996). More specifically, it is thought that photorespiration may dissipate photochemical energy produced in “excess” of what can be consumed by CO₂ assimilation and therefore serving a photoprotective function. However, a recent study highlights this may not always be the case since there is no evidence for photodamage under minimal levels of photorespiration, but the additional ATP consumption from photorespiration may help prevent feedback inhibition from ATP synthase (Smith et al., 2023). Evidence for this feedback inhibition can be seen from a decrease in ATP synthase conductivity resulting in an increase in the pH-dependent form of nonphotochemical quenching (NPQ), q_E , which occurs when photorespiration is decreased. In general, NPQ describes the dissipation of excess excitation energy as heat and comprised of multiple components (Muller et al., 2001). The major q_E component responds to the acidification of the lumen and results in the downregulation of the light reactions.

Given this consequence of decreasing photorespiration in the plant’s energetic landscape, manipulating levels of photorespiration could be used as a tool for identification of novel genes involved in dynamically responding to shifts in ATP:NADPH demand. Photorespiration and the C₃ cycle respond dynamically to environmental factors, for example under fluctuating light, which then dynamically alters the ATP:NADPH demand because the ATP:NADPH demand increases with photorespiration (Fu and Walker, 2022). Consequently, the response of the energetic landscape must be similarly dynamic to prevent photodamage and maintain optimal efficiency of metabolism. One illustration of this could be the putative H⁺/K⁺ antiporter, KEA3,

in which activity after a high to low light transition coincides with decreased ATP/ADP and NADPH/NADP⁺ ratios (Kaiser et al., 2019). As such, while some of the genes which mediate the dynamic response of the energetic landscape are known, there are likely many others which remain unknown. Questions surrounding the energy landscape during dynamic conditions can be resolved using imaging-based chlorophyll fluorescence screens (Li et al., 2019, Niyogi et al., 1997). Therefore, an imaging-based chlorophyll fluorescence screen combined with manipulating photorespiratory flux might identify additional genes involved in responding to dynamic shifts in ATP:NADPH demand.

Here, we manipulate levels of photorespiration to identify additional genes involved responding to dynamic shifts in the ATP:NADPH demand. More specifically, an imaging-based chlorophyll fluorescence screen was developed where plants were exposed to a low (2%) to high (40%) O₂ transition, referred to as an O₂ transient, in a custom chamber. Under 2% O₂ the wild type (WT) plant has high levels of NPQ from feedback regulation via ATP synthase and as it transitions to 40% O₂ there is a relaxation of ATP synthase causing a decrease in NPQ (Smith et al., 2023). We reasoned that a deviation in this response might indicate some variation in their ability to respond to shifts in ATP:NADPH demand. First, different energetic knock-out mutants were screened for a deviation in the WT response as validation of the method. We identified novel phenotypes in which NPQ was increased from WT at either the 2% or 40% O₂. Some of these mutants were followed up with steady-state measurements where the phenotype disappeared, highlighting how mechanisms which are important under dynamic measurements and steady-state can differ. Next, we performed a forward genetic screen on ethyl methanesulfonate (EMS) mutagenic plants to identify deviations from this WT response. This

identified two interesting mutant lines which may be important in responding to dynamic shifts in ATP:NADPH demands.

Materials and methods

Plant material and growth

All experiments were performed using the *Arabidopsis thaliana* ecotype Columbia-0. Homozygous seed lines were obtained for *mdh1-1* (AT1G53240, GABI_097C10), *mdh1-2* (AT1G53240, GABI_540F04), *mdh-2* (AT3G15020, SALK_126994), *altox1d* (AT1G32350, SALK_203986C), *altox2* (AT5G64210, SALK_059351), *npq4* (AT1G44575, gifted from K.K Niyogi from (Li et al., 2002)), *cat2* (AT4G35090, SALK_076998), and *hpr1-1* (AT1G68010, SALK_067724) and confirmed by PCR-based genotyping. All plants used for screening and spectrophotometry were grown in soil in a under a 12/12 day/night cycle at $\sim 100 \mu\text{mol photons m}^{-2} \text{ s}^{-1}$ at 21/16°C day/night and 60% humidity.

To generate a mutagenized initial M1 population, approximately 10,000 *A. thaliana* seeds were treated overnight with a 0.2% EMS solution and rinsed in water the following morning. The M1 seeds were then sown at the rate of 0.5 mL per pot where the resulting seed was then pooled for the M2 generation. Plants used for seed were grown in soil under a 16/8 day/night cycle at $\sim 100 \mu\text{mol photons m}^{-2} \text{ s}^{-1}$ at 21/16°C day/night and 60% humidity.

Chlorophyll fluorescence screening

The fluorescence-based screen was performed in a dynamic environmental photosynthesis imager (DEPI) (Cruz et al., 2016). A custom chamber was built which allows imaging and manipulation of O₂, nitrogen, and CO₂ using mass flow controllers connected to cylinders of CO₂ and O₂, with nitrogen produced in a nitrogen generator (Peak Scientific, Genuis 1053 230V). To minimize back-reflection of the actinic and saturating light used for fluorescence

imaging, the chamber resembled the shape of a house and the dimensions were 25" x 13" x 7" for the base with a 20° angle between the base and rafter with the ability to screen a standard flat of plants (PLAS-LABS, East Lansing, MI). The screens used for optimizing light intensity were measured for a total of one hour with 20 min at 2% O₂ and 40 min at 40% O₂ under either 400 or 700 μmol photons m⁻² s⁻¹. To screen both the M2 EMS mutagenized plants and energetic mutants, plants were measured for 40 min at 2% O₂ and one hour and 20 min at 40% at 300 μmol photons m⁻² s⁻¹. The screening method for the M2 EMS mutagenized plants was applied again to a F2 backcross between the WT and the identified "1x1" line to select plants either positive or negative for the phenotype to pool for whole genome sequencing. During the screen, image capture protocols were measured every 2 min to determine ϕ_{II} and NPQ using standard saturation pulse chlorophyll fluorescence min and raw images were processed in Visual Phenomics [described in (Cruz et al., 2016, Baker, 2008)].

Genomic DNA extraction, sequencing, and analysis

Genomic DNA was extracted from the WT, M3 generation of the 1x1 line, the positive F2 backcross, and the negative F2 backcross for sequencing (NucleoSpin Plant II Midi Kit for Plants, Macherey-Nagel). Paired-end libraries using the genomic DNA were prepared using a library kit with unique dual-indexed adapters according to the manufacturer's instructions (HyperPrep DNA library kit, Kapa Biosystems). Completed libraries were checked for quality and quantified using a combination of assays (dsDNA HS, Qubit) (TapeStation HS DNA1000, Agilent). The libraries were pooled in equimolar amounts and the pool was quantified (Collibri Quantification qPCR kit, Invitrogen). The pooled libraries were loaded onto one lane of a flow cell (SP flow cell, NovaSeq). Sequencing was performed in a 2x150bp paired end format at the Michigan State University Genomics Core (NovaSeq 6000 v1.5). To identify the single

nucleotide polymorphism (SNP) responsible for the 1x1 phenotype, comparisons were run first between positive and negative F2 backcrosses and then the WT and M3 using the SIMPLE pipeline [described in (Wachsman et al., 2017)]. The SIMPLE pipeline first mapped the corresponding sequencing data separately against the TAIR10 reference genome to identify the entirety of single nucleotide polymorphisms (SNPs) present. Next, the program identified potentially causal SNPs using a LOESS-fitted ratio variable which represented the allele frequency comparison between samples which was then plotted to the corresponding chromosomal position. The strongest candidates from the plots were then selected based on their homozygosity in addition to the SNP effect on the translated protein and listed in a table.

In vivo spectroscopic assays

All spectroscopic measurements were made using intact fully expanded leaves using an in-house constructed integrated diode emitter array spectrophotometer to measure chlorophyll *a* fluorescence and electrochromic shift (ECS) parameters [described in (Hall et al., 2013)]. O₂ concentrations (2% or 21%) were obtained using a mass flow controller system which fed into a gas exchange analyzer which mixed in 400 ppm CO₂ and was fed into the leaf cuvette of the spectrophotometer (LI-6400 XT, LI-COR Biosciences). Plants were dark adapted for 30 min prior to experimentation at the corresponding O₂ concentration. Light response curves were measured with the actinic light intensities ranging between 100-850 $\mu\text{mol photons m}^{-2} \text{s}^{-1}$. Plants were illuminated for 12 min at each individual intensity to reach a steady-state, and then dark adapted for 12 min to allow for the relaxation of q_E . Saturation pulse parameters were calculated from a multiphase flash, and used to calculate ϕ_{II} , NPQ, q_E , and q_I as previously described (Baker, 2008, Loriaux et al., 2013). In terms of ECS parameters, the relative extent of the proton motive force (pmf) was measured from the total amplitude of the absorbance shift (ECS_t) during a 300

ms dark interval after steady-state illumination (Sacksteder and Kramer, 2000). The first order rate constant of the ECS decay reflects the rate constant of transthylakoid efflux, or proton conductivity of the thylakoid membrane (g_{H^+}) and was determined by fitting the ECS decay to a first order exponential.

Data processing

Curve fitting and graphing were performed in R (dplyr and ggplot2 packages) and python (SciPy package).

Results

Development of a novel fluorescence-based screen

As discussed above, under low photorespiratory conditions there is an increase in the q_E component of NPQ resulting in higher levels of overall NPQ (Smith et al., 2023). We reasoned we could leverage this observation to create a high-throughput screening process which would identify specific genes involved in acclimating to large shifts in energy demands. More specifically, we could monitor NPQ during an O₂ transient where plants transition from 2% to 40% O₂ through imaging chlorophyll fluorescence. We expected that at 2% O₂, where both photorespiratory flux and ATP:NADPH demand are decreased, NPQ would be higher likely due to a decrease in ATP synthase conductivity. However, as the plants transitioned to 40% O₂ where photorespiratory flux and ATP:NADPH demand are increased, there would be a relaxation in ATP synthase conductivity resulting in decreased NPQ. Therefore, a deviation in this response could be indicative of a gene involved in acclimating to large shifts in ATP:NADPH demand.

To develop the screen outlined above, a chamber needed to be constructed which would allow for the direct manipulation of the surrounding atmospheric conditions while not sacrificing imaging quality from the system imaging the chlorophyll fluorescence due to reflection from the

actinic and saturating light to the measurement camera. A custom chamber was developed to interface with the dynamic environmental photosynthetic imager (DEPI) which allows for continuous and high-throughput measurements of photosynthetic parameters (Figure 3.1A) (Cruz et al., 2016). Due to the large volume of the chamber, the question then arose as to how long it would take for the chamber to transition from 2% to 40% O₂ as that would be important in the determination of the length of the screen. The transition took place over approximately 40 min with the chamber reaching around 30% O₂ after around 10 min (Figure 3.1B). Based on these results, we decided to test a screen with an hour dark adaptation at 2% O₂ followed by 20 min at 2% and then 40 min at 40% O₂.

Another important parameter in the development of the screen was the actinic light intensity because the balance of the q_E and q_I components of NPQ depend on this (Smith et al., 2023). More specifically, at 2% O₂ q_E increases whereas at 40% O₂ q_I increases. This increase in each component has a different light sensitivity, resulting in variability in the difference between total NPQ between 2% and 40%. We reasoned the optimal light intensity would have the largest difference in NPQ between 2% and 40% O₂ and thus provide a strong consistent phenotype for the WT. To determine this optimal intensity, a light intensity response curve was performed which measured NPQ in the WT within the chamber at both 2% and 40% O₂. Clear differences between the 2% and 40% O₂ were observed at 100, 400, and 700 $\mu\text{mol photons m}^{-2} \text{s}^{-1}$ which suggested these may be appropriate light intensities to use in the screen (Figure 3.2A). The difference in NPQ between 2% and 40% O₂ observed at 100 $\mu\text{mol photons m}^{-2} \text{s}^{-1}$ in which NPQ was the largest at 40% rather than 2% O₂ was likely driven by an increase in the photoinhibition-related q_I component rather than q_E in which the screen principle is based upon (Smith et al.,

2023). Therefore, the 400 and 700 $\mu\text{mol photons m}^{-2} \text{s}^{-1}$ appeared to be the optimal light intensities for conducting the screen.

The principle of the screen was tested and optimized by comparing the response of different mutants and WT at both 400 and 700 $\mu\text{mol photons m}^{-2} \text{s}^{-1}$. One of the mutants included was a knockout of hydroxypyruvate reductase (*hpr1*) which is a core enzyme in the photorespiratory pathway (Timm et al., 2008). Another mutant included was a knockout of the foliar-expressed catalase isoform (*cat2*) which shows a more subtle photorespiratory phenotype when grown under high CO_2 (Queval et al., 2007). When grown under high CO_2 , photorespiratory genes knockouts either exhibit a subtle or obvious growth phenotype, which is much more apparent or often lethal at ambient air (Timm et al., 2008, Eisenhut et al., 2017, Somerville, 1984). Therefore, we reasoned it was unlikely our screen would simply reidentify photorespiratory mutants because our plants were grown under ambient air. We expected that if our screen was successful, both *hpr1* and *cat2* would display a difference in response compared to WT at 40% O_2 because of the role photorespiration plays in maintaining the energetic landscape. We additionally examined a mutant lacking in a subunit of PsbS (*npq4*) which is involved in regulating NPQ and therefore displays constitutively low levels of NPQ and therefore should not respond to the O_2 transient (*npq4*).

The response of these mutants is shown in Figure 3.2B-C. Under 400 $\mu\text{mol photons m}^{-2} \text{s}^{-1}$ light intensity, the WT had high levels of NPQ at 2% O_2 which then decreased following the transition to 40% O_2 as expected (Figure 3.2B). However, a different response occurred under 700 $\mu\text{mol photons m}^{-2} \text{s}^{-1}$, likely due to an increase in q_I component of NPQ which increases with O_2 and light (Figure 3.2C) (Smith et al., 2023). Additionally, under 700 $\mu\text{mol photons m}^{-2} \text{s}^{-1}$, the kinetics of the WT response were similar to the mutants. Based on these results, 400 μmol

photons $\text{m}^{-2} \text{s}^{-1}$ was selected as the appropriate light intensity to perform the screen. In terms of mutants, *hpr1* had similar levels of NPQ initially at 2% O_2 and then increased NPQ at 40% compared to the WT (Figure 3.2B). Like *hpr1*, *cat2* displayed similar levels of NPQ when compared to the WT initially at 2% O_2 and then increased NPQ at 40%, although slightly less than *hpr1*. It was not expected that *npq4* would respond to the O_2 transient due its constitutively low levels of NPQ and this was indeed true. Overall, these results suggested that the design of the screen would be successful in identification of genes involved in acclimation shifts in ATP:NADPH demands.

Characterization of known energetic knockout mutants

For additional validation, mutants involved in the malate valve and alternative pathways of the mitochondrial electron transport chain were tested for their potential role in acclimating to shifts in energy demands. The screening procedure was slightly modified to both extend the length and decrease the light intensity. We lengthened the screen to 40 min at 2% O_2 followed by one hour and 20 min at 40% O_2 based on the large initial rise in NPQ at 2% O_2 observed above during light-acclimation (Figure 3.2B-C). The longer initial time at 2% O_2 and illumination allowed NPQ to reach a steady-state in the WT as seen below. Additionally, the light intensity was decreased to 300 $\mu\text{mol photons m}^{-2} \text{s}^{-1}$ to reduce some variation in the WT phenotype described in depth below which might have resulted from an increase in the q_I component.

The first category of mutants analyzed were mutants involved in the malate valve. The malate valve adjusts cellular ATP:NADPH by shuttling reducing power via malate/oxaloacetate shuttles [reviewed in (Scheibe, 2004)]. Malate dehydrogenase (MDH) is the enzyme responsible for catalyzing the oxidation of malate to oxaloacetate in presence of reductant. In the plant cell, MDH exists in several forms including the mitochondrial MDH, plastid MDH, and cytoplasmic

MDH. The mitochondrial MDH is encoded by three structural genes (*mdh1*, *mdh2*, and *mdh3*) (Yudina, 2012). It has been suggested these malate valves are important as a ‘thermodynamic buffer’ that maintains the chloroplast NADP⁺/NADPH ratio constant over a wide range of conditions (Selinski and Scheibe, 2019). Both *mdh1-1* and *mdh1-2* displayed similar rates of NPQ to WT but then had a steep rise in NPQ after the transition to 40% O₂. Interestingly, *mdh2* did not display a similar phenotype and instead resembled the WT. However, the double knockout of *mdh1-1mdh2* also resembled the WT making the results difficult to conclusively interpret (Figure 3.3A).

It has been suggested alternative pathways of the mitochondrial electron transport chain may be important in oxidizing reducing equivalents from photosynthesis or photorespiratory glycine oxidation (Gandin et al., 2012). The mitochondrial electron transport chain contains five protein complexes integrated into the inner membrane which couple electron transfer with proton translocation for the generation of ATP. Plants additionally possess non-phosphorylating pathways including an alternative oxidase (AOX). AOX oxidizes ubiquinol and reduces O₂ to water without the translocation of protons across the membrane thereby generating no ATP (Vanlerberghe, 2013). Both *altox1d* and *altox2* initially displayed a large spike in NPQ under the 2% O₂ which began to decline prior to the transition to 40% O₂. After transitioning to 40% O₂, both *altox1d* and *altox2* then reached WT levels of NPQ (Figure 3.3B).

Dynamic O₂ transients revealed phenotypes not readily available under the steady-state

We then sought to understand the potential cause for the spike in NPQ observed at 2% O₂ in the *altox1d* and *altox2* mutants. While we also observed an interesting phenotype in *mdh1* lines, the lack of phenotype in the *mdh1-1mdh2* double knockout presented cause for not exploring the mutant further at this time. Though the DEPI is useful for achieving high

throughput imaging of some photosynthetic signals, it is limited to measurements based on chlorophyll fluorescence. Oftentimes large changes in NPQ are associated with a change in the q_E component which arise from an increase in pmf which can be measured in relative terms using the electrochromic shift (ECS) (Avenson et al., 2004). Therefore, to examine the ECS we then measured *altox1d* and *altox2* mutants under steady-state conditions using *in vivo* spectroscopy. Under these steady-state conditions, there was no difference between the mutants and WT in either ϕ_{II} or NPQ at 2% O₂ (Figure 3.4A-B). These also corresponded with no observable difference in q_E or q_I components of NPQ (Figure 3.4C-D). Additionally, there were no differences between the mutants and WT in the light induced pmf (ECS_I) or ATP synthase conductivity (g_{H^+}) at 2% O₂ (Figure 3.5A-B). Ultimately, these results highlight the importance of approaches utilizing dynamic conditions (an O₂ transient) as they can unveil phenotypes which do not present under steady-state conditions.

Identifying EMS mutants with divergent responses from the WT to O₂ transients

After exploring the response of different energetic knockouts, we examined EMS mutagenized plants for a deviation in their response to O₂ transients. Approximately 1,000 homozygous M2 EMS mutagenized plants were screened for a deviation in the NPQ response with this number being chosen to ensure total genomic coverage. This identified approximately 30 mutants with responses that differed from WT. The deviations from these plants were classified broadly as “*exaggerated*”, “*opposite*”, or “*delayed*” depending on the nature of their differences from the WT response (Figure 3.6). The *exaggerated* phenotype described a plant which displayed a sharper decline in NPQ in response to the transition to 40% O₂ compared to the WT, the *opposite* described a plant in which NPQ increased instead of decreased after the transition to 40% O₂, and the *delayed* phenotype described a plant which showed a decline in

NPQ in response to the transition to 40% O₂, but delayed relative to the WT. These deviations could be caused by disruptions in several factors including changes to metabolism, ATP synthase regulation, alternative electron flow, and more, however, it is impossible to know without identification of the causal gene mutation.

Oftentimes EMS mutant screening produces phenotypes which are not dominant or otherwise heritable in the M3 generation (Henry et al., 2014, Addo-Quaye et al., 2017). Additionally, while most typical EMS screens identify obvious phenotypes, the phenotypes identified above were more subtle and often required specific conditions to be reproduced such as a particular developmental stage. To validate and confirm the heritability of the phenotypes uncovered above, the M3 generation of the 30 identified candidates were also screened. Of these candidates, two lines maintained replicable phenotypes. These lines are referred to as “1x1” and “2x24” based on the growing flat and plant number assigned during the initial screening process. The M3 generation of 1x1 first displayed a slightly higher level of NPQ at 2% O₂. However, the more prominent feature of the mutant was the steep rise following the transition to 40% O₂ where NPQ reached a peak and then declined (Figure 3.7A). In contrast, the 2x24 mutant had a lower initial NPQ which then rose following the transition to 40% O₂ (Figure 3.7A). Interestingly, the growth for 1x1 was identical to the WT which is not always typical of photosynthesis or energy-related phenotypes (Figure 3.7B). In contrast, the 2x24 line grew more irregularly as represented by the ability to only grow 2 replicates after transplanting 8 total M3 seedlings. Overall, both these mutations displayed a heritable and divergent response to the O₂ transient suggesting they might be key players in acclimating to large shifts in energy demands. However, due to the near WT growth, the 1x1 line was chosen over the 2x24 line to advance for identification of the causal single-nucleotide polymorphism (SNP).

To determine what the causal SNP might be, the M3 lines were backcrossed with the WT and the subsequent F2 generation was screened. The backcross served to reduce the number of homozygous mutations in the M3 line and ideally the number of candidate genes produced during downstream analysis. Screened F2 individuals were classified as either positive (1x1 phenotype) or negative (WT phenotype) and were accordingly pooled and sequenced. However, definitive classification of F2 plants as either positive or negative became challenging due to variation that was later observed in both the WT and 1x1 phenotypes. The variation between the WT and 1x1 phenotypes can be seen in Figure 3.8. With respect to the WT, occasionally NPQ would rise slowly over time at 40% O₂ (Figure 3.8A). Other times, the 1x1 would not display a steep rise at 40% O₂ but rather a slow rise over time (Figure 3.8B). The positive and negative populations were compared using a pipeline which generates a ratio that represents the allele frequency comparison. The allele frequency ratio should be around 0 for unlinked SNPs and approximately 0.66 for causal mutations. When comparing the positive and negative populations no candidate genes were returned using these cutoffs (Figure 3.9A).

As described above, working with a F2 population is ideal due to the significant decrease in homozygous mutations, however, comparing SNPs in the M3 and WT can reveal a more extensive list of candidate mutations. In addition to sequencing the F2 populations, the M3 and WT lines were also sequenced. When the M3 and the wild type were compared to generate an allele frequency ratio, a candidate list was generated which contained 72 genes. The candidate list was generated by first identifying SNPs with the correct allele frequency ratio as described above and then filtering those predicted non-synonymous mutations within a coding region (Figure 3.9B, Table 3.1). The number of genes in this list was larger than what would be typically returned if using a segregating F2 population.

Discussion

Overall, this work displays the utility of novel dynamic screening methods for identifying novel biological phenotypes in both knockout and EMS mutants. First, the difference in the *altox* mutants between the steady-state and dynamic phenotypes highlights how there are mechanisms important under a dynamic context which are not under the steady-state. More specifically, for *altox* the temporarily increased NPQ under 2% O₂ could suggest that alternative oxidase might play an important role in acclimating to decreased ATP:NADPH demand. Additionally, the EMS mutagenic screen revealed two interesting novel phenotypes while also highlighting some difficulties which might arise in the casual SNP identification of transient phenotypes.

A deeper understanding of photosynthetic performance under dynamic conditions is important for increasing photosynthetic productivity

Photosynthesis research is often conducted under steady-state conditions in controlled environments which has produced large advances in understanding core processes in photosynthesis. However, studies increasingly use approaches which mimic dynamic environments encountered in the field and correspondingly identify phenotypes specific to such dynamic conditions. For example, a mutant lacking the PsbS component of *qE* (*npq4*) displays both increased photodamage and decreased fitness only under fluctuating light conditions (Kulheim et al., 2002). Another example includes the recovery of growth defects in the knockouts of the photorespiratory enzymes *hpr1* and *ggt1* under fluctuating light (von Bismarck et al., 2023). The contrasting results from the dynamic conditions under the screen compared to the steady-state for the *altox* knockouts provided yet another example of how dynamic conditions can unveil phenotypes which are not present under steady-state conditions (Figure 3.3B, 3.4, 3.5). An initial spike in NPQ occurred at 2% O₂ in the *altox1d* and *altox2* knockouts.

However, when we tried to investigate the cause of the increased NPQ at 2% O₂ utilizing steady-state methods, the phenotype was no longer observed and appears to be only captured under transient conditions. The transiently increased NPQ at 2% O₂ in the *altox1d* and *altox2* knockouts could suggest that alternative oxidase might play an important role in acclimating to decreased ATP:NADPH demand perhaps involving its ability to rapidly consume reductant without additional generation of ATP. While manipulating O₂ levels is an artificial treatment not encountered in nature, it introduces changes in photorespiratory flux which can occur under fluctuations in natural conditions including temperature and light.

Additionally, the *mdh1-1* and *mdh1-2* mutants displayed an interesting transient phenotype in response to a shift in ATP:NADPH demand. More specifically, both *mdh1-1* and *mdh1-2* displayed a steep rise in NPQ after the transition to 40% O₂ where ATP:NADPH demand was increased (Figure 3.3A). Interestingly, *mdh1* was not on the candidate list for potential 1x1 causal mutations despite similarities observed between their phenotypes (Figure 3.3A, 3.7A). It is possible that the increased NPQ in *mdh1* could be caused from a substrate limitation from NADP⁺/NADPH suggesting that *mdh1* may act as an important ‘thermodynamic buffer’ when energy demands are high (40%). More specifically, the mitochondria might be important in consuming additional reductant during an increase in ATP:NADPH demand caused by an increase through photorespiration via the malate valve. However, the double knockout of *mdh1-1mdh2* resembled the WT confounding these results (Figure 3.3A).

Transient phenotypes can generate difficulties in the identification of the casual SNP

Due to the large candidate list, which was generated for the 1x1 line, the casual mutation responsible for the 1x1 phenotype has yet to be definitively identified. Comparing the sequencing results for the phenotype positive and negative bulks in the F2 screening typically

results in a narrow candidate list and a ratio plot sufficient to identify the causal mutation. However, when the sequencing results for the positive and negative populations were compared no candidate genes were returned (Figure 3.9A). No candidate genes were likely returned due to the incorrect categorization of plants as either positive (mutant) or negative (WT) in the bulk populations. The pipeline used for comparing sequencing results attempts to find a polymorphism that has only non-reference reads for the mutant and approximately 1 mutant: 2 WT ratio of reads in the WT (Wachsman et al., 2017). As a result, incorrect categorization of a plant in the screening process will influence this analysis and yield no candidates. As shown above, definitive classification of F2 plants as either positive or negative was difficult due to variation in the control phenotypes which likely led to incorrect classification and yielding no candidates (Figure 3.8).

Incorrect categorization may have occurred because transient phenotypes can be difficult to recognize. As discussed above, dynamic conditions can be very useful for unveiling novel phenotypes which are not present under steady-state conditions and increasing our knowledge of a particular system. However, dynamic conditions can introduce difficulty in replicating a particular phenotype. In the future, when working with dynamic phenotypes it might be beneficial to consider obtaining a smaller, higher-confidence population rather than focusing on gathering a large bulk population. More specifically, in this case by only including plants in the bulk populations where first the control phenotypes behaved exactly as expected then additionally the F2 classification identically matched the appropriate control.

Promising candidates for the causal mutation of the 1x1 phenotype

Although the causal gene for 1x1 phenotype remains unknown, the candidate list contains promising candidates for future verification using complementation (Table 1). The list of

candidate genes evaluated for any obvious connection to leaf energetics or photorespiration resulting in the main candidate of interest, GLU1, which encodes Fd-GOGOAT, the enzyme responsible for reassimilating ammonia released during photorespiration. However, another interesting category of candidates would be either transcriptional or post-translational regulatory factors which respond to shifts in ATP:NADPH demand. The only transcription factor which was listed was a bZIP transcription factor family protein (TGA9) which is known to be sensitive to the redox state of the cell (Lu et al., 2023). In terms of post-translational modifications, recent evidence suggests ubiquitination might be a major mechanism for regulation of the chloroplast proteome, particularly for photosynthetic proteins (Sun et al., 2022). Accordingly, a E3 ubiquitin ligase (EMB2771) was also listed as a candidate. Additionally, the lack of photorespiratory genes present on the candidate list indicates the strategy was successful in avoiding the reidentification of core photorespiratory genes.

While the C3 cycle and photorespiration comprise the largest portion of metabolic ATP:NADPH demand, other metabolic processes including nitrate assimilation require a significant contribution making GLU1 a promising initial candidate for the 1x1 mutant (Noctor and Foyer, 1998). The release and recapture of ammonia from photorespiratory glycine oxidation links photorespiration to nitrogen metabolism (Keys, 2006). Photorespiratory glycine oxidation releases ammonia as much as 10-fold more than the nitrogen assimilated from soil with most of the ammonia being recaptured through Fd-GOGAT (Keys et al., 1978). The *Arabidopsis thaliana* genome includes two distinct forms of Fd-GOGAT; with the photorespiratory function being attributed to GLU1 (Coschigano et al., 1998). Therefore, GLU1 is a key enzyme in nitrogen metabolism. With respect to energetics, production of glutamate via the GS-GOGAT pathway requires two additional electrons (equivalent to 1 NADPH) and 1 ATP with the overall estimates

for reductant demand for nitrate assimilation around ~2.5-23% of total LEF (Walker et al., 2020). As discussed above, the most prominent feature of the 1x1 mutant was the steep rise and decline in NPQ following the transition to 40% O₂. It is possible that a loss of reductant and ATP consumption from GLU1 might cause a temporary constraint on the light reactions resulting in increased NPQ. Currently the only evidence suggesting a role for GLU1 in energy transients is the decrease in GLU1 transcripts in plants lacking plastid-localized MDHs suggesting that GLU1 might represent an alternative way to remove excess electrons when malate valve capacity is diminished (Selinski and Scheibe, 2014). However, to confirm that a SNP in GLU1 is responsible for the 1x1 phenotype it will be necessary to test whether complementation of the SNP results in a loss of the phenotype.

Figures and Tables

A



B

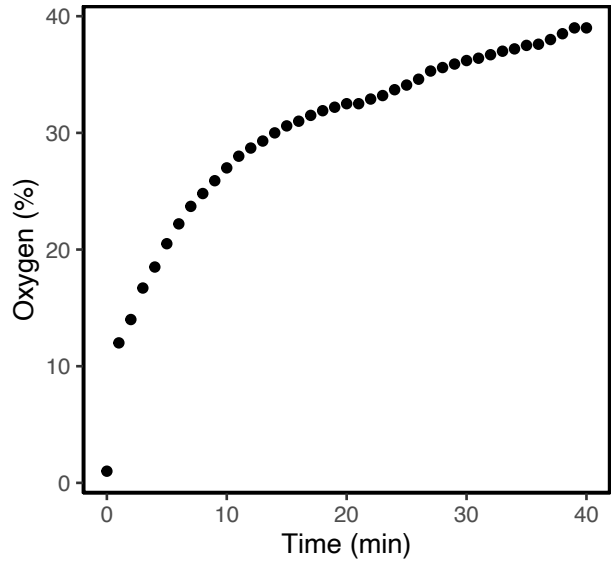


Figure 3.1. Manipulation of O₂ concentration while tracking photosynthetic performance.

A) The design of the custom Plexiglass chamber which was constructed to interface with the dynamic environmental photosynthetic imager (DEPI). The Plexiglass chamber allowed for the manipulation of atmospheric conditions while maintaining the precision of the chlorophyll fluorescence imaging. The chamber was tested for B) the time in which it took for the O₂ concentration of the chamber to reach 40% from 2%.

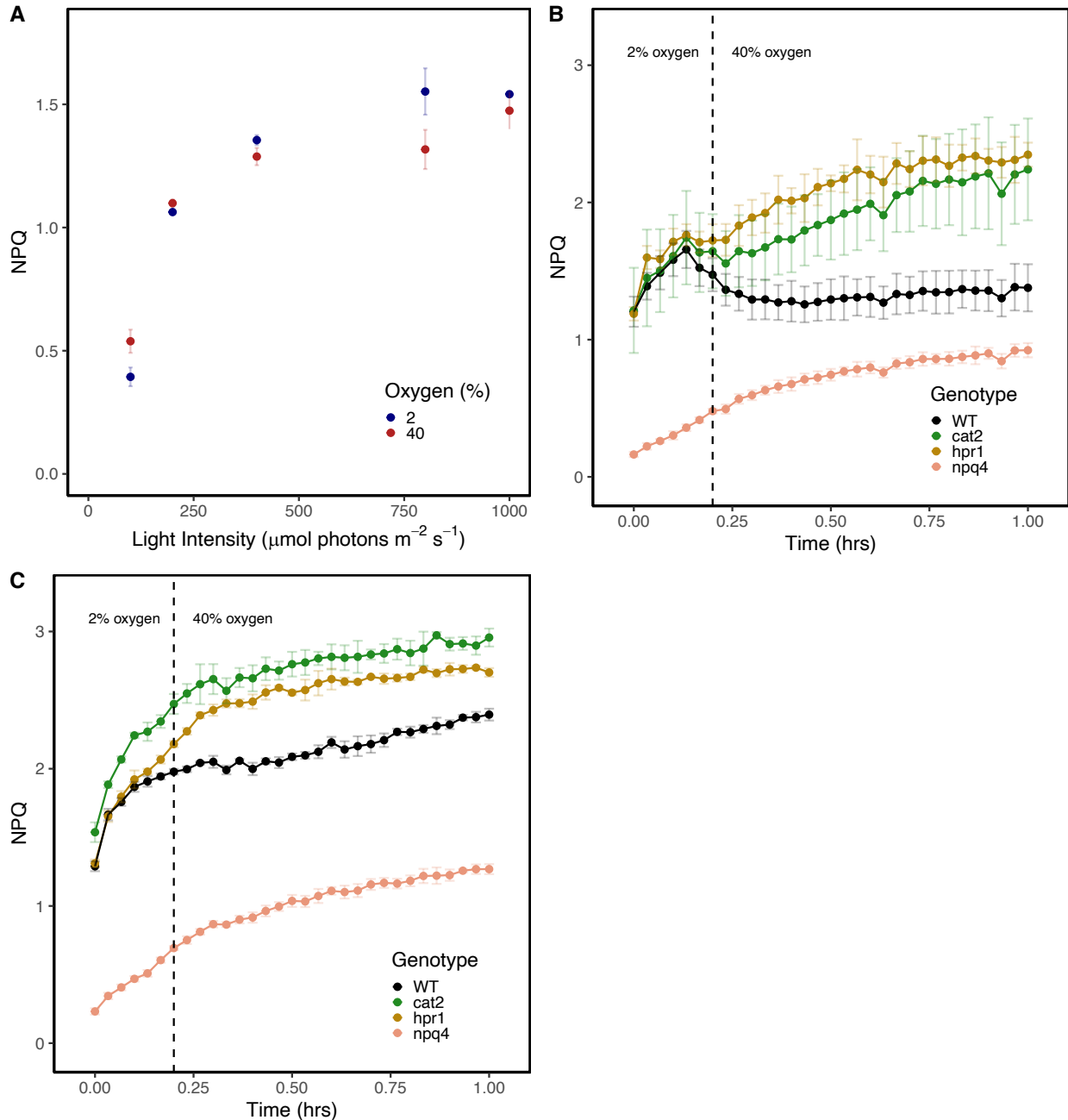


Figure 3.2. Development and optimization of the light intensity utilized for the fluorescence-based screen. First, A) light intensity screen curve was performed at 2% and 40% O₂ to identify the largest difference in NPQ. Next, two light intensities were tested by comparing the response of different mutants and the WT at both B) 400 and C) 700 $\mu\text{mol photons m}^{-2} \text{s}^{-1}$. NPQ was measured over the course of one hour where after 20 min at 2% O₂ the O₂ concentration was changed to 40% O₂. The colored lines represent the mutants utilized. The black line represents the WT used in the corresponding screen. Mean \pm SD, n = 4.

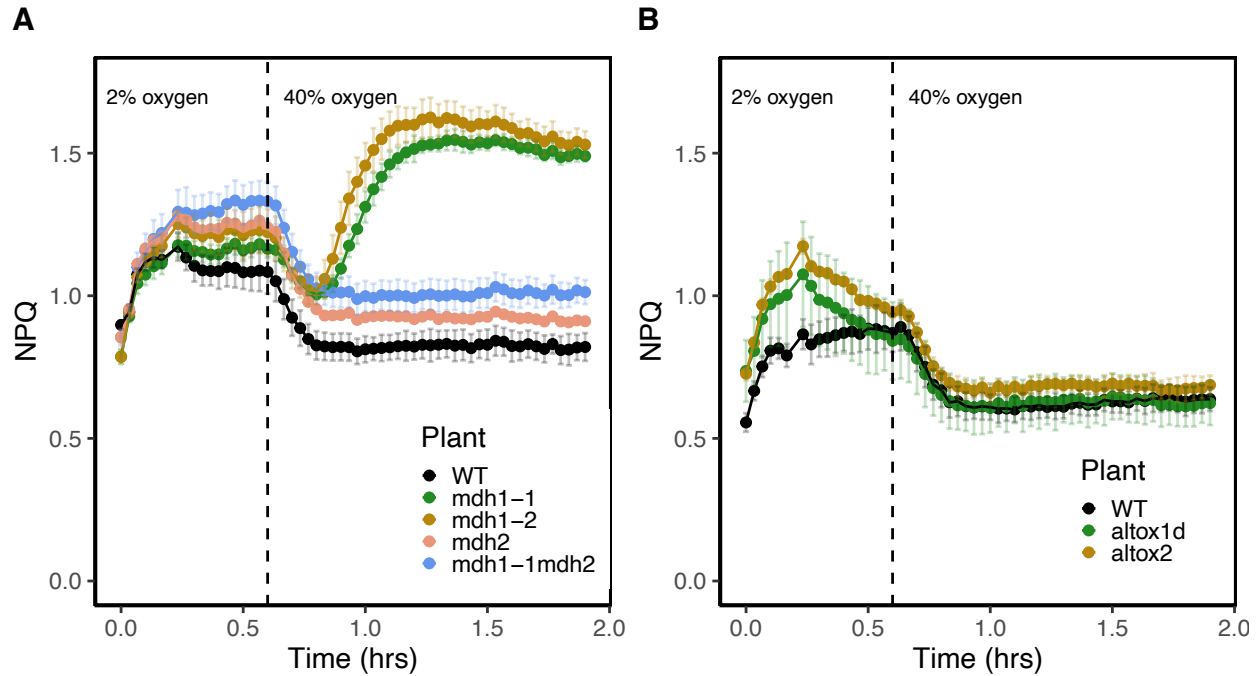


Figure 3.3. Deviations in the NPQ response to an O₂ transient in known energetic mutants. Displayed is the A) response of malate valve mutants and B) alternative oxidase mutants. NPQ was measured over the course of two hours where after 40 min at 2% O₂ the O₂ concentration was changed to 40% O₂. The colored lines represent mutants utilized. The black line represents the WT used in the corresponding screen. Mean \pm SD, n = 4.

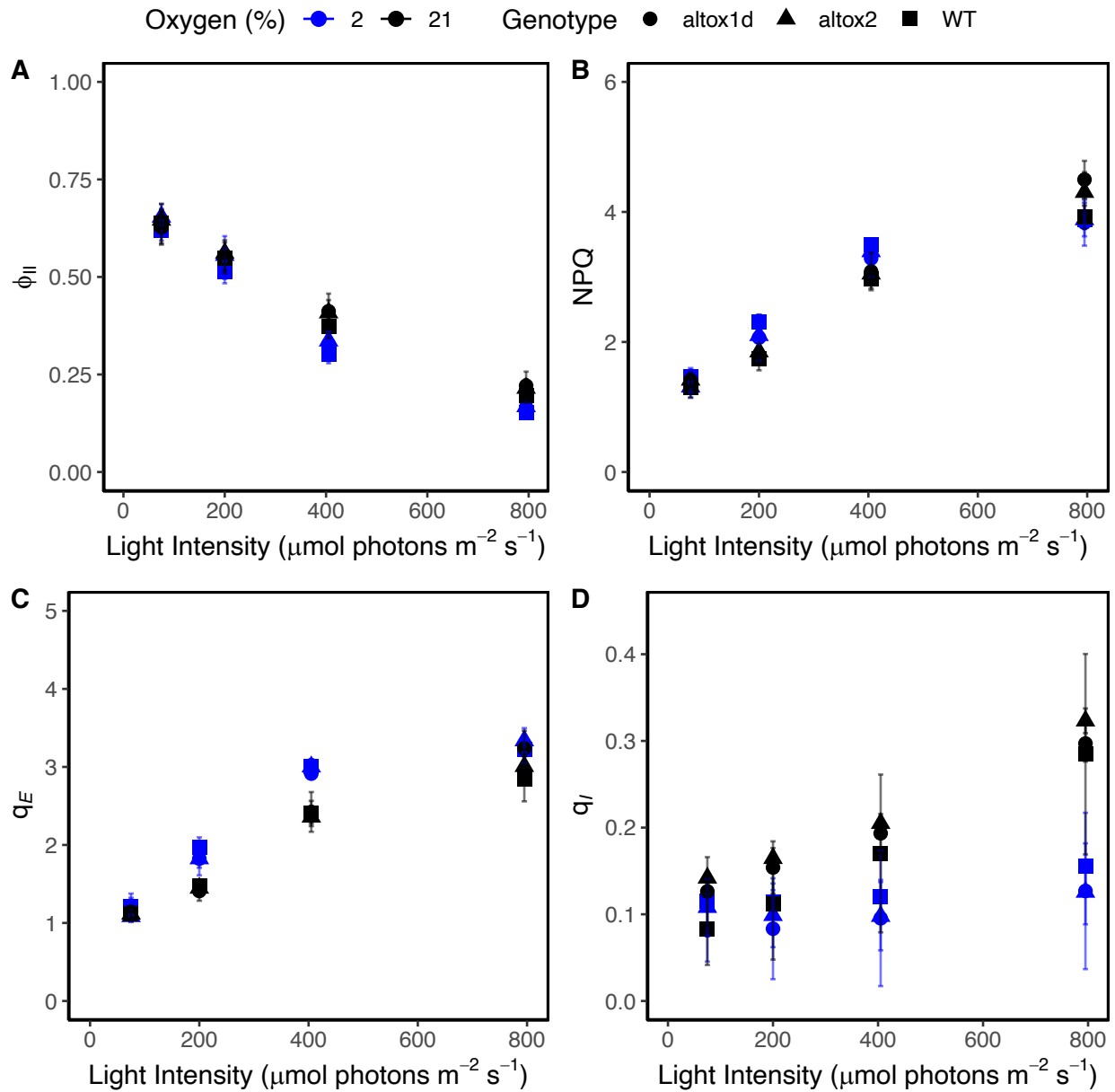


Figure 3.4. The response of the light reactions to altered photorespiratory flux in alternative oxidase mutants. A) Changes in photosynthetic efficiency (ϕ_{II}), B) nonphotochemical quenching (NPQ), C) the rapidly reversible pH dependent component of NPQ (q_E) and D) the long-lived component of NPQ (q_I). Plants were measured at 2% and 21% O_2 with 400 ppm CO_2 as a steady state function of light intensity. Shown are the means \pm SD ($n = 4$).

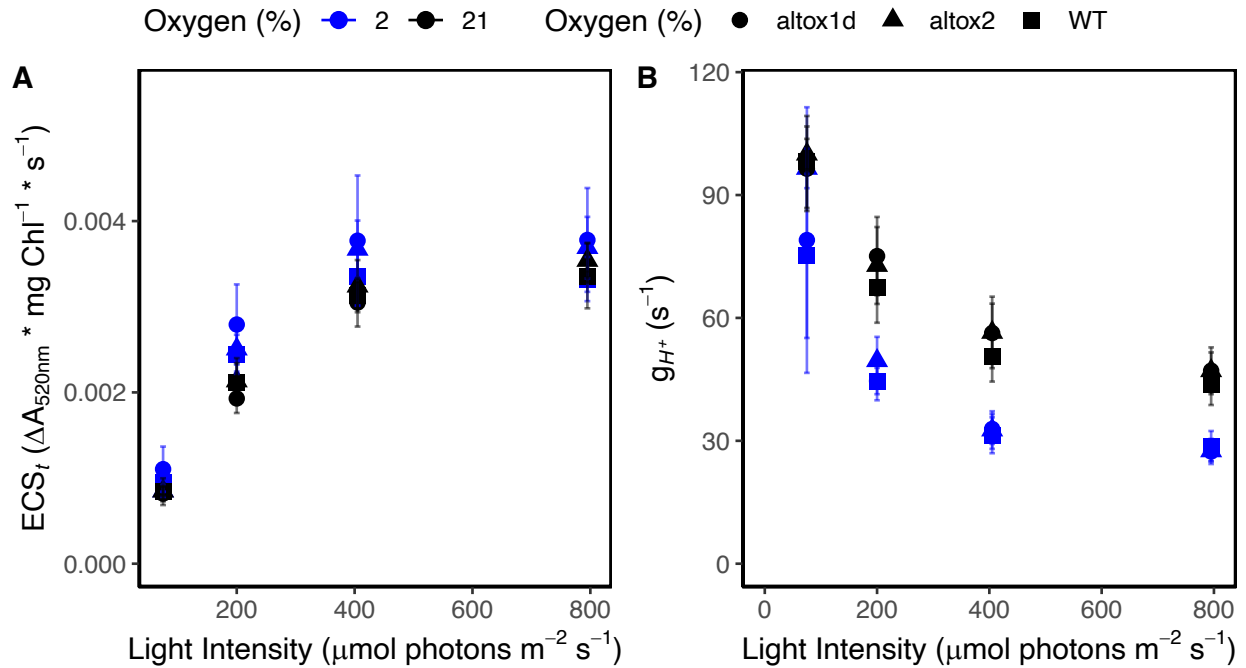


Figure 3.5. The response of the proton circuit to altered photorespiratory flux in alternative oxidase mutants. A) The total extent of *pmf* (as measured by ECS_t) and B) the response of ATP synthase kinetics as measured by the rate constant of transthylakoid proton efflux (g_{H^+}). Plants were measured at 2% and 21% O₂ with 400 ppm CO₂ as a steady state function of light intensity. Shown are the means \pm SD ($n = 4$).

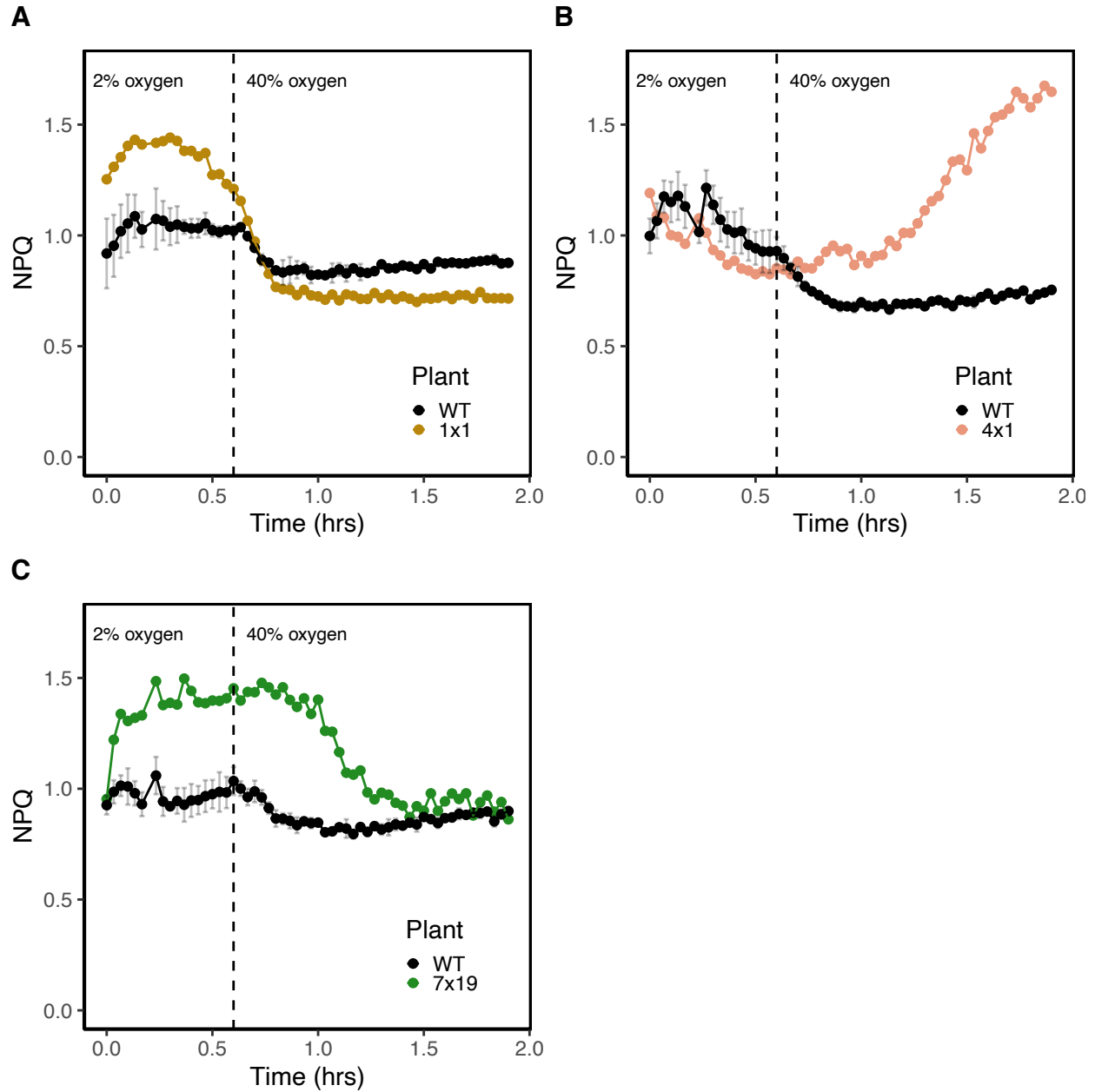


Figure 3.6. Deviations in the NPQ response to an O₂ transient in selected EMS mutants. NPQ was measured over the course of two hours where after 40 min at 2% O₂ the O₂ concentration was changed to 40% O₂. The colored lines represent the individual mutagenized plant selected from different screens. The black line represents the WT used in the corresponding screen. Mean \pm SD, n = 3 for WT.

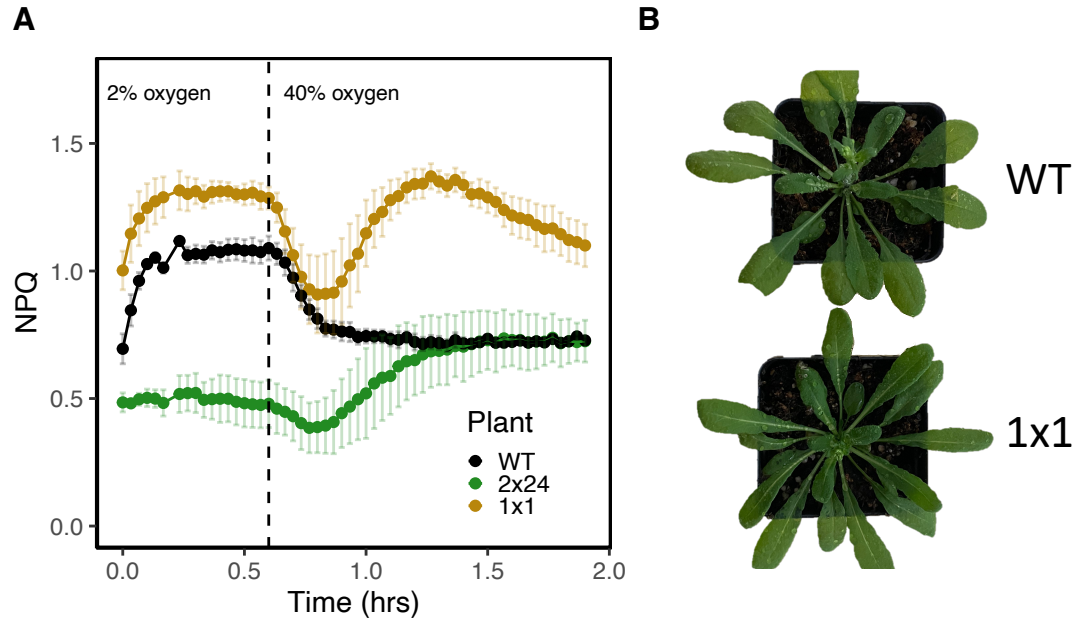


Figure 3.7. Replication of the identified EMS mutations in the M3 line. Displayed is the A) Replication of the identified phenotypes in the M3 generation. Additionally, the B) comparison of growth between 1x1 mutant and WT. NPQ was measured over the course of two hours where after 40 min at 2% O₂ the O₂ concentration was changed to 40% O₂. The green line and yellow lines represent the identified EMS lines named “1x1” and “2x24”. The black line represents the WT used in the corresponding screen. Mean ± SD, n = 4 for WT and 1x1. Mean ± SD, n = 2 for 2x24.

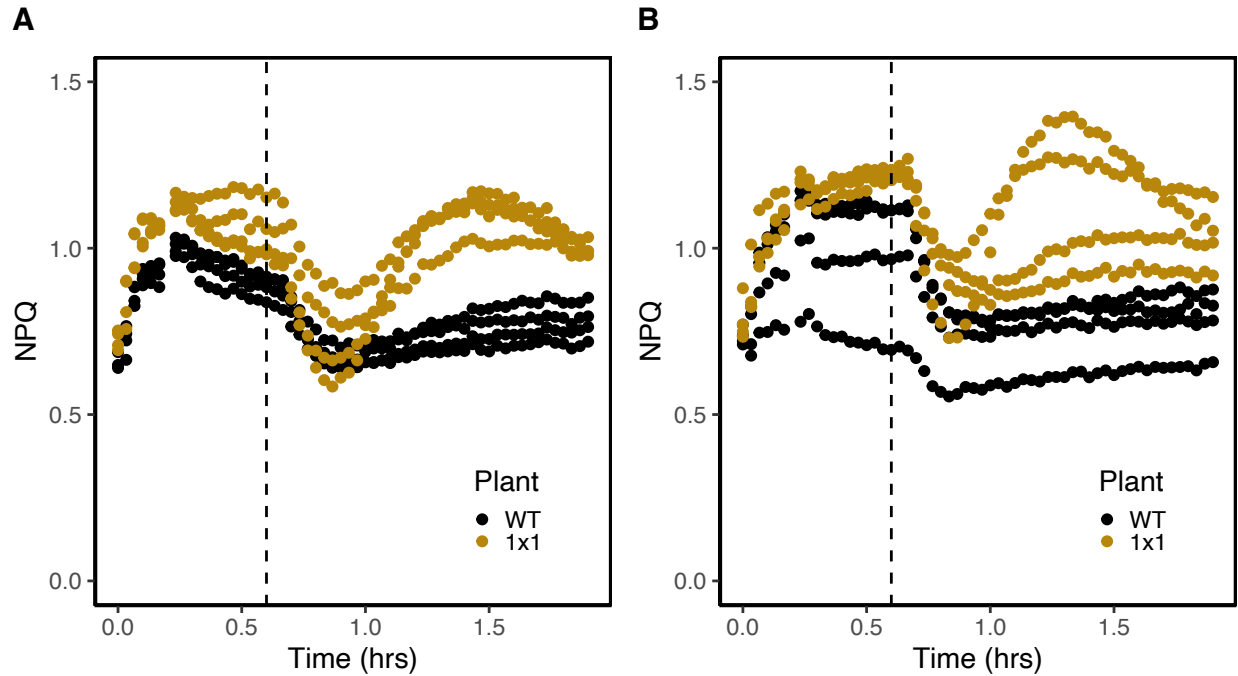


Figure 3.8. Variation in the line 1x1 and WT phenotypes observed when screening F2. For both A) and B) displayed are the positive and negative controls utilized in different F2 screen where the WT and 1x1 are positive and negative, respectively. NPQ was measured over the course of two hours where after 40 min at 2% O₂ the O₂ concentration was changed to 40% O₂. Shown in yellow and black are the individual replicates for 1x1 and WT, respectively.

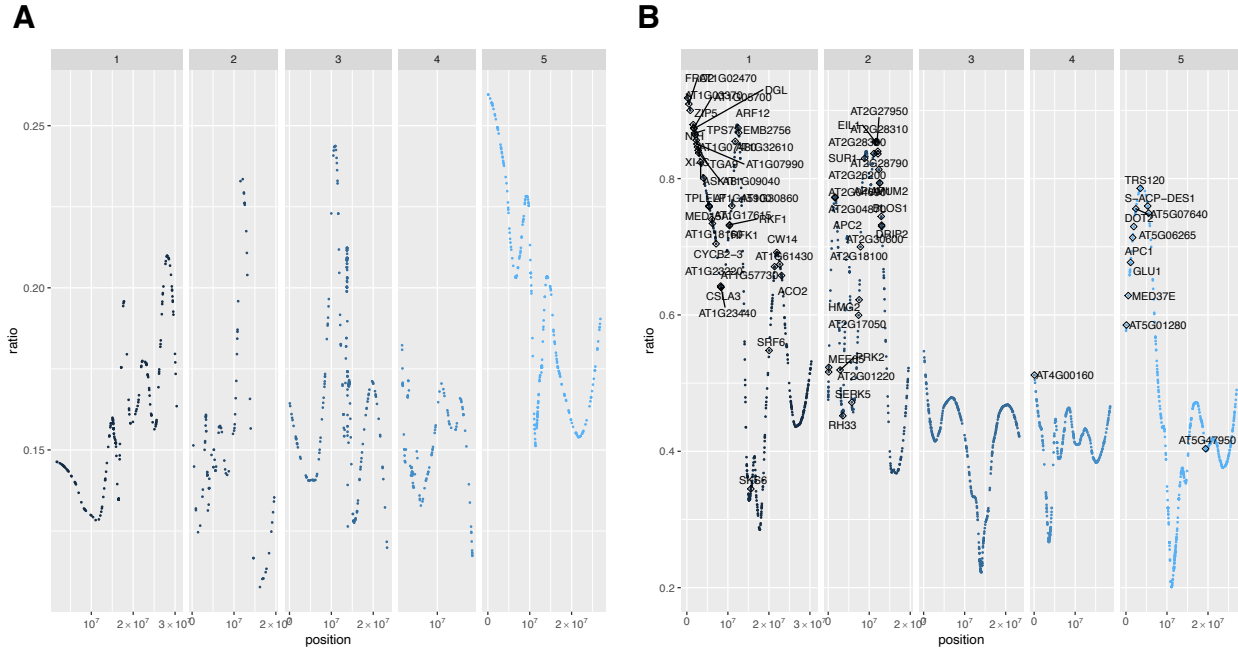


Figure 3.9. Allele frequency ratio for mapping of EMS mutant 1x1. Displayed are the allele frequency ratios across the chromosomal locations when comparing A) the positive and negative M2 populations and B) the M3 and WT. The strongest candidates are labeled with text.

Table 3.1. The strongest identified EMS candidates. Shown are the strongest candidate genes for the line “1x1” when comparing the M3 and the WT. Candidates were selected based on the allele frequency ratio in addition to having a significant effect on the protein.

Chromosome	Position	Reference	Alternate	Mutation effect	Gene name	Locus
1	211113	G	A	Missense variant	FRO2	AT1G01580
1	513503	G	A	Missense variant	AT1G02470	AT1G02470
1	832541	G	A	Missense variant	AT1G03370	AT1G03370
1	1545508	G	A	Missense variant	ZIP5	AT1G05300
1	1711313	G	A	Missense variant	AT1G05700	AT1G05700
1	1742039	G	A	Missense variant	DGL	AT1G05800
1	1957193	G	A	Missense variant	TPS7	AT1G06410
1	2045076	G	A	Missense variant	NIH	AT1G06670
1	2298868	G	A	Missense variant	AT1G07480	AT1G07480
1	2480731	G	A	Missense variant	AT1G07990	AT1G07990
1	2623723	G	A	Missense variant	TGA9	AT1G08320
1	2787047	G	A	Missense variant	XI-C	AT1G08730
1	2914903	G	A	Missense variant	AT1G09040	AT1G09040
1	3355774	G	A	Missense variant	ASK18	AT1G10230
1	4090297	G	A	Missense variant	ELP	AT1G12090
1	5418756	G	A	Missense variant	TPL	AT1G15750
1	5432571	G	A	Missense variant	MED15A	AT1G15780
1	5464397	G	A	Stop gained	AT1G15900	AT1G15900
1	6060042	G	A	Missense variant	AT1G17615	AT1G17615
1	6251842	G	A	Missense variant	AT1G18160	AT1G18160
1	7135204	C	T	Missense variant & splice region variant	CYCB2-3	AT1G20610
1	8242779	C	T	Missense variant	AT1G23220	AT1G23220
1	8321955	C	T	Missense variant	AT1G23440	AT1G23440
1	8335173	C	T	Missense variant	CSLA3	AT1G23480
1	10395274	C	T	Missense variant	RFK1	AT1G29720
1	10415268	C	T	Missense variant	RKF1	AT1G29750
1	10986766	C	T	Missense variant	AT1G30860	AT1G30860
1	11795908	C	T	Missense variant	AT1G32610	AT1G32610
1	12511345	C	T	Missense variant	ARF12	AT1G34310
1	12649478	C	T	Missense variant & splice region variant	EMB2756	AT1G34550
1	15605159	C	T	Missense variant & splice region variant	SKS6	AT1G41830
1	20064122	C	T	Stop gained	SRF6	AT1G53730
1	21380952	C	T	Missense variant	AT1G57730	AT1G57730
1	21922231	C	T	Missense variant	CW14	AT1G59650
1	22665905	C	T	Missense variant	AT1G61430	AT1G61430
1	23084019	C	T	Missense variant	ACO2	AT1G62380
2	124894	G	A	Missense variant	AT2G01220	AT2G01220
2	145918	G	A	Missense variant	MEE65	AT2G01280
2	1625980	G	A	Missense variant	APC2	AT2G04660
2	1645918	G	A	Stop gained	AT2G04690	AT2G04690
2	1716187	C	T	Missense variant	AT2G04870	AT2G04870
2	2014373	G	A	Missense variant	AT2G05500	AT2G05500
2	2916790	G	A	Missense variant	PRK2	AT2G07040
2	3579727	G	A	Missense variant	RH33	AT2G07750
2	5753960	G	A	Missense variant	SERK5	AT2G13800
2	7414281	G	A	Missense variant	AT2G17050	AT2G17050
2	7550382	G	A	Missense variant	HMG2	AT2G17370
2	7869827	G	A	Missense variant	AT2G18100	AT2G18100
2	8879983	G	A	Missense variant	SUR1	AT2G20610
2	8945990	G	A	Missense variant	GCL2	AT2G20770
2	11155265	G	A	Missense variant	AT2G26200	AT2G26200
2	11547356	G	A	Missense variant	EIL1	AT2G27050
2	11901030	G	A	Stop gained	AT2G27950	AT2G27950
2	12086547	G	A	Missense variant	AT2G28310	AT2G28310
2	12126862	G	A	Missense variant	AT2G28360	AT2G28360
2	12354717	G	A	Missense variant	AT2G28790	AT2G28790
2	12548064	G	A	Missense variant	APUM2	AT2G29190
2	12553178	G	A	Missense variant	APUM1	AT2G29200
2	12929634	C	T	Missense variant	BLOS1	AT2G30330
2	13026535	C	T	Missense variant	DRIP2	AT2G30580
2	13038915	G	A	Missense variant	AT2G30600	AT2G30600
4	64317	C	T	Missense variant	AT4G00160	AT4G00160
5	114782	G	A	Stop gained	AT5G01280	AT5G01280
5	554302	G	A	Missense variant	MED37E	AT5G02500
5	1130822	G	A	Missense variant	GLU1	AT5G04140
5	1645726	G	A	Missense variant	APC1	AT5G05560
5	1906722	G	A	Missense variant	AT5G06265	AT5G06265
5	2415502	G	A	Missense variant	AT5G07640	AT5G07640
5	3496724	G	A	Missense variant & splice region variant	TRS120	AT5G11040
5	5309571	G	A	Missense variant	S-ACP-DES1	AT5G16240
5	5520488	G	A	Missense variant	DOT2	AT5G16780
5	19417955	G	A	Missense variant	AT5G47950	AT5G47950

LITERATURE CITED

- ADDO-QUAYE, C., BUESCHER, E., BEST, N., CHAIKAM, V., BAXTER, I. & DILKES, B. P. 2017. Forward Genetics by Sequencing EMS Variation-Induced Inbred Lines. *G3 (Bethesda)*, 7, 413-425.
- AVENSON, T. J., CRUZ, J. A. & KRAMER, D. M. 2004. Modulation of energy-dependent quenching of excitons in antennae of higher plants. *Proceedings of the National Academy of Sciences*, 101, 5530-5535.
- BAKER, N. R. 2008. Chlorophyll fluorescence: a probe of photosynthesis in vivo. *Annu. Rev. Plant Biol.*, 59, 89-113.
- COSCHIGANO, K. T., MELO-OLIVEIRA, R., LIM, J. & CORUZZI, G. M. 1998. Arabidopsis gls mutants and distinct Fd-GOGAT genes. Implications for photorespiration and primary nitrogen assimilation. *Plant Cell*, 10, 741-52.
- CRUZ, J. A., SAVAGE, L. J., ZEGARAC, R., HALL, C. C., SATOH-CRUZ, M., DAVIS, G. A., KOVAC, W. K., CHEN, J. & KRAMER, D. M. 2016. Dynamic environmental photosynthetic imaging reveals emergent phenotypes. *Cell Systems*, 2, 365-377.
- EISENHUT, M., BRÄUTIGAM, A., TIMM, S., FLORIAN, A., TOHGE, T., FERNIE, A. R., BAUWE, H. & WEBER, A. P. M. 2017. Photorespiration Is Crucial for Dynamic Response of Photosynthetic Metabolism and Stomatal Movement to Altered CO₂ Availability. *Mol Plant*, 10, 47-61.
- FU, X. & WALKER, B. J. 2022. Dynamic Response of Photorespiration in Fluctuating Light Environments. *Journal of Experimental Botany*.
- GANDIN, A., DUFFES, C., DAY, D. A. & COUSINS, A. B. 2012. The Absence of Alternative Oxidase AOX1A Results in Altered Response of Photosynthetic Carbon Assimilation to Increasing CO₂ in Arabidopsis thaliana. *Plant and Cell Physiology*, 53, 1627-1637.
- GUAN, X. & GU, S. 2009. Photorespiration and photoprotection of grapevine (*Vitis vinifera* L. cv. Cabernet Sauvignon) under water stress. *Photosynthetica*, 47, 437-444.
- HALL, C. C., CRUZ, J., WOOD, M., ZEGARAC, R., DEMARS, D., CARPENTER, J., KANAZAWA, A. & KRAMER, D. 2013. Photosynthetic measurements with the idea spec: an integrated diode emitter array spectrophotometer/fluorometer. *Photosynthesis Research for Food, Fuel and the Future*. Springer.
- HANGARTER, R. P. & GOOD, N. E. 1982. Energy thresholds for ATP synthesis in chloroplasts. *Biochimica et Biophysica Acta (BBA)-Bioenergetics*, 681, 397-404.
- HENRY, I. M., NAGALAKSHMI, U., LIEBERMAN, M. C., NGO, K. J., KRASILEVA, K. V., VASQUEZ-GROSS, H., AKHUNOVA, A., AKHUNOV, E., DUBCOVSKY, J., TAI, T. H. & COMAI, L. 2014. Efficient Genome-Wide Detection and Cataloging of EMS-

- Induced Mutations Using Exome Capture and Next-Generation Sequencing. *Plant Cell*, 26, 1382-1397.
- KAISER, E., CORREA GALVIS, V. & ARMBRUSTER, U. 2019. Efficient photosynthesis in dynamic light environments: a chloroplast's perspective. *Biochemical Journal*, 476, 2725-2741.
- KEYS, A., BIRD, I., CORNELIUS, M., LEA, P., WALLSGROVE, R. M. & MIFLIN, B. 1978. Photorespiratory nitrogen cycle. *Nature*, 275, 741-743.
- KEYS, A. J. 2006. The re-assimilation of ammonia produced by photorespiration and the nitrogen economy of C3 higher plants. *Photosynth Res*, 87, 165-75.
- KOZAKI, A. & TAKEBA, G. 1996. Photorespiration protects C3 plants from photooxidation. *Nature*, 384, 557-560.
- KRAMER, D. M. & EVANS, J. R. 2011. The importance of energy balance in improving photosynthetic productivity. *Plant Physiol*, 155, 70-8.
- KULHEIM, C., ÅGREN, J. & JANSSON, S. 2002. Rapid regulation of light harvesting and plant fitness in the field. *Science*, 297, 91-93.
- LI, J., TIETZ, S., CRUZ, J. A., STRAND, D. D., XU, Y., CHEN, J., KRAMER, D. M. & HU, J. 2019. Photometric screens identified Arabidopsis peroxisome proteins that impact photosynthesis under dynamic light conditions. *The Plant Journal*, 97, 460-474.
- LI, X.-P., MÜLLER-MOULÉ, P., GILMORE, A. M. & NIYOGI, K. K. 2002. PsbS-dependent enhancement of feedback de-excitation protects photosystem II from photoinhibition. *Proceedings of the National Academy of Sciences*, 99, 15222-15227.
- LORIAUX, S., AVENSON, T., WELLES, J., MCDERMITT, D., ECKLES, R., RIENSCHKE, B. & GENTY, B. 2013. Closing in on maximum yield of chlorophyll fluorescence using a single multiphase flash of sub-saturating intensity. *Plant, cell & environment*, 36, 1755-1770.
- LU, C., LIU, X., TANG, Y., FU, Y., ZHANG, J., YANG, L., LI, P., ZHU, Z. & DONG, P. 2023. A comprehensive review of TGA transcription factors in plant growth, stress responses, and beyond. *International Journal of Biological Macromolecules*, 128880.
- MIYAKE, C. 2010. Alternative electron flows (water–water cycle and cyclic electron flow around PSI) in photosynthesis: molecular mechanisms and physiological functions. *Plant and Cell Physiology*, 51, 1951-1963.
- MULLER, P., LI, X. P. & NIYOGI, K. K. 2001. Non-photochemical quenching. A response to excess light energy. *Plant Physiol*, 125, 1558-66.

- NIYOGI, K. K., BJORKMAN, O. & GROSSMAN, A. R. 1997. Chlamydomonas Xanthophyll Cycle Mutants Identified by Video Imaging of Chlorophyll Fluorescence Quenching. *The Plant Cell*, 9, 1369-1380.
- NOCTOR, G. & FOYER, C. H. 1998. A re-evaluation of the ATP :NADPH budget during C3 photosynthesis: a contribution from nitrate assimilation and its associated respiratory activity? *Journal of Experimental Botany*, 49, 1895-1908.
- OSEI-BONSU, I., MCCLAIN, A. M., WALKER, B. J., SHARKEY, T. D. & KRAMER, D. M. 2021. The roles of photorespiration and alternative electron acceptors in the responses of photosynthesis to elevated temperatures in cowpea. *Plant Cell Environ*, 44, 2290-2307.
- QUEVAL, G., ISSAKIDIS-BOURGUET, E., HOEBERICHTS, F. A., VANDORPE, M., GAKIÈRE, B., VANACKER, H., MIGINIAC-MASLOW, M., VAN BREUSEGEM, F. & NOCTOR, G. 2007. Conditional oxidative stress responses in the Arabidopsis photorespiratory mutant *cat2* demonstrate that redox state is a key modulator of daylength-dependent gene expression, and define photoperiod as a crucial factor in the regulation of H₂O₂-induced cell death. *The Plant Journal*, 52, 640-657.
- SACKSTEDER, C. A. & KRAMER, D. M. 2000. Dark-interval relaxation kinetics (DIRK) of absorbance changes as a quantitative probe of steady-state electron transfer. *Photosynthesis research*, 66, 145-158.
- SCHEIBE, R. 2004. Malate valves to balance cellular energy supply. *Physiologia plantarum*, 120, 21-26.
- SELINSKI, J. & SCHEIBE, R. 2014. Lack of malate valve capacities lead to improved N-assimilation and growth in transgenic *A. thaliana* plants. *Plant Signal Behav*, 9, e29057.
- SELINSKI, J. & SCHEIBE, R. 2019. Malate valves: old shuttles with new perspectives. *Plant Biology*, 21, 21-30.
- SMITH, K., STRAND, D. D., KRAMER, D. M. & WALKER, B. J. 2023. The role of photorespiration in preventing feedback regulation via ATP synthase in *Nicotiana tabacum*. *Plant, Cell & Environment*.
- SOMERVILLE, C. 1984. analysis of photosynthetic carbon dioxide fixation and photorespiration by mutant selection. *Oxford surveys of plant molecular and cell biology*.
- STRAND, D. D. & WALKER, B. J. 2023. Energetic considerations for engineering novel biochemistries in photosynthetic organisms. *Front Plant Sci*, 14, 1116812.
- SUN, Y., YAO, Z., YE, Y., FANG, J., CHEN, H., LYU, Y., BROAD, W., FOURNIER, M., CHEN, G., HU, Y., MOHAMMED, S., LING, Q. & JARVIS, R. P. 2022. Ubiquitin-based pathway acts inside chloroplasts to regulate photosynthesis. *Science Advances*, 8, eabq7352.

- TIMM, S., NUNES-NESE, A., PARNIK, T., MORGENTHAL, K., WIENKOOP, S., KEERBERG, O., WECKWERTH, W., KLECZKOWSKI, L. A., FERNIE, A. R. & BAUWE, H. 2008. A cytosolic pathway for the conversion of hydroxypyruvate to glycerate during photorespiration in Arabidopsis. *The Plant Cell*, 20, 2848-2859.
- VANLERBERGHE, G. C. 2013. Alternative oxidase: a mitochondrial respiratory pathway to maintain metabolic and signaling homeostasis during abiotic and biotic stress in plants. *Int J Mol Sci*, 14, 6805-47.
- VON BISMARCK, T., WENDERING, P., PEREZ DE SOUZA, L., RUS, J., STRANDBERG, L., HEYNEKE, E., WALKER, B. J., SCHÖTTLER, M. A., FERNIE, A. R., NIKOLOSKI, Z. & ARMBRUSTER, U. 2023. Growth in fluctuating light buffers plants against photorespiratory perturbations. *Nature Communications*, 14, 7052.
- WACHSMAN, G., MODLISZEWSKI, J. L., VALDES, M. & BENFEY, P. N. 2017. A SIMPLE Pipeline for Mapping Point Mutations *Plant Physiology*, 174, 1307-1313.
- WALKER, B. J., KRAMER, D. M., FISHER, N. & FU, X. 2020. Flexibility in the energy balancing network of photosynthesis enables safe operation under changing environmental conditions. *Plants*, 9, 301.
- WALKER, B. J., VANLOOKE, A., BERNACCHI, C. J. & ORT, D. R. 2016. The Costs of Photorespiration to Food Production Now and in the Future. *Annu Rev Plant Biol*, 67, 107-29.
- YUDINA, R. S. 2012. Malate dehydrogenase in plants: Its genetics, structure, localization and use as a marker. *Advances in Bioscience and Biotechnology*, 3, 370-377.

CHAPTER 4:

The acclimatory response to periods with altered ATP:NADPH demand

Kaila Smith, Larry Wu, Xinyu Fu, Polly Hsu and Berkley J. Walker

Abstract

For photosynthesis to operate efficiently and without the risk of photodamage it requires a balance between the ATP and reductant (referred to in terms of NADPH) supplied from the light reactions with the demand from metabolism. The exact ATP:NADPH demand from metabolism is dynamic and depends on flux through specific metabolic pathways which respond to the surrounding environment. These periods with altered metabolic demands can be prolonged during periods such as drought and impact photosynthetic efficiency which ultimately poses the question as to how the plant acclimates to periods with both increased and decreased ATP:NADPH demand. To answer this question, we first examined the response of the light reactions over a 7-hour period at both 2% and 40% O₂ which decreased and increased ATP:NADPH demand, respectively. We found photosynthetic efficiency (ϕ_{II}) did restore to initial levels after approximately 4 hours at 2% O₂ but not at 40% O₂. To investigate mechanisms driving these responses, we characterized the transcriptional response early (1 hour) and later (7 hours) in the 7-hour period. There were little overall changes in the transcriptional response after 1 hour. After 7 hours, there was a strong response of the transcriptome at 2%, however, most of the genes were not related to photosynthetic processes. As the transcriptome and proteome are not necessarily correlated, we next characterized the proteomic response after 7 hours and found an increased abundance in numerous photosynthetic-related proteins at both 2% and 40% O₂. These more highly abundant proteins, together with the lack of transcriptional response, suggest the regulatory response to periods with altered ATP:NADPH demand could involve post-translational modifications which could improve protein stability.

Introduction

The energy costs associated with downstream rubisco activity explains much of the energy demand from metabolism in plants. The carboxylation of rubisco drives carbon assimilation in photosynthetic organisms by initiating the first step of the C₃ cycle. Each carboxylation reaction produces two molecules of 3-phosphoglycerate (3PGA) which are metabolized by the C₃ cycle to either regenerate RuBP or be exported as triose phosphates for starch and sucrose biosynthesis. The C₃ cycle requires 3 ATP and 2 NADPH per CO₂ fixed by rubisco. Rubisco additionally catalyzes the oxygenation of RuBP which produces a molecule of 2-phosphoglycolate (2PG) alongside a molecule of 3PGA (Bowes et al., 1971). The 2PG is a potent inhibitor of several C₃ cycle enzymes and is therefore recycled into 3PGA through a series of reactions known as photorespiration (Anderson, 1971, Flügel et al., 2017, Kelly and Latzko, 1976). During the photorespiratory cycle, the process consumes 3.5 ATP and 2 reductant (referred to later in terms of NADPH for simplicity). Note that these demands assume steady-state processing of photorespiratory intermediates and the export of either glycine or serine from the photorespiratory cycle can additionally decrease these demands (Fu et al., 2023, Fu and Walker, 2022, Harley and Sharkey, 1991a, Busch et al., 2018).

The ATP and reductant required by metabolism is mostly provided by linear electron flow (LEF) through the light reactions. However, the situation is complicated by the fact that LEF produces a fixed stoichiometry of ~1.33 ATP:NADPH which is less than what is demanded by metabolism generating an ATP deficit (Kramer and Evans, 2010, Walker et al., 2020). The exact value of ATP:NADPH demanded by metabolism varies based mostly on the flux through the C₃ cycle and photorespiration (Foyer et al., 2012). The C₃ cycle and photorespiration demand 1.5 and 1.75 ATP:NADPH, respectively, and flux through the C₃ cycle and photorespiration varies

based on environmental conditions (for example light and temperature) meaning the demand will be somewhere in that range depending on the flux through these pathways (Long et al., 1993, Farquhar et al., 1980, Noctor and Foyer, 1998). Mechanisms exist to correct the imbalance between LEF and metabolism including cyclic electron flow (CEF), the malate valve, and the water-water cycle (Scheibe, 2004, Miyake, 2010, Kramer and Evans, 2010). However, how the plants might deploy these or other as-yet undescribed mechanisms in the long-term in response to changes in ATP:NAPH demand is unclear (Walker et al., 2020). For example, after transfer to sustained high light expression and protein levels of malate dehydrogenase increases suggesting an increased capacity of the malate valve under high light (Becker et al., 2006). Similarly, protein content for proteins involved with different CEF pathways change under different growth conditions (Alric et al., 2005).

The role of photorespiration within the energetic landscape is an evolving area of research. Some experiments have been interpreted to indicate that the reductant consumption from photorespiration provides a photoprotective function by dissipating “excess” photochemical energy and preventing damage to the photosystems (Guan et al., 2004, Guan and Gu, 2009, Kozaki and Takeba, 1996). This idea is challenged by an alternative model where the primary link between photorespiration and the light reactions are that the additional ATP consumption helps prevent feedback regulation from ATP synthase (Smith et al., 2023). This phenomenon is associated with a decrease in photosynthetic efficiency (ϕ_{II}) and proposed to occur because the plant does not relax alternative ATP generating pathway(s) leading to the inability to turnover excess ATP which leads to substrate limitation of ATP synthase. Additionally, the energetic costs and CO₂ release make photorespiration an attractive target for metabolic engineering and crop improvement with several strategies already being implemented in plants (Kebeish et al., 2007,

South et al., 2019, Maier et al., 2012). These strategies are expected to alter the ATP and reductant demands of photorespiration (Peterhansel et al., 2013b). Together, this raises the question of how the plants might acclimate to situations where ATP and reductant consumption are altered over prolonged periods of time? The answer to this question is important for not only informing bioengineering strategies but also for answering fundamental questions in leaf energetics.

Here, we characterize the short-term acclimatory response to periods (1-7 hours) under altered ATP:NADPH demand. First, we examined whether the decrease in ϕ_{II} associated with altered ATP:NADPH demand could restore over a 7 hour period and found that at 2% O₂ ϕ_{II} restored to ambient levels but at 40 O₂ it did not. To identify processes potentially driving the acclimatory response observed at 2% O₂, the response of the transcriptome was measured at the beginning of the acclimatory period (1 hour) and at the end (7 hours). However, there were little changes to the transcriptome after 1 hour. While there were a number of genes differentially expressed after 7 hours, most of the genes were not related photosynthetic processes. As the transcriptome and proteome are not often correlated, we then examined the proteomic response after 7 hours. Unlike the transcriptome, there was increased abundance in numerous photosynthetic-related proteins. These more highly abundant proteins, together with the lack of transcriptional response, suggest the regulatory response to periods with altered ATP:NADPH demand could involve post-translational modifications which could improve protein stability.

Materials and methods

Material and growth

All experiments were performed using the *Arabidopsis thaliana* ecotype Columbia-0 on plants with fully grown rosettes just prior to bolting. All plants were grown in soil under a 12/12 day/night cycle at $\sim 100 \mu\text{mol photons m}^{-2} \text{s}^{-1}$ at 21/16°C day/night and 60% humidity.

Chlorophyll a fluorescence imaging

Pulse-amplitude modulated chlorophyll *a* fluorescence was measured in a dynamic environmental photosynthesis imager which is used for imaging chlorophyll *a* fluorescence (Cruz et al., 2016). A custom chamber was built which allows imaging as well as manipulation of the O₂, N₂, and CO₂ atmosphere using mass flow controllers connected to cylinders of CO₂ and O₂, with N₂ produced in a N₂ generator (Genuis 1053 230V, Peak Scientific). The chamber top was angled (resembling the roof of a house) and the dimensions were 63.5 cm x 33 cm x 18 cm for the base with a 20° angle between the base and rafter with the ability to screen a standard flat of plants (PLAS-LABS, East Lansing, MI, USA). Plants were dark adapted within the chamber at the corresponding O₂ concentration for 30 min prior to the initial saturating pulse. Image capture protocols were then taken every 2 min for 7 hours to measure ϕ_{II} and NPQ using standard saturation pulse chlorophyll fluorescence and raw images were processed in Visual Phenomics [described in (Cruz et al., 2016, Baker, 2008)]. Measurements were taken under $300 \mu\text{mol photons m}^{-2} \text{s}^{-1}$. This time course was repeated on 3 consecutive days at 2%, 21%, and 40% O₂ with new plants each day and the order of the conditions were randomly generated. The protocol was repeated to harvest leaf tissue for transcriptome and proteome analysis where the time course was either stopped after 1 or 7 hours for sampling. The sampling was performed over 6 consecutive days at 2%, 21%, and 40% O₂ and either removed after 1 or 7 hours again with new

plants being utilized each day and the order of the conditions randomly generated. Plants were rapidly removed from the chamber and the entire rosette was collected and flash frozen in liquid N₂ within a few minutes of opening the chamber.

RNA extraction and sequencing

RNA was extracted for sequencing (Quick-RNA Plant Kit, Zymo Research) and treated for DNase (DNase I Kit, Zymo Research) according to manufacturer's instructions and then the RNA integrity number was measured for each sample to ensure intact RNA prior to library preparation. Ribosomal RNA was then depleted (QIAseq FastSelect – rRNA Plant Kit, Qiagen) and sequencing libraries were prepared from depleted samples (Stranded Total RNA Library Kit with IDT for Illumina Unique Dual Index adapters, Illumina) following manufacturer's recommendations except with half reaction volumes. Completed libraries were checked for quality control and quantified using a combination of assays (dsDNA HS, Qubit) (TapeStation HS DNA1000, Agilent). The libraries were combined in equimolar amounts for multiplexed sequencing, and the pool was quantified (Collibri Quantification qPCR kit, Invitrogen). The pool was loaded onto one lane of a flow cell (NovaSeq 6000 SP flow cell, Illumina) and sequencing was performed in a 2x150bp paired end format (NovaSeq 6000 v1.5, Illumina).

RNA data analysis

Adaptor sequences attached during library preparation were removed using trimmomatic v0.39 with the following parameters: ILLUMINACLIP:\$Adapters:2:40:15 SLIDINGWINDOW:4:20 MINLEN:50 (the \$Adapters is the path to the adaptor file NexteraPE-PE.fa (Bolger et al., 2014). The paired-end sequence files were quantified with Kallisto v0.46.1 based on Araport11 annotation (Bray et al., 2016, Cheng et al., 2017). The -b 100 parameter was used for kallisto quant step for carrying out 100 bootstrap steps. The kallisto results were

imported to R v4.2.1 by the tximport package and analyzed by the DESeq2 package with Wald test (Soneson et al., 2015, Love et al., 2014). Only genes with greater than 30 total pseudo counts from all samples were considered. The GO term analysis was done with agriGO v2.0 (Tian et al., 2017).

Total protein leaf extraction

Total protein extraction was performed as previously described with modifications adapted to plant tissues (Humphrey et al., 2018). Frozen leaves were homogenized under cryogenic conditions (FastPrep-24 instrument with a CoolPrep Adapter, MP biomedical, Irvine, CA, USA) and dry ice. Ground tissues were suspended in cold sodium deoxycholate (SDC) lysis buffer (100 mM Tris-HCl, pH 8.5, 4% [w/v] sodium deoxycholate). The lysates were immediately heat-treated at 95°C for 10 min and then homogenized with sonication (6 cycles of 5s on and 5s off at 80% output power). Samples were centrifuged for 20 min at 10,000g and 4°C, and supernatants containing the total protein extract were collected. Protein concentration was determined using the BCA method (Pierce BCA Protein Assay Kit, 23227, Thermo Scientific).

Proteolytic digestion

Protein samples (100ug) were mixed with 100mM Tris-HCl (pH 8.5) supplemented to 4% (w/v) sodium deoxycholate (SDC), reduced and alkylated by adding TCEP and chloroacetamide at 10mM and 40mM, respectively, and incubated for 5min at 45C with shaking at 2000 rpm (ThermoMixer C, Eppendorf, Germany). Trypsin, in 50mM ammonium bicarbonate, was added at a 1:100 ratio (wt/wt) and the mixture was incubated at 37°C overnight with shaking at 1500 rpm in the Thermomixer. Final volume of each digest was ~300uL. After digestion, SDC was removed by phase extraction. The samples were acidified to 1% TFA and subjected to C18

solid phase clean up using StageTips to remove salts (Rappsilber et al., 2007). Eluted peptides were dried by vacuum centrifugation and stored at -20°C.

Isotopic/isobaric peptide labeling

Peptide samples were re-suspended in 100uL of 100mM TEAB and labeled (TMTpro reagents, Thermo Scientific) according to manufacturers' instructions. Aliquots of 2 uL were taken from each labeled sample and reserved for testing labeling/mixing efficiency by MS according to Erdjument-Bromage (Erdjument-Bromage et al., 2018). Remaining labeled peptides were then mixed and purified by solid phase extraction using C18 StageTips. Eluted peptides were dried by vacuum centrifugation and stored at -20°C.

Fractionation

The dried peptide sample was re-suspended in 2% acetonitrile/0.1% trifluoroacetic acid in water to 60uL and injected onto a column (Acquity UPLC BEH 2.1mm x 250mm C18, Waters) using an Ultra Performance Liquid Chromatography system (UPLC) (Acquity H-class UPLC, Waters). Bound peptides were washed using 100% water for 2min and then separated over 65min using a gradient of 2%B to 40%B in 53min raised to 80%B in 1min and held at 80%B for the duration of the run. Fractions were collected at 1.5min intervals (FC403B fraction collector, Gilson) and then concatenated into 12 total fractions post-run. Peptides were dried by vacuum centrifugation to ~2uL and frozen at -20°C.

LC/MS/MS analysis

Dried peptides were re-suspended in 2% acetonitrile/0.1% trifluoroacetic acid in water to 20uL. An injection of 10uL was automatically made (EASYNLC 1200, Thermo Scientific) onto a trapping column (Acclaim PepMap RSLC 0.1mm x 20mm C18, Thermo Scientific) and washed for ~5min with buffer A. Bound peptides were then eluted over 95min onto a resolving column

(Acclaim PepMap RSLC 0.075mm x 500mm, Thermo Scientific) with a linear gradient of 8%B to 42%B in 84 min at a constant flow rate of 300ul/min. After the gradient the column was washed with 90%B for 10 min (Buffer A = 99.9% Water/0.1% Formic Acid, Buffer B = 80% Acetonitrile/0.1% Formic Acid/19.9% Water). Column temperature was maintained at a constant temperature of 50°C using an integrated column oven (PRSO-V2, Sonation GmbH, Biberach, Germany). Eluted peptides were sprayed into a spectrometer (Q-Exactive HF-X, Thermo Scientific) using a FlexSpray spray ion source. Survey scans were taken in the Orbitrap (120000 resolution, determined at m/z 200) and the top 15 ions in each survey scan are then subjected to automatic higher energy collision induced dissociation with fragment spectra acquired at a resolution of 45000.

DDA data analysis

The resulting MS/MS spectra were converted to peak lists using MaxQuant and searched against a reference protein database containing all *A. thaliana* sequences available for background and appended with common laboratory contaminants (Cox and Mann, 2008, Cox et al., 2011). The output was then analyzed using Scaffold to probabilistically validate protein identifications where assignments validated using the 1%FDR confidence filter are considered true (Searle, 2010). Student's *t* test was performed to uncover differential expression between two treatments. All *p* values were adjusted by Benjamini–Hochberg correction for multiple testing at the level of 0.05. MaxQuant parameters for all databases were as follows: allow up to 2 missed tryptic sites, fixed modification of carbamidomethyl cysteine, variable modification of oxidation of methionine, deamidation of asparagine and glutamine, peptide tolerance of +/- 4.5ppm, MS/MS tolerance of 20ppm, and FDR calculated using randomized database search.

Results

Photosynthetic efficiency is restored to ambient levels at 2% O₂ but not at 40% O₂

As discussed above, ATP:NADPH demand depends on the ratio of flux through the C3 cycle and photorespiration and therefore can be manipulated by atmospheric conditions. More specifically, because changes in atmospheric conditions alter the availability of CO₂ to rubisco which impacts the relative ratio of the oxygenation to carboxylation rate (Von Caemmerer, 2013, Abadie et al., 2018). For example, at 2% O₂ the availability of CO₂ increases and as a result photorespiratory flux decreases causing a decrease in ATP:NADPH demand with the reverse true at 40% O₂. Manipulating CO₂ is sometimes considered to have similar effects as O₂ on altering photorespiration. However, we reasoned utilizing 2% O₂ rather than elevated CO₂ might serve as a stronger driver because the ATP:NADPH demand is significantly lower with O₂ compared to CO₂ (Smith et al., 2023).

To determine whether the decrease in ϕ_{II} associated with altered ATP:NADPH demand could restore over a 7 hour period, we measured ϕ_{II} at 2%, 21%, and 40 O₂. For the first 4 hours, at 2% and 40% O₂, ϕ_{II} decreased relative to ambient (21%) with the lowest values being at 40% (Figure 4.1A). At 40% O₂, ϕ_{II} remained lower than both ambient and 2% O₂ over the 7-hour time frame. Interestingly, at 2% O₂ ϕ_{II} slowly rose to reach ambient levels after around 4 hours. Ultimately, this suggests there might be an acclimatory response occurring at the 2% O₂ during the initial 4 hours.

We hypothesized the restoration in ϕ_{II} to ambient levels observed above might occur from a decrease in nonphotochemical quenching (NPQ). NPQ describes processes which dissipate excess excitation energy including but not limited to a pH-dependent form as well as photoinhibition-related form [reviewed in (Muller et al., 2001)]. Accordingly, we examined

corresponding NPQ levels over the 7-hour time frame (Figure 4.1B). After approximately 1 hour, the 2% O₂ and 40% O₂ displayed higher levels of NPQ compared to ambient. Unexpectedly, the rise in ϕ_{II} at 2% O₂ over time to reach ambient levels did not correspond with a decrease in NPQ suggesting there could be multiple factors driving the acclimatory response observed at 2% O₂.

The transcriptional response was the strongest after 7 hours at 2% O₂, however, only a small proportion of the differentially regulated genes were related to photosynthesis

To identify mechanisms possibly involved in the acclimatory response, we examined the response of the transcriptome after 1 and 7 hours at 2%, 21%, and 40% O₂. We reasoned transcriptome analysis was an effective method for dissecting what might be driving both the acclimatory response at 2% O₂ as well as the lack of response at 40% O₂. These time points were chosen specifically to capture both the period in which ϕ_{II} was rising as well as after ϕ_{II} reached ambient levels. Principle component analysis (PCA) was performed on the variance stabilized transcript data for each sample to examine the effect of both time and O₂. PCA identified time as the primary component (74%) and O₂ as the secondary (11%) (Figure 4.2A). The O₂ component was primarily driven by the 7-hour time point where the 2% O₂ samples were clearly separated from 21% and 40% O₂ samples. This suggests that the transcriptional response to altered ATP:NADPH demand began somewhere between the 1-hour and 7-hour time points. The transcriptional response after 7 hours was the strongest at 2% O₂ with 434 differentially expressed genes when compared to the compared to 21% O₂. More specifically, there were 379 significantly downregulated and 55 upregulated genes (Figure 4.2B). In comparison, the response after 7 hours at 40% O₂ was much weaker with only 106 significantly differentially expressed genes with 44 genes being downregulated and 62 upregulated. These results are consistent with the stronger acclimatory response observed in ϕ_{II} at 2% over 40% O₂.

Despite the large number of differentially expressed genes observed at 2% O₂, less than 20 were related to photosynthesis or energy related processes. Previous studies at elevated CO₂, which is thought to be comparable to low O₂, do suggest that elevated CO₂ modestly alters several photosynthetic-related genes including changes to transcripts related to the thylakoid electron transport chain, photorespiration, and carbon fixation (Gupta et al., 2005, Taylor et al., 2005, Ainsworth et al., 2006, Foyer et al., 2012). Therefore, we reasoned that some of the differentially expressed genes observed at 2% O₂ might be both related to photosynthetic processes and potentially responsible for the acclimatory response. However, only a small proportion of the differentially expressed genes at 2% O₂ were related to photosynthetic processes. More specifically, at 2% O₂ only 13 photosynthetic-related genes were downregulated and 1 upregulated when compared to the ambient condition (Figure 4.3). Additionally, these genes were mostly related to nitrogen metabolism with a few relating to carbon assimilation, photorespiration, and the light reactions. We found only 1 gene involved in starch and sucrose synthesis was downregulated at 40% O₂.

The proteomic response displayed a large proportion of photosynthetic proteins with increased abundance

Given the small proportion differentially regulated genes which were related to photosynthetic processes, it seemed unlikely a transcriptional response was driving the acclimatory response observed in ϕ_{II} at 2% O₂. Several studies have evaluated the correlation between mRNA measurements and corresponding protein measurements and report varying levels of correlation due to factors such as protein degradation and turnover (Tuller et al., 2007, Wu et al., 2008, Gygi et al., 1999). Therefore, we reasoned the proteome might reveal additional insight into a potential regulatory mechanism. We examined response of the proteome after 7

hours at 2%, 21%, and 40% O₂ to examine how photosynthetic proteins responded to altered ATP:NADPH demand. Proteomic analysis was conducted only on the 7-hour timepoint because of the minimal response in the 1-hour timepoint above. PCA was conducted on the peptide levels of each sample to identify the effect of O₂. O₂ was the secondary component (20.58%) with the primary component (50.55%) likely driven by variation in the samples (Figure 4.4A). Larger variation is often observed between samples in proteomic studies can make detecting significant changes in protein abundance difficult (Kammers et al., 2015). Therefore, a fold change cutoff for changes in protein abundance was not included to wholistically capture all possible changes in protein abundance. Unlike the transcriptional response seen above, the proteomic response was more similar between the 2% and 40% O₂ conditions (Figure 4.4B). For example, at 2% O₂ there was a total of 410 proteins with changes in abundance with 225 decreased and 185 increased. At 40% O₂, there was a total of 525 proteins with changes in abundance with 333 decreased and 192 increased. These results begin to highlight the divergent responses observed between the transcriptome and proteomes.

Unlike the transcriptome, there were numerically more changes in the abundance of photosynthetic-related proteins at both 2% and 40% O₂. Given the response from the transcriptome observed above, we reasoned there was a possibility the proteome would also have little changes in photosynthetic related proteins. However, there were a total of 70 proteins with changes in abundance between both conditions (Figure 4.5-4.6). In general, most photosynthetic-related proteins had increased abundance except for 3. Of the photosynthetic-related proteins 60% were categorically related to the light reactions at both 2% and 40% O₂.

There was little agreement between O₂-dependent differences in the transcriptome and to the proteome

Given the apparent discrepancies between the response of photosynthetic-related processes between the proteome and transcriptome, this raised the question as to how similar the responses were overall. For example, we reasoned there should be some instances where a change in a differentially expressed gene resulted in the same directional change in protein abundance under the same conditions between both datasets. However, when we compared common elements between data sets this was only true for a limited number of situations (Figure 4.7). In fact, the greatest overlap occurred between the proteins with decreased abundance under both O₂ conditions. One of the second largest overlaps occurred between proteins which with increased abundance under both O₂ conditions. Finally, the other second largest overlap occurred between genes which were oppositely upregulated at 40% and downregulated at 2% O₂. These interactions suggest more commonalities within datasets rather than across. The interactions of the specific genes and corresponding proteins in common across the datasets can be further illustrated within the heat map depicted Figure 4.8. A few of the genes included are in fact photosynthetic-related genes including rubisco activase (RCA), violaxanthin de-epoxidase 1 (VDE1), and phosphoribulokinase (PRK), however, do not display consistent expression patterns between the datasets. Overall, these interactions suggest little similarities in the expression patterns between transcriptional and proteomic response even in common elements.

Discussion

One of the primary questions raised in this study is how the plant might respond to prolonged periods with altered ATP:NADPH demand and whether the associated decrease in ϕ_{II} might restore. The decreases in ϕ_{II} at both high and low O₂ is somewhat surprising given the

opposite changes in ATP:NADPH demand and are attributed to increases in different components of NPQ (Smith et al., 2023). At 2% O₂ the decrease in ϕ_{II} results from an increase in the pH-dependent form due to a decrease in ATP synthase conductivity. Whereas, at 40% O₂ the decrease in ϕ_{II} occurs from an increase in the photoinhibition-related form. Ultimately, we did find that ϕ_{II} did increase to ambient (21%) levels and after around four hours which unexpectedly did not correspond to decreased NPQ. This suggests that there might be an increase in ϕ_{II} which does not seem to involve decreased NPQ and ultimately restoration of ATP synthase conductivity. Instead, the cause of the increased ϕ_{II} might be potentially from a change in the redox state of the acceptor side of PSII. Ultimately, this suggests that there is an acclimatory response to prolonged periods with lowered ATP:NADPH demand which potentially involves a change in the redox state of the acceptor side of PSII. There did not appear to be any adjustments in the light reactions at 40% O₂ which might be because the decrease in ϕ_{II} at 40% results from an increase in the photoinhibition-related form of NPQ rather than the pH-dependent form like at 2% O₂.

The overall upregulation of photosynthetic related proteins might be involved in the acclimatory response to altered ATP:NADPH demand. Despite the minimal transcriptional response, there were many photosynthetic proteins with increased abundance in both O₂ conditions (Figure 4.5). One interpretation of this could be that the acclimatory response the plant utilizes to respond to prolonged periods of altered ATP:NADPH demand might involve post-translational modifications which decrease protein degradation. Post-translational modifications can control a protein's stability through interactions with specific amino acids localized within regulatory domains of target proteins which either expedite or forestall protein degradation [reviewed in (Lee et al., 2023)].

Forestalling protein degradation in photosynthetic related proteins offers advantages for both O₂ conditions. For situations like at 40% O₂ where the ATP:NADPH demand is increased, photosynthetic proteins utilize approximately 50% of ATP costs associated with protein degradation and synthesis (Li et al., 2017). By potentially forestalling protein degradation when ATP:NADPH demand is increased, the ATP could then be utilized in metabolism rather than in protein degradation and synthesis. With respect to the 2% O₂, it has been shown that a reduction in photosynthetic protein abundance reduces maximal electron transport rate and because electron transport is calculated using ϕ_{II} this also likely equates to a reduction in ϕ_{II} (Violet-Chabrand et al., 2017, Pao et al., 2019). Therefore, the increased abundance of photosynthetic-related proteins might begin to explain the acclimatory response in ϕ_{II} at 2% O₂. Additionally, meta-analyses of the plant response to elevated CO₂ suggests a selective loss of rubisco compared to proteins involved in light conversion which is consistent with our data (Long et al., 2004, Ainsworth and Long, 2005). However, the log2FoldChange in abundance on all the photosynthetic-related proteins were relatively small so an alternative explanation might be that photosynthetic capacity itself is sufficient to recover without any substantial re-programming.

There was an intersection of a few comment elements related to photosynthesis between the transcriptome and proteome raising the question as to whether these might play a more active role in energy balancing. Although we observed a larger proportion of photosynthetic proteins which were not present in the transcriptome, there were a couple of intersections between the two data sets including RCA, VDE1, PRK. As seen above, the level of RCA, VDE1, and PRK were both commonly altered between both the proteome and transcriptome which presents the question as there were a select number of transcriptionally regulated genes which aid in the acclimatory response to periods with altered ATP:NADPH demand (Figure 4.7-4.8). However, as

outlined above, we reasoned if there were significant effects from transcriptional expression that the gene expression would be similarly mirrored in the protein expression which was not the case. Thus, the inconsistencies in these patterns do not suggest any significant form of regulation occurring from these specific genes. With respect to RCA, it was that the protein was more abundant at 40% whereas gene expression was downregulated at 2% O₂. In terms of VDE1, it was found that the protein was more highly abundant at both conditions whereas gene expression was downregulated at 2% O₂. Finally, gene expression of PRK was downregulated at 2% but the protein was more abundant under both conditions. While these genes still might be involved in energy balancing on a functional level, their inconsistencies in expression changes make it hard to decipher.

Conclusion

The acclimatory response observed at low O₂ to prolonged periods with altered ATP:NADPH demand is important in the context of both fundamental leaf energetics as well as metabolic engineering. For example, there is concern that novel engineering strategies which alter the ATP:NADPH demand might result in a down-regulation of photosynthetic efficiency (Strand and Walker, 2023). However, this work highlights how there might be longer term acclimatory responses the plant could use to meet new synthetic energy demands. More specifically, the evidence of the recovery of decreased ϕ_{II} at low O₂ when ATP:NADPH demand is low could indicate the regulatory mechanisms in place which will assist in the plant adapting to novel biochemical pathways. Additionally, this work suggests these regulatory mechanisms might include post-translational modifications which could decrease protein degradation.

Figures and Tables

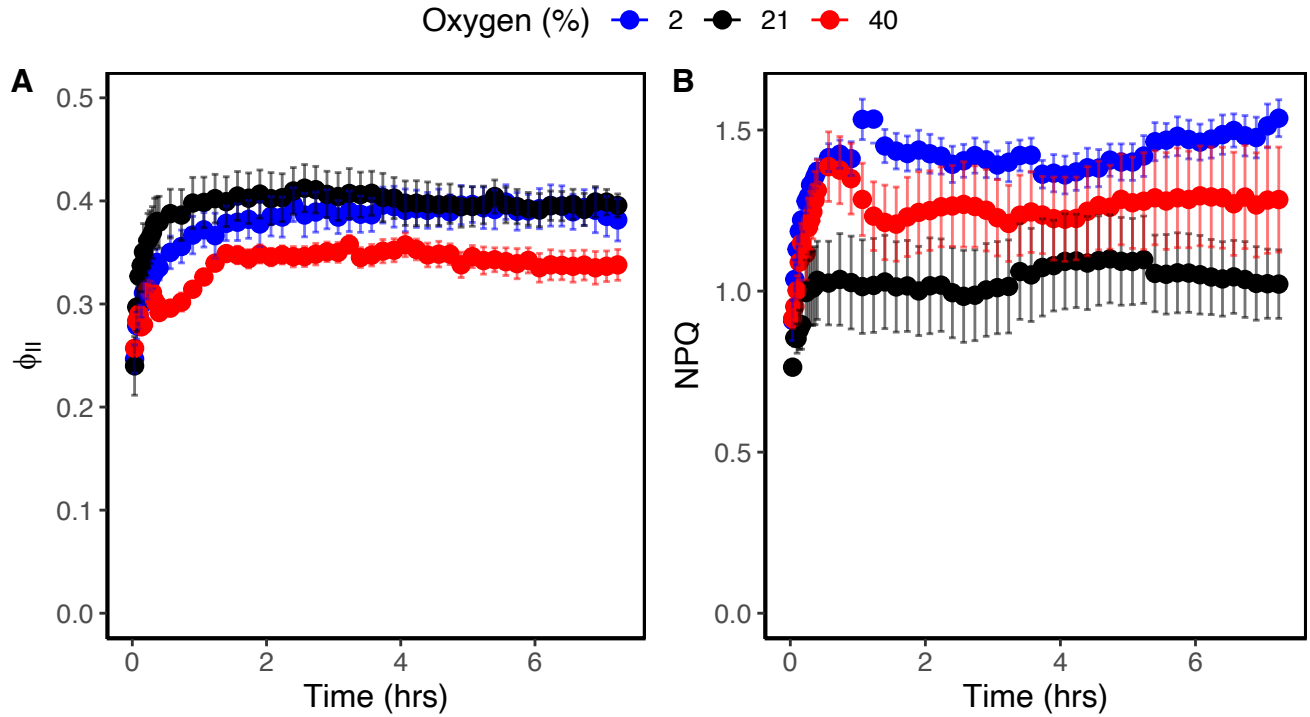


Figure 4.1. The response of the light reactions in response to changing O₂ over time. The figure displays the response of the light reactions as represented by measurements of A) photosynthetic efficiency (ϕ_{II}) and B) nonphotochemical quenching (NPQ). Plants were measured at 300 $\mu\text{mol photons m}^{-2} \text{s}^{-1}$ at 2%, 21%, and 40% O₂ with 400 ppm CO₂. Shown are the means \pm SD (n = 4).

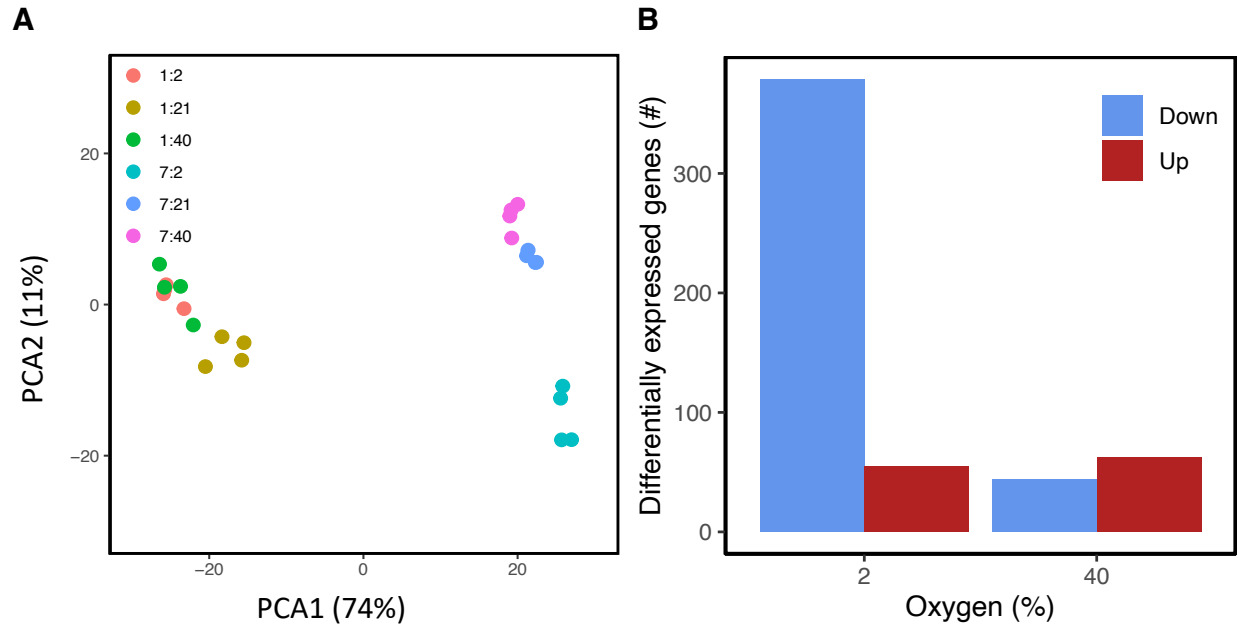


Figure 4.2. Effect of altered O₂ concentration on the transcriptome over time. The figure depicts A) principal component analysis of normalized transcript data. For the samples, the first number in the legend denotes the time (in hours) and the second number denotes the O₂ concentration (%). Additionally, B) the number of differentially expressed genes at both 2% and 40% O₂ when compared to the ambient (21%) at the 7-hour time point.

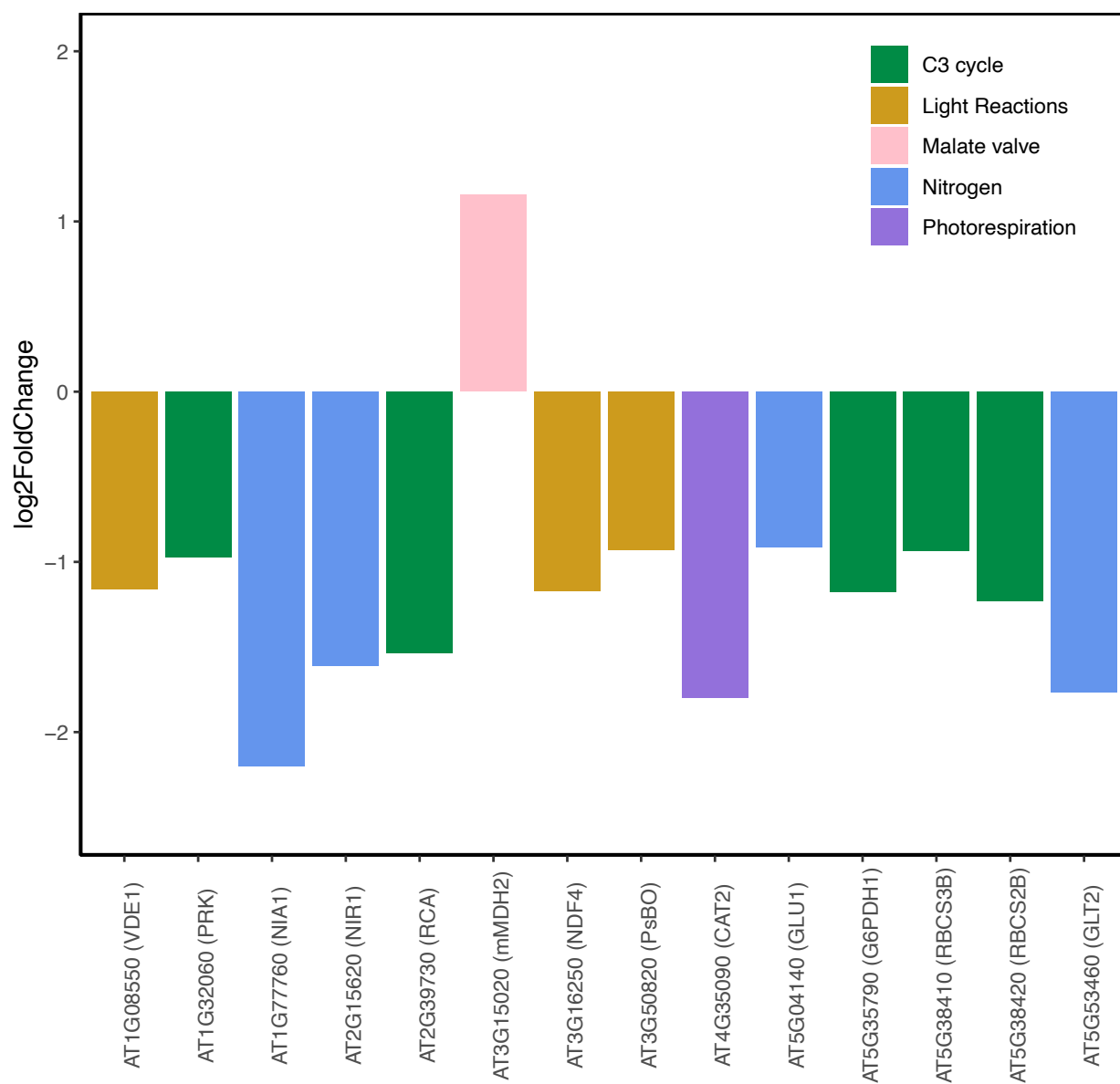


Figure 4.3. Differentially expressed genes related to photosynthetic and energetic processes at 2% O₂. Displayed is the log₂FoldChange in expression of photosynthetic genes at 2% O₂ compared to ambient (21%). The colors depict the associated pathway.

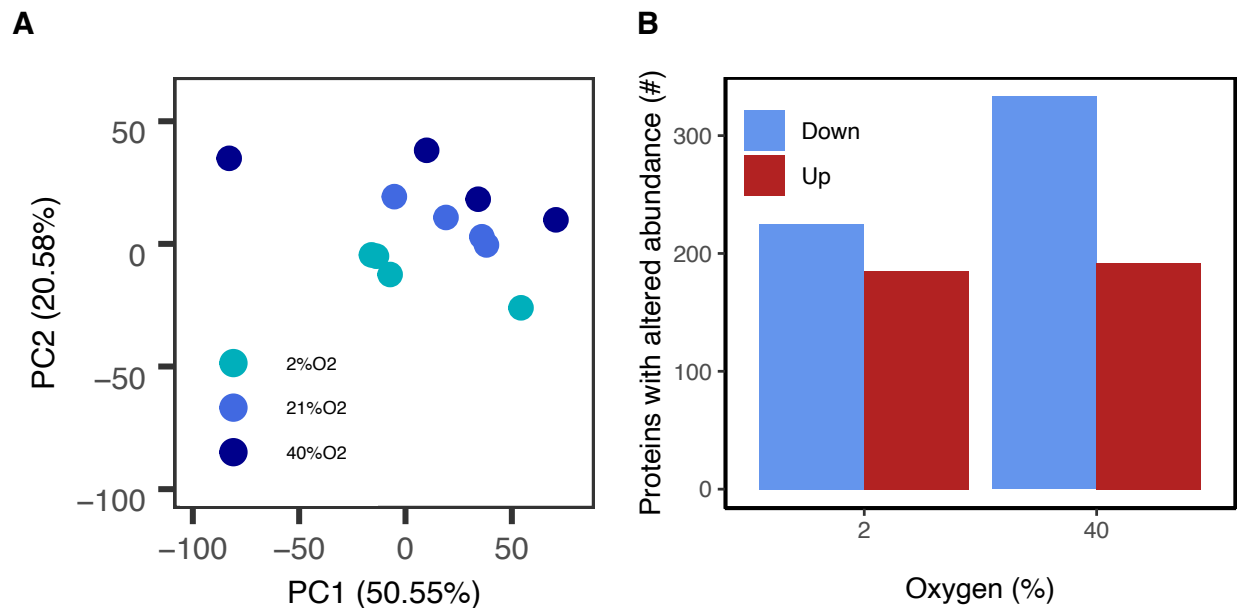


Figure 4.4. Effect of altered O₂ concentration on the proteome. The figure depicts A) principal component analysis of normalized peptide data. Additionally, B) the number of proteins with altered abundances at both 2% and 40% O₂ when compared to the ambient (21%) at the 7-hour time point.

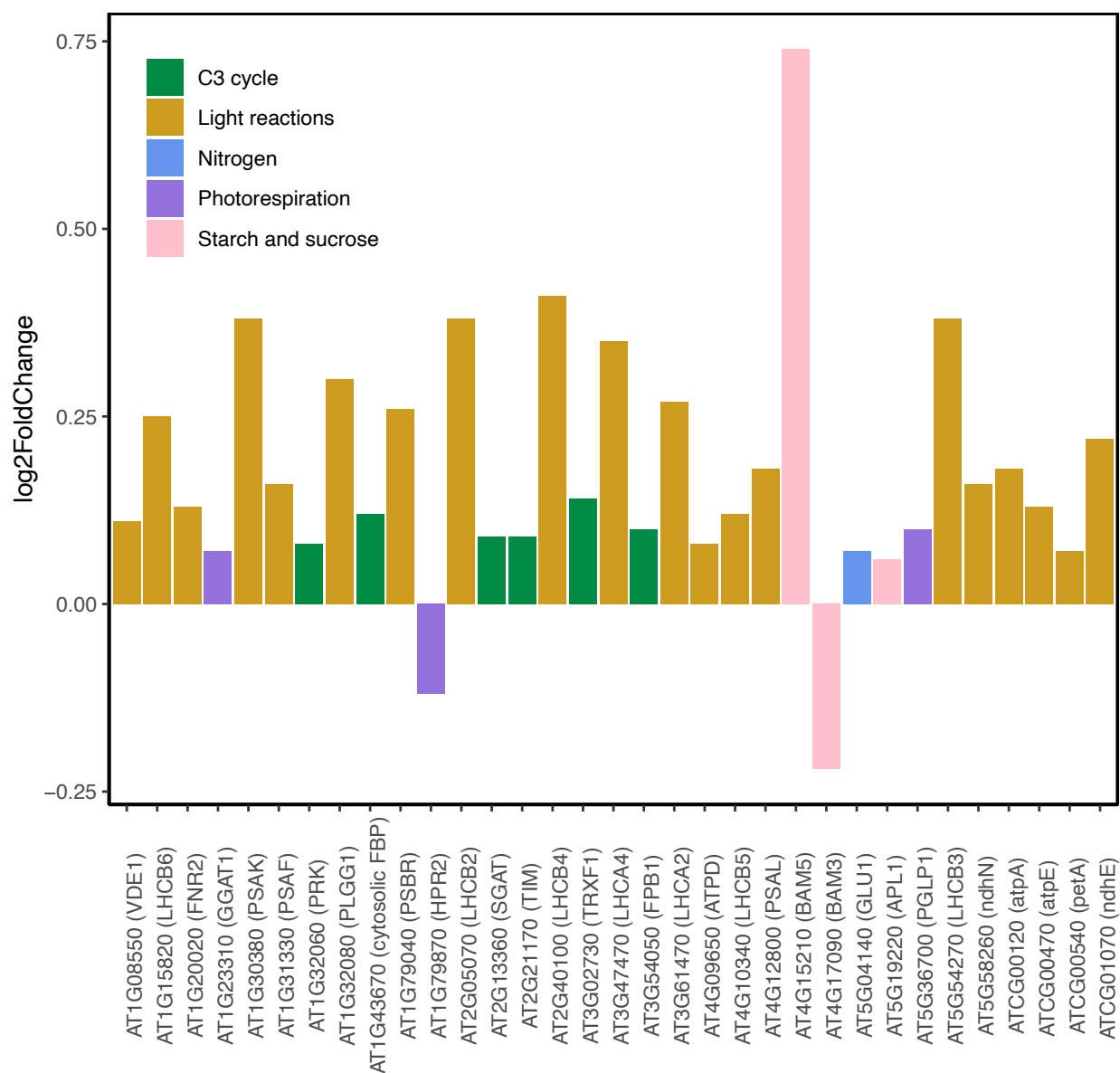


Figure 4.5. Photosynthetic-related proteins with altered abundance at 2% O₂. Displayed is the log₂FoldChange in expression of photosynthetic proteins at 2% O₂ compared to ambient (21%). The colors depict the associated pathway.

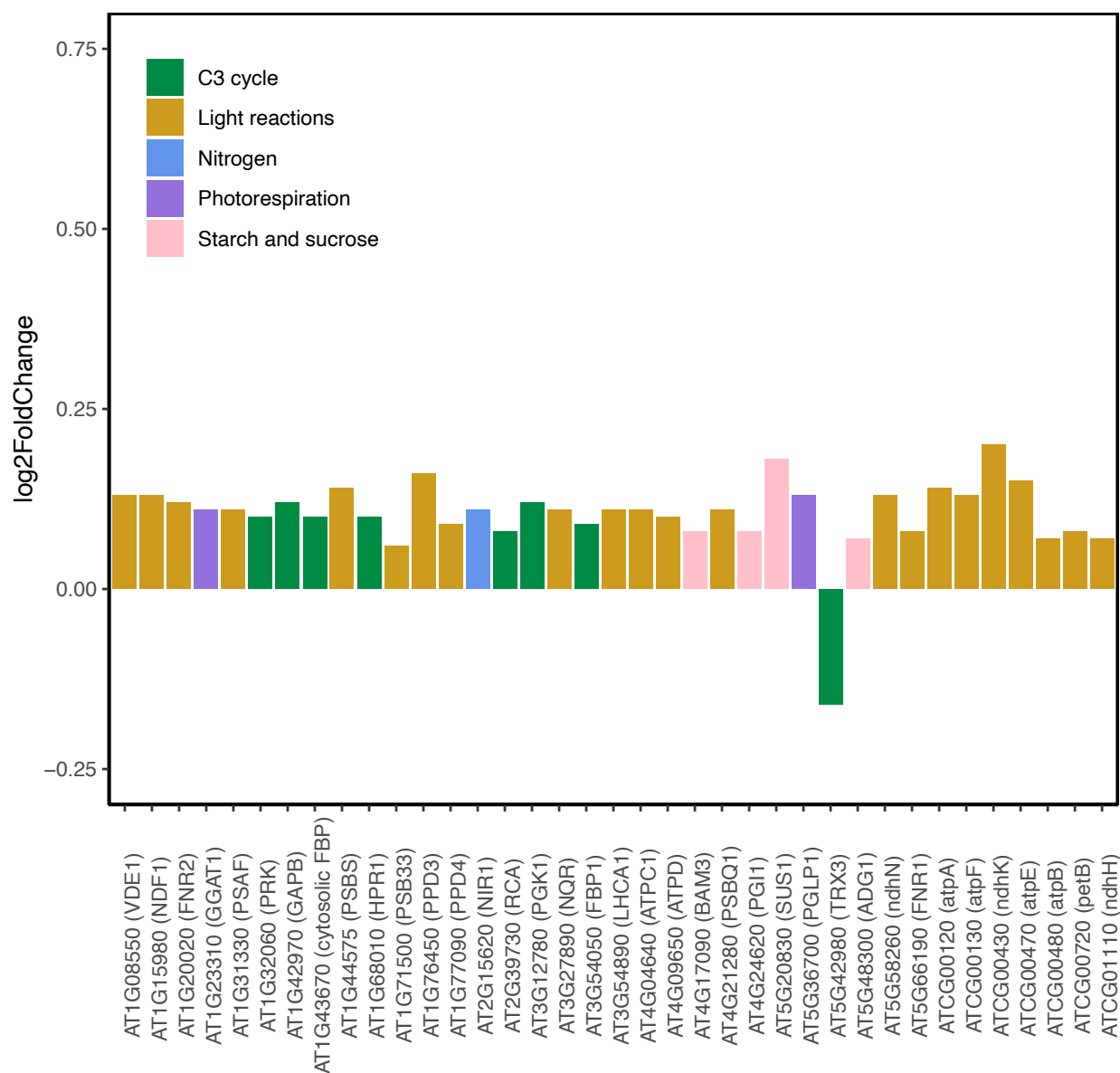


Figure 4.6. Photosynthetic-related proteins with altered abundance at 40% O₂. Displayed is the log₂FoldChange in expression of photosynthetic proteins at 40% O₂ compared to ambient (21%). The colors depict the associated pathway.

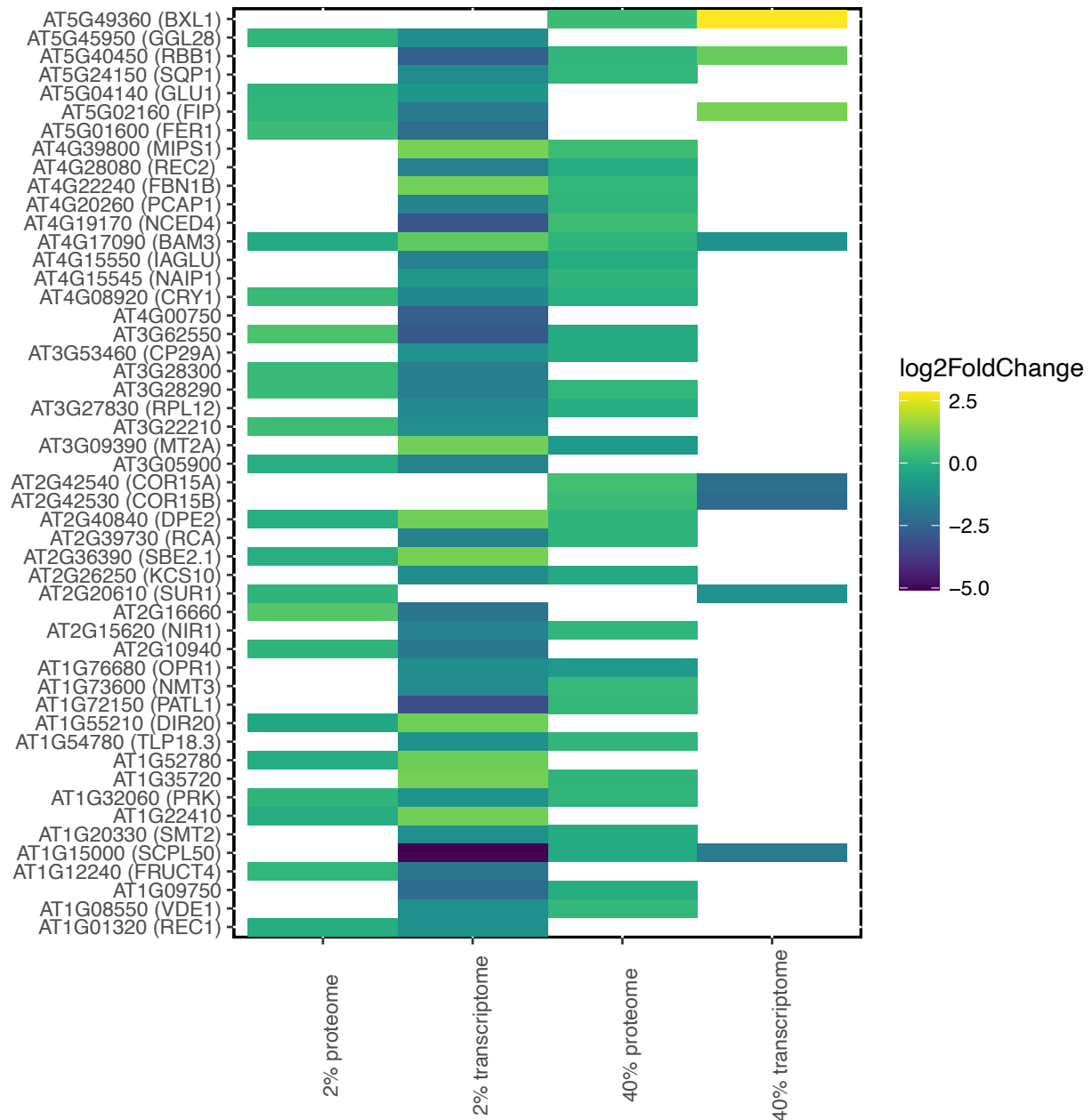


Figure 4.8. Expression changes in common elements between the transcriptome and proteome. Presented are the log2FoldChanges for the elements which were commonly altered between the transcriptome and proteome for both 2% and 40% when compared to 21% O₂.

LITERATURE CITED

- ABADIE, C., BATHELLIER, C. & TCHERKEZ, G. 2018. Carbon allocation to major metabolites in illuminated leaves is not just proportional to photosynthesis when gaseous conditions (CO₂ and O₂) vary. *New Phytologist*, 218, 94-106.
- AINSWORTH, E. A. & LONG, S. P. 2005. What have we learned from 15 years of free-air CO₂ enrichment (FACE)? A meta-analytic review of the responses of photosynthesis, canopy properties and plant production to rising CO₂. *New Phytologist*, 165, 351-372.
- AINSWORTH, E. A., ROGERS, A., VODKIN, L. O., WALTER, A. & SCHURR, U. 2006. The effects of elevated CO₂ concentration on soybean gene expression. An analysis of growing and mature leaves. *Plant Physiology*, 142, 135-147.
- ALRIC, J., PIERRE, Y., PICOT, D., LAVERGNE, J. & RAPPAPORT, F. 2005. Spectral and redox characterization of the heme c_i of the cytochrome b₆ f complex. *Proceedings of the National Academy of Sciences*, 102, 15860-15865.
- ANDERSON, L. E. 1971. Chloroplast and cytoplasmic enzymes II. Pea leaf triose phosphate isomerases. *Biochimica et Biophysica Acta (BBA)-Enzymology*, 235, 237-244.
- BAKER, N. R. 2008. Chlorophyll fluorescence: a probe of photosynthesis in vivo. *Annu. Rev. Plant Biol.*, 59, 89-113.
- BECKER, B., HOLTGREFE, S., JUNG, S., WUNRAU, C., KANDBINDER, A., BAIER, M., DIETZ, K.-J., BACKHAUSEN, J. E. & SCHEIBE, R. 2006. Influence of the photoperiod on redox regulation and stress responses in *Arabidopsis thaliana* L.(Heynh.) plants under long-and short-day conditions. *Planta*, 224, 380-393.
- BOLGER, A. M., LOHSE, M. & USADEL, B. 2014. Trimmomatic: a flexible trimmer for Illumina sequence data. *Bioinformatics*, 30, 2114-20.
- BOWES, G., OGREN, W. & HAGEMAN, R. 1971. Phosphoglycolate production catalyzed by ribulose diphosphate carboxylase. *Biochemical and biophysical research communications*, 45, 716-722.
- BRAY, N. L., PIMENTEL, H., MELSTED, P. & PACTER, L. 2016. Erratum: Near-optimal probabilistic RNA-seq quantification. *Nat Biotechnol*, 34, 888.
- BUSCH, F. A., SAGE, R. F. & FARQUHAR, G. D. 2018. Plants increase CO₂ uptake by assimilating nitrogen via the photorespiratory pathway. *Nature plants*, 4, 46-54.
- CHENG, C. Y., KRISHNAKUMAR, V., CHAN, A. P., THIBAUD-NISSEN, F., SCHOBEL, S. & TOWN, C. D. 2017. Araport11: a complete reannotation of the *Arabidopsis thaliana* reference genome. *Plant J*, 89, 789-804.

- COX, J. & MANN, M. 2008. MaxQuant enables high peptide identification rates, individualized p.p.b.-range mass accuracies and proteome-wide protein quantification. *Nature Biotechnology*, 26, 1367-1372.
- COX, J., NEUHAUSER, N., MICHALSKI, A., SCHELTEMA, R. A., OLSEN, J. V. & MANN, M. 2011. Andromeda: a peptide search engine integrated into the MaxQuant environment. *J Proteome Res*, 10, 1794-805.
- CRUZ, JEFFREY A., SAVAGE, L. J., ZEGARAC, R., HALL, CHRISTOPHER C., SATOH-CRUZ, M., DAVIS, GEOFFRY A., KOVAC, WILLIAM K., CHEN, J. & KRAMER, DAVID M. 2016. Dynamic Environmental Photosynthetic Imaging Reveals Emergent Phenotypes. *Cell Systems*, 2, 365-377.
- ERDJUMENT-BROMAGE, H., HUANG, F. K. & NEUBERT, T. A. 2018. Sample Preparation for Relative Quantitation of Proteins Using Tandem Mass Tags (TMT) and Mass Spectrometry (MS). *Methods Mol Biol*, 1741, 135-149.
- FARQUHAR, G. D., VON CAEMMERER, S. & BERRY, J. A. 1980. A biochemical model of photosynthetic CO₂ assimilation in leaves of C₃ species. *Planta*, 149, 78-90.
- FLÜGEL, F., TIMM, S., ARRIVAUULT, S., FLORIAN, A., STITT, M., FERNIE, A. R. & BAUWE, H. 2017. The photorespiratory metabolite 2-phosphoglycolate regulates photosynthesis and starch accumulation in Arabidopsis. *The Plant Cell*, 29, 2537-2551.
- FOYER, C. H., NEUKERMANS, J., QUEVAL, G., NOCTOR, G. & HARBINSON, J. 2012. Photosynthetic control of electron transport and the regulation of gene expression. *Journal of Experimental Botany*, 63, 1637-1661.
- FU, X., GREGORY, L. M., WEISE, S. E. & WALKER, B. J. 2023. Integrated flux and pool size analysis in plant central metabolism reveals unique roles of glycine and serine during photorespiration. *Nature Plants*, 9, 169-178.
- FU, X. & WALKER, B. J. 2022. Dynamic Response of Photorespiration in Fluctuating Light Environments. *Journal of Experimental Botany*.
- GUAN, X. & GU, S. 2009. Photorespiration and photoprotection of grapevine (*Vitis vinifera* L. cv. Cabernet Sauvignon) under water stress. *Photosynthetica*, 47, 437-444.
- GUAN, X., ZHAO, S., LI, D. & SHU, H. 2004. Photoprotective function of photorespiration in several grapevine cultivars under drought stress. *Photosynthetica*, 42, 31-36.
- GUPTA, P., DUPLESSIS, S., WHITE, H., KARNOSKY, D. F., MARTIN, F. & PODILA, G. K. 2005. Gene expression patterns of trembling aspen trees following long-term exposure to interacting elevated CO₂ and tropospheric O₃. *New Phytologist*, 167, 129-142.
- GYGI, S. P., ROCHON, Y., FRANZA, B. R. & AEBERSOLD, R. 1999. Correlation between protein and mRNA abundance in yeast. *Molecular and cellular biology*.

- HARLEY, P. C. & SHARKEY, T. D. 1991. An improved model of C₃ photosynthesis at high CO₂: reversed O₂ sensitivity explained by lack of glycerate reentry into the chloroplast. *Photosynthesis Research*, 27, 169-178.
- KAMMERS, K., COLE, R. N., TIENGWE, C. & RUCZINSKI, I. 2015. Detecting significant changes in protein abundance. *EuPA Open Proteomics*, 7, 11-19.
- KEBEISH, R., NIESSEN, M., THIRUVEEDHI, K., BARI, R., HIRSCH, H.-J., ROSENKRANZ, R., STÄBLER, N., SCHÖNFELD, B., KREUZALER, F. & PETERHÄNSEL, C. 2007. Chloroplastic photorespiratory bypass increases photosynthesis and biomass production in *Arabidopsis thaliana*. *Nature biotechnology*, 25, 593-599.
- KELLY, G. & LATZKO, E. 1976. Inhibition of spinach-leaf phosphofructokinase by 2-phosphoglycollate. *FEBS letters*, 68, 55-58.
- KOZAKI, A. & TAKEBA, G. 1996. Photorespiration protects C₃ plants from photooxidation. *Nature*, 384, 557-560.
- KRAMER, D. M. & EVANS, J. R. 2010. The Importance of Energy Balance in Improving Photosynthetic Productivity *Plant Physiology*, 155, 70-78.
- LEE, J. M., HAMMARÉN, H. M., SAVITSKI, M. M. & BAEK, S. H. 2023. Control of protein stability by post-translational modifications. *Nature Communications*, 14, 201.
- LI, L., NELSON, C. J., TRÖSCH, J., CASTLEDEN, I., HUANG, S. & MILLAR, A. H. 2017. Protein Degradation Rate in *Arabidopsis thaliana* Leaf Growth and Development. *The Plant Cell*, 29, 207-228.
- LONG, S., BAKER, N. & RAINES, C. 1993. Analysing the responses of photosynthetic CO₂ assimilation to long-term elevation of atmospheric CO₂ concentration. *CO₂ and biosphere*, 33-46.
- LONG, S. P., AINSWORTH, E. A., ROGERS, A. & ORT, D. R. 2004. Rising atmospheric carbon dioxide: plants FACE the future. *Annu. Rev. Plant Biol.*, 55, 591-628.
- LOVE, M. I., HUBER, W. & ANDERS, S. 2014. Moderated estimation of fold change and dispersion for RNA-seq data with DESeq2. *Genome Biol*, 15, 550.
- MAIER, A., FAHNENSTICH, H., VON CAEMMERER, S., ENGQVIST, M., WEBER, A., FLUGGE, U. & MAURINO, V. 2012. Glycolate oxidation in *A. thaliana* chloroplasts improves biomass production. *Frontiers in Plant Science*, 3, 38.
- MIYAKE, C. 2010. Alternative electron flows (water–water cycle and cyclic electron flow around PSI) in photosynthesis: molecular mechanisms and physiological functions. *Plant and Cell Physiology*, 51, 1951-1963.

- MULLER, P., LI, X. P. & NIYOGI, K. K. 2001. Non-photochemical quenching. A response to excess light energy. *Plant Physiol*, 125, 1558-66.
- NOCTOR, G. & FOYER, C. H. 1998. A re-evaluation of the ATP :NADPH budget during C3 photosynthesis: a contribution from nitrate assimilation and its associated respiratory activity? *Journal of Experimental Botany*, 49, 1895-1908.
- PAO, Y. C., STÜTZEL, H. & CHEN, T. W. 2019. A mechanistic view of the reduction in photosynthetic protein abundance under diurnal light fluctuation. *J Exp Bot*, 70, 3705-3708.
- PETERHANSEL, C., KRAUSE, K., BRAUN, H. P., ESPIE, G. S., FERNIE, A. R., HANSON, D. T., KEECH, O., MAURINO, V. G., MIELEWCZIK, M. & SAGE, R. F. 2013. Engineering photorespiration: current state and future possibilities. *Plant Biol (Stuttg)*, 15, 754-8.
- RAPPSILBER, J., MANN, M. & ISHIHAMA, Y. 2007. Protocol for micro-purification, enrichment, pre-fractionation and storage of peptides for proteomics using StageTips. *Nat Protoc*, 2, 1896-906.
- SCHEIBE, R. 2004. Malate valves to balance cellular energy supply. *Physiologia plantarum*, 120, 21-26.
- SEARLE, B. C. 2010. Scaffold: a bioinformatic tool for validating MS/MS-based proteomic studies. *Proteomics*, 10, 1265-9.
- SMITH, K., STRAND, D. D., KRAMER, D. M. & WALKER, B. J. 2023. The role of photorespiration in preventing feedback regulation via ATP synthase in *Nicotiana tabacum*. *Plant, Cell & Environment*.
- SONESON, C., LOVE, M. I. & ROBINSON, M. D. 2015. Differential analyses for RNA-seq: transcript-level estimates improve gene-level inferences. *F1000Res*, 4, 1521.
- SOUTH, P. F., CAVANAGH, A. P., LIU, H. W. & ORT, D. R. 2019. Synthetic glycolate metabolism pathways stimulate crop growth and productivity in the field. *Science*, 363, eaat9077.
- STRAND, D. D. & WALKER, B. J. 2023. Energetic considerations for engineering novel biochemistries in photosynthetic organisms. *Front Plant Sci*, 14, 1116812.
- TAYLOR, G., STREET, N. R., TRICKER, P. J., SJÖDIN, A., GRAHAM, L., SKOGSTRÖM, O., CALFAPIETRA, C., SCARASCIA-MUGNOZZA, G. & JANSSON, S. 2005. The transcriptome of *Populus* in elevated CO2. *New Phytologist*, 167, 143-154.
- TIAN, T., LIU, Y., YAN, H., YOU, Q., YI, X., DU, Z., XU, W. & SU, Z. 2017. agriGO v2.0: a GO analysis toolkit for the agricultural community, 2017 update. *Nucleic Acids Res*, 45, W122-w129.

- TULLER, T., KUPIEC, M. & RUPPIN, E. 2007. Determinants of protein abundance and translation efficiency in *S. cerevisiae*. *PLoS Comput Biol*, 3, e248.
- VIALET-CHABRAND, S., MATTHEWS, J. S., SIMKIN, A. J., RAINES, C. A. & LAWSON, T. 2017. Importance of fluctuations in light on plant photosynthetic acclimation. *Plant physiology*, 173, 2163-2179.
- VON CAEMMERER, S. 2013. Steady-state models of photosynthesis. *Plant, Cell & Environment*, 36, 1617-1630.
- WALKER, B. J., KRAMER, D. M., FISHER, N. & FU, X. 2020. Flexibility in the energy balancing network of photosynthesis enables safe operation under changing environmental conditions. *Plants*, 9, 301.
- WU, G., NIE, L. & ZHANG, W. 2008. Integrative analyses of posttranscriptional regulation in the yeast *Saccharomyces cerevisiae* using transcriptomic and proteomic data. *Current microbiology*, 57, 18-22.

CHAPTER 5:

Conclusions and future directions

Kaila Smith

Summary

Population growth predicts the global population to reach 9.7 billion by 2050 calling for double the current annual food production (McGuire, 2015). One of the ways in which food production can be increased is through larger agricultural yields which may be limited by photosynthetic efficiency. For example, carbon assimilation reaches a theoretical maximum of 4.6%, however, the highest reported values are closer to 2-3% in plants conducting C3 photosynthesis (Zhu et al., 2008, Walker et al., 2016). One strategy to improve photosynthesis is the modification of the photorespiratory pathway which could substantially alter metabolic ATP:NADPH demand (Peterhansel et al., 2013a). This is problematic since the ATP:NADPH demand from metabolism must be matched with that supplied from the light reactions to operate efficiently without photodamage in a process referred to as energy balancing. Ultimately, to implement novel photosynthetic improvement strategies successfully, further knowledge surrounding how energy balance is regulated is required (Kramer and Evans, 2010).

There is a lot of focus regarding how supply-side processes including linear electron flow, cyclic electron flow (CEF), and the malate valve mediate energy balancing, however, there is less focus surrounding on how changes in the ATP:NADPH demand from metabolism drive these responses (Walker et al., 2020, Kramer et al., 2004a, Cruz et al., 2005, Laisk et al., 2007, Scheibe, 2004, Scheibe et al., 2005). In terms of metabolism in the light of photoautotrophic tissues, photorespiration consumes substantial amounts of energy in the forms of ATP and reductant making the pathway an important component in leaf energetics. The energetic costs of photorespiration are often discussed; however, less emphasis is placed on how the energy demands from photorespiration might be involved in achieving energy balance remains (Busch, 2020, Noctor and Foyer, 1998, Peterhansel et al., 2010, Huma et al., 2018). Within this

dissertation, I elucidated how the energy demands from photorespiration might be involved in achieving energy balance.

The C3 cycle and photorespiration are thought to require the largest amount of ATP and reductant in photosynthetic tissues. Many key physiological approaches (for example measurements of mesophyll conductance to CO₂ using chlorophyll fluorescence as well as the water-water cycle from rates oxygen evolution and concurrent gas exchange) depend upon this assumption (Loreto et al., 1992, Gilbert et al., 2011, Warren, 2006, Ruuska et al., 2000). While these simplifications can be useful, they only reflect a portion of the total ATP and NADPH demand in the cell due to the contribution of additional metabolic processes. One approach for determining how each individual metabolic pathway contributes to the ATP:NADPH demand is to leverage metabolic flux networks. These metabolic flux networks can be used to resolve cellular energy flux by coupling the flux of each individual reaction to its associated ATP and NADPH demand. This approach was taken in Chapter 1 to quantify how individual metabolic pathways contribute to the overall energy demand of the cell. As expected, the C3 cycle and photorespiration did represent most of the ATP and reductant demands (Figure 1.1). Due to the large ATP and reductant demands from the C3 cycle and photorespiration, cellular ATP:NADPH demand is thought to be determined mainly from the distribution of flux through photorespiration and the C3 cycle. However, the distribution of flux through photorespiration and the C3 cycle did not entirely explain cellular ATP:NADPH (Figure 5.1C). Instead, starch and sucrose synthesis also substantially altered the cellular ATP:NADPH demand (Figure 1.6A). Ultimately, these results highlighted that while other metabolic pathways may have more energetic significance than expected, the C3 cycle and photorespiration still dominate in terms of absolute flux further validating key assumptions in plant physiology.

Given the large amount of ATP and NADPH consumed by photorespiration, it is important to understand how the pathway interacts with the light reactions of photosynthesis which supply the ATP and NADPH. Chapter 2 examined how downstream changes in energy demand driven by manipulating flux through photorespiration impacted the flexibility of the light reactions. Low photorespiratory flux decreased photosynthetic efficiency (ϕ_{II}) which was attributed to increased feedback regulation at ATP synthase (Figure 2.4A, 2.5A, and 2.6B). One proposed function of the large reductant consumption from photorespiration is to dissipate “excess” photochemical energy produced in excess of that which can be consumed by CO₂ assimilation, thus acting a photoprotective mechanism (Walker et al., 2016, Sharkey, 1988, Osei-Bonsu et al., 2021, Guan and Gu, 2009). However, ϕ_{II} decreased under high photorespiratory flux, possibly from the accumulation of photoinhibition, contrary to the proposed role of photorespiration as a photoprotective electron sink (Figure 2.5B). Additionally, the accumulation of photoinhibition might be driven by changes in O₂ rather than by photorespiratory flux. Instead of the proposed role as a photoprotective electron sink, the results from this chapter suggest a novel role for the ATP consumption from photorespiration in maintaining ATP synthase activity.

Photorespiration and the C₃ cycle respond dynamically to environmental factors, for example under fluctuating light, which then alters the ATP:NADPH demand which increases with photorespiration (Fu and Walker, 2022). Consequently, the energy balancing response must be similarly dynamic to prevent photodamage and maintain optimal efficiency of metabolism. While some of the genes that mediate this dynamic response are known, there are likely many others which remain unknown. To identify additional genes involved in responding to these dynamic shifts in ATP:NADPH demand, Chapter 3 leveraged the phenotype identified in Chapter 2 to develop an imaging-based fluorescence screen. The screen revealed how mechanisms which

are important under dynamic measurements and steady-state can differ (Figure 3.3B and Figure 3.4). Additionally, a mutagenic screen revealed two interesting novel phenotypes and highlighted some difficulties which might arise in the casual SNP identification of transient phenotypes (Figure 3.7, 3.8 and 3.9).

In addition to dynamic changes in ATP:NADPH demand, the ATP:NADPH demand from metabolism can be altered during prolonged periods such as drought raising the question as to how the plant might respond to prolonged periods with altered ATP:NADPH. For example, if the decreased in ϕ_{II} observed in Chapter 2 might restore. Under 2% O₂, ϕ_{II} did restore to ambient levels after approximately 4 hours despite a lack of change in NPQ (Figure 4.1A). The acclimatory response was then examined through transcriptomic and proteomic analyses. There were few changes in energy and photosynthetic-related transcripts, however, there were changes in numerous photosynthetic proteins which were mostly an increase in abundance at both 40% and 2% O₂ (Figure 4.3, 4.5, and 4.6). These more highly abundant proteins, together with the lack of transcriptional response, suggested the regulatory response to periods with altered ATP:NADPH demand might involve post-translational modifications which could improve protein stability. However, the log₂FoldChange in abundance on all the photosynthetic-related proteins were relatively small so an alternative explanation might be that photosynthetic capacity itself is sufficient to recover without any substantial re-programming.

Together the results in this dissertation highlight the inherent capability of C3 plants in managing substantial changes in energy demand driven by photorespiration. With respect to the decreased energy demand at 2% O₂, there was an initial decline in ϕ_{II} driven by decreased ATP synthase conductivity ultimately from a loss of ATP consumption from photorespiration. However, ϕ_{II} did restore to ambient levels which displayed how the plant has innate acclimatory

mechanisms to address situations of decreased demand. With respect to the increased demand at 40% O₂, there appeared to be little response to the increased demands and rather any responses observed were likely driven by changes in O₂ itself. While this dissertation began to explore the innate acclimatory mechanisms responsible for the inherent capability of C3 plants in managing these substantial changes in energy demand, clearly there are many unanswered questions.

Future directions

The findings in this dissertation increase our overall understanding of the role of the energy demands from photorespiration in achieving energy balance. Additionally, these findings begin to address some of the associated regulatory mechanisms involved. However, as often is the case, these findings also raised many new unanswered questions. Some of these questions raised but not thoroughly addressed in this dissertation includes the specific timing for activation or deactivation of the malate valve, how photorespiration might operate with other energy-demanding metabolisms to achieve energy balance, as well as specific regulatory mechanisms in place which will assist in the plant adapting to novel biochemical pathways.

The chloroplast has many possible routes of alternative electron transfer to augment an ATP deficit including the CEF and the malate valve, however, there are a lot of questions as to when these mechanisms are specifically employed. In Chapter 2, an increase in CEF under 40% O₂ was expected to meet the higher ATP:NADPH demand and a decrease in CEF under 2% O₂ to meet the lower demand. Instead, the *in vivo* assays for CEF indicated no substantial changes in the relative rates of electron transfer from CEF which suggested that CEF does not respond to short term changes in ATP:NADPH demand (Figure 2.10). The lack of CEF activation instead argues that other alternative electron transport pathways, such as the malate valve, may be more involved in supplying a dynamic ATP deficit. Malate valve activity does rapidly activate during a

high-light transition which could alleviate surplus NADPH as the C3 cycle gradually reaches steady-state (Scheibe and Stitt, 1988, Scheibe, 2019). In Chapter 3, under similarly dynamic conditions, *mdh1-1* and *mdh1-2* mutants displayed an interesting transient phenotype in response to a shift in ATP:NADPH demand (Figure 3.3A). The transient response of the *mdh1* knockout supports the malate valve might be involved in supplying a dynamic ATP deficit. However, the double knockout of *mdh1-1mdh2* resembled the WT, confounding these results.

A major theme which arose throughout this work was how photorespiration might operate with other energy-demanding metabolisms to achieve energy balance. For example, in Chapter 1 there was a substantial contribution from starch and sucrose synthesis in determining cellular ATP:NADPH demand which led to the hypothesis that the ATP demand from starch and sucrose synthesis might counterbalance that from photorespiration to help maintain a more similar ATP:NADPH demand (Figure 1.6). The potential maintenance of a more similar ATP:NADPH demand amongst conditions might explain why there were not larger responses in either the transcriptome or proteome in Chapter 4 and perhaps examining metabolic changes might offer more insight into the acclimatory response at 2% O₂. One way to test the proposed relationship would be to examine how starch and sucrose synthesis knockouts respond to dynamic changes in ATP:NADPH demand by using the screen developed in Chapter 3. The benefit of this relationship might be to potentially decrease the need for rapid adjustments from alternative ATP generating processes which could lead to a downregulation of the light reactions and photosynthesis (Livingston et al., 2010b, Alric and Johnson, 2017, Allen, 2003b). This could be assessed by examining the response of CEF in starch and sucrose synthesis knockouts at changing O₂. Additionally, a decreased need for rapid adjustments in ATP generating processes might begin to resolve why altering flux through the C3 cycle or photorespiration does not

always appear to activate CEF as expected from changes in energetic demands as seen in Chapter 2 (Figure 2.10).

In addition to starch and sucrose synthesis, there were also connections between how photorespiration might operate with nitrogen metabolism to achieve energy balance. Chapter 3 revealed that *GLU1*, which encodes Fd-GOGAT an important enzyme in nitrogen metabolism, might be the SNP candidate responsible for the mutagenic 1x1 phenotype (Table 3.1). However, to confirm that a SNP in *GLU1* is responsible for the 1x1 phenotype it will be necessary to test whether complementation of the SNP results in a loss of the phenotype. Alternatively, as discussed extensively in the chapter, there were a lot of challenges associated with classifying the transient phenotype and it may be beneficial to repeat the screening and subsequent sequencing of the F2 population with these difficulties now in mind. For example, only including plants in the bulk populations where first the control phenotypes behaved exactly as expected then additionally the F2 classification identically matched the appropriate control.

There is concern that novel engineering strategies which alter the ATP:NADPH demand might result in a down-regulation of photosynthetic efficiency (Strand and Walker, 2023). This idea is supported by the findings in Chapter 2 where photosynthetic efficiency is decreased under both 2% and 40% O₂ where ATP:NADPH demand is altered (Figure 2.4). However, the work in Chapters 3 and 4 begins to address how there might both short and long term acclimatory responses the plant could use to meet new synthetic energy demands. Although Chapter 3 has yet to conclusively identify any specific mechanisms, the work highlighted the importance in using dynamic methodology to uncover physiological responses not readily available in the steady-state as well as developed a platform for examining how plants with novel metabolisms might respond to dynamic shifts in ATP:NADPH demand. In Chapter 4, the recovery of decreased ϕ_{II} at

low O₂ when ATP:NADPH demand is low could indicate there are regulatory mechanisms in place which will assist in the plant adapting to novel biochemical pathways (Figure 4.1). More specifically, these regulatory mechanisms might include post-translational modifications which could decrease protein degradation, however, to gain further insight into whether these types of post-translational modifications might be occurring modification-specific proteomics must be conducted.

LITERATURE CITED

- ALLEN, J. F. 2003. Cyclic, pseudocyclic and noncyclic photophosphorylation: new links in the chain. *Trends in Plant Science*, 8, 15-19.
- ALRIC, J. & JOHNSON, X. 2017. Alternative electron transport pathways in photosynthesis: a confluence of regulation. *Curr Opin Plant Biol*, 37, 78-86.
- BUSCH, F. A. 2020. Photorespiration in the context of Rubisco biochemistry, CO₂ diffusion and metabolism. *Plant Journal*, 101, 919-939.
- CRUZ, J. A., AVENSON, T. J., KANAZAWA, A., TAKIZAWA, K., EDWARDS, G. E. & KRAMER, D. M. 2005. Plasticity in light reactions of photosynthesis for energy production and photoprotection. *Journal of experimental botany*, 56, 395-406.
- FU, X. & WALKER, B. J. 2022. Dynamic Response of Photorespiration in Fluctuating Light Environments. *Journal of Experimental Botany*.
- GILBERT, M. E., POU, A., ZWIENIECKI, M. A. & HOLBROOK, N. M. 2011. On measuring the response of mesophyll conductance to carbon dioxide with the variable J method. *Journal of Experimental Botany*, 63, 413-425.
- GUAN, X. & GU, S. 2009. Photorespiration and photoprotection of grapevine (*Vitis vinifera* L. cv. Cabernet Sauvignon) under water stress. *Photosynthetica*, 47, 437-444.
- HUMA, B., KUNDU, S., POOLMAN, M. G., KRUGER, N. J. & FELL, D. A. 2018. Stoichiometric analysis of the energetics and metabolic impact of photorespiration in C₃ plants. *The Plant Journal*, 96, 1228-1241.
- KRAMER, D. M., AVENSON, T. J. & EDWARDS, G. E. 2004. Dynamic flexibility in the light reactions of photosynthesis governed by both electron and proton transfer reactions. *Trends Plant Sci*, 9, 349-57.
- KRAMER, D. M. & EVANS, J. R. 2010. The Importance of Energy Balance in Improving Photosynthetic Productivity *Plant Physiology*, 155, 70-78.
- LAISK, A., EICHELMANN, H., OJA, V., TALTS, E. & SCHEIBE, R. 2007. Rates and roles of cyclic and alternative electron flow in potato leaves. *Plant and Cell Physiology*, 48, 1575-1588.
- LIVINGSTON, A. K., CRUZ, J. A., KOHZUMA, K., DHINGRA, A. & KRAMER, D. M. 2010. An Arabidopsis mutant with high cyclic electron flow around photosystem I (hcef) involving the NADPH dehydrogenase complex. *The Plant cell*, 22, 221-233.
- LORETO, F., HARLEY, P. C., DI MARCO, G. & SHARKEY, T. D. 1992. Estimation of Mesophyll Conductance to CO₂ Flux by Three Different Methods. *Plant Physiol*, 98, 1437-43.

- MCGUIRE, S. 2015. FAO, IFAD, and WFP. The State of Food Insecurity in the World 2015: Meeting the 2015 International Hunger Targets: Taking Stock of Uneven Progress. Rome: FAO, 2015. *Adv Nutr*, 6, 623-4.
- NOCTOR, G. & FOYER, C. H. 1998. A re-evaluation of the ATP: NADPH budget during C3 photosynthesis: a contribution from nitrate assimilation and its associated respiratory activity? *Journal of Experimental Botany*, 49, 1895-1908.
- OSEI-BONSU, I., MCCLAIN, A. M., WALKER, B. J., SHARKEY, T. D. & KRAMER, D. M. 2021. The roles of photorespiration and alternative electron acceptors in the responses of photosynthesis to elevated temperatures in cowpea. *Plant Cell Environ*, 44, 2290-2307.
- PETERHANSEL, C., BLUME, C. & OFFERMANN, S. 2013. Photorespiratory bypasses: how can they work? *J Exp Bot*, 64, 709-15.
- PETERHANSEL, C., HORST, I., NIESSEN, M., BLUME, C., KEBEISH, R., KÜRKCÜOĞLU, S. & KREUZALER, F. 2010. Photorespiration. *Arabidopsis Book*, 8, e0130.
- RUUSKA, S. A., BADGER, M. R., ANDREWS, T. J. & VON CAEMMERER, S. 2000. Photosynthetic electron sinks in transgenic tobacco with reduced amounts of Rubisco: little evidence for significant Mehler reaction. *Journal of Experimental Botany*, 51, 357-368.
- SCHEIBE, R. 2004. Malate valves to balance cellular energy supply. *Physiologia plantarum*, 120, 21-26.
- SCHEIBE, R. 2019. Maintaining homeostasis by controlled alternatives for energy distribution in plant cells under changing conditions of supply and demand. *Photosynthesis research*, 139, 81-91.
- SCHEIBE, R., BACKHAUSEN, J. E., EMMERLICH, V. & HOLTGREFE, S. 2005. Strategies to maintain redox homeostasis during photosynthesis under changing conditions. *Journal of experimental botany*, 56, 1481-1489.
- SCHEIBE, R. & STITT, M. 1988. Comparison of NADP-malate dehydrogenase activation, QA reduction and O₂ evolution in spinach leaves. *Plant Physiol Biochem*, 26, 473-481.
- SHARKEY, T. D. 1988. Estimating the rate of photorespiration in leaves. *Physiologia Plantarum*, 73, 147-152.
- STRAND, D. D. & WALKER, B. J. 2023. Energetic considerations for engineering novel biochemistries in photosynthetic organisms. *Front Plant Sci*, 14, 1116812.
- WALKER, B. J., KRAMER, D. M., FISHER, N. & FU, X. 2020. Flexibility in the energy balancing network of photosynthesis enables safe operation under changing environmental conditions. *Plants*, 9, 301.

- WALKER, B. J., VANLOOCKE, A., BERNACCHI, C. J. & ORT, D. R. 2016. The Costs of Photorespiration to Food Production Now and in the Future. *Annu Rev Plant Biol*, 67, 107-29.
- WARREN, C. 2006. Estimating the internal conductance to CO₂ movement. *Funct Plant Biol*, 33, 431-442.
- ZHU, X.-G., LONG, S. P. & ORT, D. R. 2008. What is the maximum efficiency with which photosynthesis can convert solar energy into biomass? *Current opinion in biotechnology*, 19, 153-159.